Chromatin accessibility dynamics of neurogenic niche cells reveal defects in neural stem cell adhesion and migration during aging

Robin W. Yeo[1,*], Olivia Y. Zhou[1,2,3,*], Brian L. Zhong[4], Eric D. Sun[1,5], Paloma Navarro Negredo[1], Surag Nair[1,6], Mahfuza Sharmin[1,6], Tyson J. Ruetz[1], Mikaela Wilson[1], Anshul Kundaje[1,6], Alexander R. Dunn[4], Anne Brunet[1,7,8]

Affiliations

[1] Department of Genetics, Stanford University, Stanford, CA, USA

[2] Stanford Biophysics Program, Stanford University, Stanford, CA, USA

[3] Stanford Medical Scientist Training Program, Stanford University, Stanford, CA, USA

[4] Department of Chemical Engineering, Stanford University, Stanford, CA, USA

[5] Biomedical Informatics Graduate Program, Stanford University, Stanford, CA, USA

[6] Department of Computer Science, Stanford University, Stanford, CA, USA

[7] Glenn Laboratories for the Biology of Aging, Stanford University, Stanford, CA, USA

[8] email: abrunet1@stanford.edu

* These authors contributed equally

Abstract

Aging is accompanied by a deterioration in the regenerative and repair potential of stem cell niches in the brain[1-5]. However, the mechanisms underlying this decline are largely unknown. Here we characterize genome-wide chromatin accessibility in young and old neurogenic niche cells *in vivo*, revealing defects in neural stem cell (NSC) adhesion and migration during aging. Interestingly, chromatin accessibility at cell adhesion and migration genes decreases with age in quiescent NSCs but increases with age in activated (proliferative) NSCs, and this is accompanied by corresponding expression changes in these genes. We experimentally validate that quiescent and activated NSCs exhibit opposing adhesion and migration behaviors with age: quiescent NSCs become less adhesive (and more migratory) whereas activated NSCs and progeny become more adhesive (and less migratory) during aging. We also show that the ability of activated NSCs and progeny to mobilize out of the niche during *in vivo* neurogenesis diminishes during aging. Using tension sensors with single molecule resolution, we find that one of the cellular mechanisms by which aging impairs the migration of old activated NSCs and progeny involves increased force-producing adhesions. We identify inhibition of the cytoskeletal-regulating kinase ROCK[6,7] as a way to reduce force-producing adhesions and restore migration in old activated NSCs *in vitro*. Interestingly, inhibition of ROCK in the neurogenic niche of old mice boosts neurogenesis to the olfactory bulb *in vivo*. These results have important implications for restoring the migratory potential of NSCs and progeny and for improving neurogenesis in the aged brain.

47 **Main text**

48

49 The adult brain contains regenerative neural stem cell (NSC) niches, with progenitors that
50 can migrate to distal brain regions to generate new neurons and glial cells[1-5]. The regenerative
51 potential of stem cell niches in the brain declines with age, and this is accompanied by a
52 corresponding deterioration in aspects of sensory and cognitive function as well as repair
53 ability[2,8-10]. The subventricular zone (SVZ) neurogenic niche provides an excellent model system
54 for studying NSC function and migration during aging. In this niche, quiescent NSCs line the
55 ventricular wall[11-13]. Quiescent NSCs can activate and in turn generate progenitors and
56 neuroblasts that migrate through the rostral migratory stream towards the olfactory bulb to
57 produce new neurons[14]. NSC progeny also migrate to sites of injury to mitigate damage by
58 generating new neurons[15] and astrocytes[16]. Both the regenerative potential and repair abilities of
59 the SVZ neurogenic region decline with age[17-21]. Previous transcriptomic studies have started to
60 uncover defects in inflammation, signaling pathways, and cell cycle in SVZ neurogenic niches
61 during aging[22-25]. However, the mechanisms underlying regenerative decline during aging – and
62 how defects in migratory potential might be involved – remain largely unknown.

63

64 Epigenomic changes that affect chromatin states play an important role in the regulation
65 of cell fate[26] and aging[27]. So far, however, epigenomic studies of NSCs have been limited to
66 whole tissues *in vivo*[28,29], developmental studies[30], or culture systems[29,31-33]. Importantly, age-
67 dependent epigenomic changes in different cell types of the neurogenic niche *in vivo* remain
68 unknown. Such changes to the chromatin landscape of NSCs could have a longer-lasting impact
69 on progeny and reveal features of aging that were previously undetected. Identifying chromatin

70 changes in different cell types from the neurogenic niche during aging could also help identify
71 novel ways to reverse age-dependent defects in regeneration and repair and counter brain aging.
72
73 **Chromatin profiling of five cell types freshly isolated from the SVZ neurogenic region**
74 **reveals opposing changes with age in quiescent and activated NSCs involving cell adhesion**
75 **and migration pathways**
76
77 To determine the impact of aging on the chromatin landscape of cells in the neurogenic
78 niche *in vivo*, we generated chromatin accessibility profiles from 5 distinct cell types freshly
79 isolated from the subventricular zone (SVZ) neurogenic niche of young and old mice. We aged
80 cohorts of transgenic mice expressing green fluorescent protein driven by the human promoter
81 for glial fibrillary acidic protein (GFAP-GFP)[34], which, in combination with other markers (see
82 Methods), enables the isolation of 5 different cell types by fluorescence-activated cell sorting
83 (FACS)[35] (Fig. 1a, Extended Data Fig. 1a). The SVZ neurogenic niches of young (3-5 months
84 old) and old (20-24 months old) GFAP-GFP mice were micro-dissected, and 5 cell populations
85 from this region were freshly isolated by this FACS method[35,36]– endothelial cells, astrocytes,
86 quiescent NSCs (qNSCs), activated NSCs (aNSCs), and neural progenitor cells (NPCs) (Fig. 1a,
87 Extended Data Fig. 1a). We verified that FACS markers mostly did not change with age in
88 isolated quiescent and activated NSCs (though there was a small increase in EGFR in old
89 activated NSCs) (Extended Data Fig. 1a-d). This observation suggests that quiescent and
90 activated NSCs isolated from young and old animals are largely similar in terms of cell identity,
91 consistent with our previous findings[36] (see also below for independent single cell RNA-seq
92 validation and examination of cell identity, Extended Data Fig. 5, 6).

93

94 To assess chromatin accessibility genome-wide on these rare cell populations (~100-1000
95 cells per individual), we used ATAC-seq[37-41] (Fig. 1a) (see Methods). ATAC-seq libraries across
96 all conditions exhibited stereotypical 147-bp nucleosome periodicity (Extended Data Fig. 1e) and
97 strong enrichment of accessibility around transcription start sites (TSSs) (Extended Data Fig. 1f).
98 Principal component analysis (PCA) (Fig. 1b) and hierarchical clustering (Extended Data Fig.
99 2a) on accessible chromatin peaks separated endothelial cells from other brain cells (PC1), and
100 quiescent cells (qNSCs and astrocytes) from activated ones (aNSCs and NPCs) (PC2). The locus
101 for *Ascl1*, a neural lineage gene involved in NSC activation[42], shows accessible chromatin peaks
102 in all neural cell types (but not in endothelial cells) and more accessible peaks in aNSCs and
103 NPCs compared to qNSCs and astrocytes (Fig. 1c), consistent with *Ascl1* bulk mRNA
104 expression[36] (Extended Data Fig. 2b). Additionally, chromatin accessibility at genome-wide
105 promoters positively correlated with gene expression from single cell RNA-seq data[24] (Extended
106 Data Fig. 2c). Thus, these genome-wide chromatin accessibility datasets represent a useful
107 resource for studying age-related chromatin changes in 5 different cell types freshly isolated
108 from the regenerative SVZ neurogenic niche during aging.

109

110 Chromatin accessibility allowed separation of quiescent and activated NSCs by age (Fig.
111 1d for PC2, Extended Data Fig. 3a for PC3). In line with transcriptional studies[24,25,36], more
112 chromatin peaks change with age in qNSCs (7,354) than in aNSCs (2,311) (FDR < 0.05)
113 (Extended Data Fig. 3b, Supplementary Table 2). As expected, chromatin peaks were largely
114 located either at promoters or at intronic and distal regions, which are known to contain non-
115 coding regulatory elements such as enhancers (Extended Data Fig. 3c). Chromatin peaks that

116 overlap with marks of enhancers (H3K27ac and p300 binding[31], see Methods), as well as those at
117 distal and intronic regions, were sufficient to separate NSCs based on age whereas chromatin
118 peaks at promoters alone were not (Fig. 1e, Extended Data Fig. 3d-g). Furthermore, chromatin
119 peaks that dynamically change with age in qNSCs and aNSCs were almost entirely distal or
120 intronic (Extended data Fig. 3h, Supplementary Table 2). Thus, non-coding regulatory elements
121 may be particularly sensitive to changes during aging.
122
123 Surprisingly, aging had opposing effects on chromatin accessibility dynamics in qNSCs
124 and aNSCs. While most dynamic chromatin peaks in activated NSCs open with age, dynamic
125 chromatin peaks in quiescent NSCs largely closed with age (Fig. 1f, Extended Data Fig. 3i).
126 Likewise, the genome-wide chromatin landscape of old aNSCs contained more accessible
127 chromatin peaks and less nucleosomes than that of young aNSCs while the opposite was true for
128 qNSCs (Extended Data Fig. 3j,k). These data suggest that chromatin of quiescent NSCs becomes
129 more repressed with age while that of their activated counterparts become more permissive.
130
131 Cell adhesion and migration was a defining hallmark of genes with opposing chromatin
132 aging changes in both quiescent and activated NSCs. Indeed, Gene Ontology (GO) biological
133 pathway enrichment revealed that old qNSCs had decreased chromatin accessibility (open in
134 young) at regulatory regions of genes involved in promoting cell adhesion and inhibiting cell
135 migration ("response to forskolin", "cAMP-mediated signaling", "negative regulation of cell
136 migration" (Fig. 1g, Supplementary Table 3). We also noted a "Cell-cell adhesion (plasma
137 membrane)" signature enriched in genes with increased chromatin accessibility in old qNSCs
138 (Fig. 1g, see Extended Data Fig. 5e for gene expression). Conversely, old aNSCs had increased

139 chromatin accessibility (open in old) at regulatory regions of genes associated with increased cell
140 adhesion, especially genes involved in cell-cell interactions ("cell-cell adhesion (cadherins)",
141 "homophilic cell adhesion (plasma membrane)", "adherens junction organization") and some
142 cell-matrix interactions ("extracellular matrix assembly") (Fig. 1h, Supplementary Table 3).
143 Consistently, young qNSCs and old aNSCs were grouped together along the principal
144 component 2 (PC2) axis in PCA, based largely on cell adhesion pathways (Extended Data Fig.
145 4a, Supplementary Tables 4,5).
146
147 As for specific genes, old qNSCs freshly isolated from the brain showed reduced
148 chromatin accessibility at regulatory regions of genes involved in cell adhesion to the
149 extracellular matrix (e.g. *Itga3*, *Itgae, Itgb6*, *Itgb8*), in cell-cell adhesion (e.g. cadherins (*Cdh)*
150 and protocadherins (*Pcdh*)) (Fig. 1i), and negative regulation of cell migration (e.g. *Jag1, Nav3,*
151 *Ptpru*) (Fig. 1j). Conversely, old aNSCs exhibited increased chromatin accessibility at regulatory
152 regions of genes implicated in cell adhesion to the extracellular matrix (e.g. *Itgb1*, *Itgb6, Itga2,*
153 *Itga3*), in cell-cell adhesion (e.g. cadherins and *Pcdh18* (proto-cadherin 18)) (Fig. 1i), and
154 negative regulation of cell migration (e.g. *Jag1, Nav3, Ptpru*) (Fig. 1j, Supplementary Tables
155 2,3). A number of cell adhesion genes enriched in young qNSCs were shared with those enriched
156 in old aNSCs (Extended Data Fig. 4b). Thus, chromatin accessibility dynamics suggest that
157 quiescent and activated NSCs exhibit opposing changes at cell migration and adhesion genes
158 with age.
159 Other cell types in the niche also showed changes in chromatin accessibility with age,
160 including at genes involved in adhesion pathways (Extended Data Fig. 4c-e, Supplementary
161 Table 3). For example, endothelial cells had increased chromatin accessibility at several cell

162 adhesion pathways with age (Extended Data Fig. 4d, Supplementary Table 3). Old neural
163 progenitor cells (NPCs) exhibited increased accessibility at adhesion pathways with age
164 (Extended Data Fig. 4e). Interestingly, a number of cell adhesion genes that showed age-related
165 chromatin changes in old aNSCs and old NPCs were shared, suggesting that some of these
166 changes may be preserved in downstream progeny (Extended Data Fig. 4f).
167
168 Collectively, these results indicate that aging has opposing effects on the global
169 chromatin landscape of quiescent and activated NSCs (and NPC progeny), including opposing
170 changes to chromatin accessibility in regulatory regions involved in cell adhesion and migration.
171
172 **Opposing chromatin changes in quiescent and activated NSCs during aging are associated**
173 **with gene expression changes and functional defects in cell adhesion and migration**
174
175 We next asked if the opposing changes to chromatin in quiescent and activated NSCs
176 during aging are associated with expression changes in cell adhesion and migration genes and
177 manifest in individual cells. Analysis of available single cell RNA-seq datasets from neurogenic
178 niches of young and old mice[24,43] revealed that old quiescent and activated NSCs showed
179 opposing expression changes in gene signatures involved in cell adhesion, negative regulation of
180 migration, cell-cell adhesion, and cell-matrix adhesion (Fig. 2a,b, Extended Data Fig. 5),
181 consistent with predictions from chromatin changes (with the exception of "cell-cell adhesion
182 (plasma membrane)" which showed increased chromatin accessibility in old qNSCs but
183 decreased gene expression in old qNSCs (Fig. 1g, Extended Data Fig. 5e)). Some of these gene
184 signature changes were also preserved in neuroblasts, suggesting that they can persist in

185 downstream progeny (Extended Data Fig. 5h, j). Specifically, old qNSCs/astrocytes showed
186 downregulation of genes involved in cell adhesion, including adhesion to the extracellular matrix
187 (ECM) (e.g. *Itgb8*) or to cells (e.g. *Alcam, Ctnnd2*) (Fig. 2c, Extended data Fig. 5k). Conversely,
188 old aNSCs/NPCs showed upregulation of genes involved in cell-cell adhesion (e.g. *Alcam,*
189 *Lsamp, Ntm*) (Fig. 2c, Extended data Fig. 5l), consistent with chromatin accessibility changes at
190 these genetic loci (Fig. 2d). Thus, changes in gene expression of cell adhesion and migration
191 pathways by single cell RNA-seq (which is not dependent on gating with FACS markers for cell
192 type classification) corroborate opposing changes in chromatin states in quiescent and activated
193 NSCs. We also noted a few genes for which there was not a one-to-one correlation between
194 chromatin and expression (e.g. *Cadm2, Itgb1, Src* for quiescent NSCs and *Ccdc80, Epdr1,*
195 *Flbn1, Megf10* for activated NSCs). In these cases, age-dependent chromatin changes may be
196 poising these loci to regulate future gene expression in downstream progeny (e.g. neuroblasts).
197
198 We used single cell RNA-seq data to examine whether changes in migration and
199 adhesion genes occurred at the level of individual cells or were due to changes in NSC
200 subpopulations. For most cell migration and adhesion pathways, single cell gene expression data
201 were not bimodal (Fig. 2a,b, Extended Data Fig. 5), suggesting that changes occur in individual
202 cells. In addition, while cell cycle analysis of single cell RNA-seq data indicated a small shift
203 toward a subpopulation of more "quiescent-like" cells in old activated NSCs/NPCs (Extended
204 Data Fig. 6a,b), not all age-dependent adhesion changes occurred in this subpopulation
205 (Extended Data Fig. 6c). Thus, while subpopulation shifts in old NSCs may contribute to some
206 of the observed changes in adhesion gene expression, age-dependent changes also occur in
207 individual cells (see also below, immunostaining).

208

209 To experimentally test the prediction that adhesion and migration properties of NSCs
210 change during aging, we used a culture system for quiescent NSCs and proliferative NSCs (a mix
211 of aNSCs/NPCs)[31,36,44-46] (Fig. 2e). In this culture system, cells are directly isolated from the
212 SVZ neurogenic niches of young and old mice, and cell identity is maintained in culture with
213 specific growth factors (Fig. 2e, see Methods). We verified that the chromatin landscape of
214 cultured NSCs was similar to that of freshly isolated NSCs (Extended Data Fig. 7a-d,
215 Supplementary Tables 2,3,4), notably in age-related changes to cell adhesion and migration
216 pathways (Fig. 2f,g, Supplementary Table 3).

217

218 To examine specific adhesion proteins or pathways identified by changes in chromatin
219 and gene expression, we performed immunostaining on young and old primary cultures of
220 qNSCs and aNSCs/NPCs (Fig. 2e, Extended Data Fig. 7e). We first stained for ALCAM – a
221 transmembrane glycoprotein directly involved in cell-cell adhesion[47,48] and indirectly implicated
222 in cell-matrix adhesion[49] – and whose gene exhibits opposing chromatin and gene expression
223 changes in quiescent and activated NSCs with age (see Fig. 2c,d). Consistently, ALCAM
224 immunostaining quantification revealed that while old qNSCs exhibited a modest (non-
225 significant) decrease in ALCAM protein levels (Fig. 2h,i, Extended Data Fig. 7f), old
226 aNSCs/NPCs showed a significant increase in ALCAM protein levels compared to their young
227 counterparts (Fig. 2h,j, Extended Data Fig. 7g). We also stained for paxillin (PXN) – a marker of
228 focal adhesions and cell-matrix adhesion[50,51] – given that integrin (*Itg*) genes, which regulate
229 focal adhesions, exhibit opposing age-dependent chromatin changes in quiescent and activated
230 NSCs with age and some of them also show gene expression changes (see Fig. 1i, Fig. 2c,d).

231 Paxillin immunostaining quantification revealed that consistently, old qNSCs had fewer focal
232 adhesions than their young counterparts, whereas old aNSCs/NPCs had more focal adhesions
233 compared to young counterparts (Fig. 2k-m, Extended Data Fig. 7h,i). These opposing changes
234 in PXN staining were also observed within the subpopulation of cells containing at least one
235 focal adhesion (Extended Data Fig. 7j,k), suggesting that aging induces changes at the individual
236 cell level (though there are also subpopulation changes). These immunostaining data corroborate
237 the opposing changes in adhesion in quiescent and activated NSCs with age predicted by
238 chromatin and transcriptional data and indicate that at least some of the age-related changes in
239 adhesion molecules occur at the level of individual cells.
240
241 We next functionally assessed if aging impacts cell adhesion in quiescent and activated
242 NSCs. To probe age-related changes to cell adhesion, we adapted a detachment assay used in
243 other cell types[52,53] for NSCs. In this assay, cultured NSCs are plated as a monolayer and imaged
244 before and after enzymatic dissociation (see Methods). Old qNSCs became less adhesive (i.e.
245 detached more easily) than their young counterparts, whereas old aNSCs/NPCs became more
246 adhesive (i.e. detached less easily) (Fig. 2n-p). Using this detachment assay, we next tested the
247 functional importance of a member of the NFI family of transcription factors, which regulates
248 cell adhesion[31] and is enriched in the accessible chromatin landscape of old aNSCs (Extended
249 Data Fig. 8a,b). Interestingly, CRISPR/Cas9 knock-out of the NFIC transcription factor family
250 member blunted the difference in cell adhesion between young and old aNSCs, with
251 aNSCs/NPCs knocked out for NFIC no longer exhibiting increased adhesion with age (Extended
252 Data Fig. 8c-g). These observations support predictions about age-related adhesion changes in

253 NSCs and are consistent with the possibility that changes in NFIC regulation during aging are
254 among the factors that contribute to the adhesive phenotype of old aNSCs.
255
256 To assess the migratory properties of NSCs, we performed continuous live-cell imaging
257 of cultured NSCs over the course of 20 hours (Fig. 2q). Whereas old qNSCs were slightly more
258 migratory than their young counterparts (non-significant) (Fig. 2r, Extended Data Fig. 7l), old
259 aNSCs/NPCs were significantly less migratory than their young counterparts (Fig. 2s, Extended
260 Data Fig. 7m). We also quantified the dispersion of cultured aNSCs/NPCs through Matrigel, an
261 assay that integrates migration as well as other factors (e.g. proliferation). In this assay,
262 aNSCs/NPCs cultured from old brains also exhibited impaired ability to disperse through
263 extracellular matrix compared to their young counterparts (Fig. 2t,u). These dispersion
264 differences are likely due to defects in migration (rather than proliferation) because they already
265 manifest at early time points (12 hours, before NSCs would have time to significantly expand)
266 and we did not detect significant proliferation differences in cultured young and old
267 aNSCs/NPCs (Extended Data Fig. 7n). Collectively, these results indicate that aNSCs/NPCs
268 become more adhesive and less migratory during aging.
269
270 Hence, aging has opposing effects on the adhesive and migratory properties of quiescent
271 and activated NSCs in culture, with qNSCs becoming less adhesive/more migratory and
272 aNSCs/NPCs becoming more adhesive/less migratory in old age.
273
274 **Age-dependent location defects of quiescent and activated NSCs and progeny *in vivo* in the**
275 **niche, the rostral migratory stream, and the olfactory bulb**

276

277 In the subventricular zone neurogenic niche, quiescent NSCs line the ventricles and can
278 become activated (aNSCs) to give rise to neural progenitors (NPCs) and neuroblasts[1-4].
279 Neuroblasts then migrate long distances along the rostral migratory stream (RMS) to the
280 olfactory bulb (OB) to give rise to new neurons (neurogenesis)[3,14,54]. While NSC/NPC and
281 neuroblast migration has begun to be examined in older animals[55-59], the adhesive and migratory
282 properties of quiescent and activated NSCs (and their progenitors) has not been systematically
283 studied *in vivo* during aging.

284

285 Location within the subventricular zone niche is important for NSC function[60,61], and
286 adhesion and migration defects in quiescent and activated NSCs during aging could manifest as
287 changes to their niche location. We therefore assessed the location of quiescent and activated
288 NSCs with respect to the ventricle in the SVZ neurogenic niches during aging. To this end, we
289 performed immunostaining of brain sections – either serial coronal sections or sagittal sections
290 that contain the rostral migratory stream – from young and old individuals. To identify specific
291 NSC populations, we used GFAP (which marks NSCs and astrocytes), S100a6 (which marks
292 NSCs in the adult SVZ neurogenic niche[62]), Ki67 (which marks proliferating cells), and in some
293 cases DCX (which marks neuroblasts).

294

295 To determine the location of quiescent and activated NSCs within the SVZ neurogenic
296 niche (and to avoid including striatal astrocytes), we quantified cells that line the ventricle within
297 200 µm of the ventricle border (the vast majority of cells were located within 50µm of the
298 ventricle border) (Fig. 3a,b). For coronal sections, the ventricle border was demarcated by

299 vinculin staining (for GFAP staining, Extended Data Fig. 9a) or ARL13b staining (for S100a6
300 staining, see Methods). We found that in coronal sections from old brains, GFAP+/Ki67- cells
301 (which include qNSCs and niche astrocytes) and S100a6+/Ki67- cells (which include mostly
302 qNSCs) were located farther away from the ventricle than in young counterparts, consistent with
303 the possibility that quiescent NSCs (and perhaps some astrocytes) move away from their location
304 with age (Fig. 3c,d, Extended Data Fig. 9b-d). In contrast, GFAP+/Ki67+ (which include aNSCs
305 and proliferative niche astrocytes) and S100a6+/Ki67+ (which include mostly aNSCs) were
306 located closer to the ventricle than in young brains (Fig. 3c,d, Extended Data Fig. 9b-d),
307 consistent with the possibility that activated NSCs may not move as far with age. Although
308 GFAP+/Ki67+ or S100a6+/Ki67 cells could also include repairing SVZ astrocytes that
309 intercalate in the ependymal layer in old mice[19,63] or reactive astrocytes[64-68], we observed only 4
310 ependymal-repairing SVZ astrocytes and no reactive astrocytes in our single cell RNA-seq
311 dataset of 21,458 cells in both young and old animals[43] (Extended Data Fig. 9e, markers[19,63,69,70],
312 Supplementary Table 8, similar results with our other single cell RNA-seq dataset[24]). These data
313 suggest that aging disrupts the location of quiescent and activated NSCs in the SVZ neurogenic
314 niche (though we cannot exclude that some repairing or reactive astrocytes may also contribute).
315

316 We also determined the location of quiescent and activated NSCs (and progeny) in
317 sagittal sections. We quantified distance to the ventricle for GFAP+/Ki67- (qNSCs/astrocytes),
318 GFAP+/Ki67+ (aNSCs), DCX-/Ki67+ (aNSCs/NPCs), and DCX+/Ki67+ or DCX+/Ki67-
319 (neuroblasts) from sagittal sections that contained the rostral migratory stream as an anatomical
320 landmark (Fig. 3b,e). Consistent with results from coronal sections, we also observed opposing
321 changes in location of qNSCs/astrocytes and aNSCs/NPCs with age in sagittal sections (Fig.

322 3f,d,g, Extended Data Fig. 9d,f). Similar to aNSCs/NPCs, neuroblasts were also located closer to
323 the ventricles in old brain sections (Fig. 3h, Extended Data Fig. 9g). While location changes in
324 the neurogenic niche could be due to factors other than adhesion/migration, the opposing
325 location changes of qNSCs and aNSCs/NPCs (and neuroblasts) are consistent with *in vitro*
326 results. This opposing directionality also suggests that location changes are unlikely to solely be
327 due to the age-dependent thinning of the ventricle (or repairing or reactive astrocytes)[17,19,63,67].
328
329 To follow NSCs along their migratory path *in vivo*, we quantified the location of newborn
330 NSCs and their progeny (NPCs, neuroblasts) in the SVZ niche, along the rostral migratory
331 stream (RMS), and in the olfactory bulb (OB) during aging. To this end, we injected young and
332 old mice with the thymidine analog 5-Ethynyl-2'-deoxyuridine (EdU), which incorporates into
333 the DNA of replicating cells, to label and trace activated NSCs and their progeny (Fig. 3e). We
334 verified that EdU labeling efficiency was similar in young and old individuals (Extended Data
335 Fig. 9h,i). We then assessed the number of EdU-positive (EdU+) cells in the SVZ neurogenic
336 niche, the migration route (RMS), and distal destination (OB), at a short (4 hours), mid- (2 days),
337 or longer (7 days) time point after EdU injection (Fig. 3e,i-p, Extended Data Fig. 9j). In young
338 individuals, EdU+ cells were numerous in the niche and along the RMS 4 hours after EdU
339 injection (Fig. 3k, l, Extended Data Fig. 9j). After 7 days, young animals showed a dramatic
340 reduction of EdU+ cells in the SVZ neurogenic niche and RMS, and a corresponding increase in
341 EdU+ cells in the OB, consistent with mobilization of labelled cells out of the neurogenic niche
342 and clearance from the RMS towards the OB (Fig. 3j-m, Extended Data Fig. 9j). In old
343 individuals, EdU+ cells were less numerous overall, as expected[19-21,71] (Fig. 3n-p, Extended Data
344 Fig. 9h). Interestingly, after 7 days, old animals showed no reduction of EdU+ cells in the SVZ

345 neurogenic niche and no corresponding increase in EdU+ cells in the OB (Fig. 3n,j,p), consistent
346 with reduced mobilization of NSCs (and progeny) out of the niche. There was some clearance of
347 EdU+ cells through the old RMS after 7 days in old animals (Fig. 3o), suggesting that old
348 neuroblasts retain motility in the RMS[55] but migrate more slowly than young neuroblasts. While
349 this experimental design integrates cell migration as well as other factors (e.g. EdU dilution,
350 differences in cell cycle, survival, etc.), these results suggest that aging decreases the
351 mobilization of aNSCs and progeny (NPCs, neuroblasts) out of the neurogenic niche and
352 diminishes the migratory ability of neuroblasts to reach their distal destination *in vivo*.
353
354 **Molecular tension sensors reveal an increase in the occurrence of force-producing**
355 **adhesions in old aNSCs/NPCs which can be eliminated by ROCK inhibition**
356
357 We next used molecular tension sensors to assess the cellular properties underlying the
358 increased adhesion observed in aNSCs and progenitors during aging, focusing on cell-matrix
359 adhesion. To directly visualize the mechanical forces exerted by aNSCs/NPCs interacting with
360 their ECM substrate, we leveraged Förster resonance energy transfer (FRET)-based molecular
361 tension sensors (Fig. 4a)[72,73]. Molecular tension sensors can reveal cellular forces on surfaces
362 coated with synthetic arginine-glycine-aspartate (RGD) peptides known to bind integrins and
363 mediate adhesion[73] at single molecule resolution, with higher forces corresponding to a reduction
364 in FRET efficiency (Fig. 4a,b). We verified that cells in this assay were generally healthy and did
365 not express DCX, a marker of differentiation into neuroblasts and immature neurons (Extended
366 Data Fig. 10a,b).
367

368 FRET measurements revealed that aNSCs/NPCs primarily exert force through discrete
369 adhesion complexes at their periphery (Fig. 4b), consistent with PXN staining for focal
370 adhesions (see Fig. 2k). To investigate how aging affects NSC adhesion, we quantified the
371 adhesive force patterns for young and old cultured aNSCs/NPCs. Old aNSCs/NPCs exhibit
372 higher average adhesion force (P=0.032) (Fig. 4e, Extended Data Fig. 10c), without changes in
373 cell size (Extended Data Fig. 10d), compared to young aNSCs/NPCs. Furthermore, old
374 aNSCs/NPCs were more likely to exhibit force-producing adhesions than young aNSCs/NPCs
375 (Fig. 4f) (P=0.006, combined Fisher's exact test). In the subset of cells that had force-producing
376 adhesions, old aNSCs/NPCs showed a trending (non-significant) increase in average adhesion
377 force (Extended Data Fig. 10f), consistent with increased immunostaining with paxillin (PXN), a
378 marker of focal adhesions (see Fig. 2m, Extended Data Fig. 7k). Together, these data indicate
379 that aging not only increases the proportion of aNSCs/NPCs that exhibit focal adhesions but also
380 increases the average adhesion strength of individual old aNSCs/NPCs. These cellular changes
381 with age could contribute to the adhesion/migration defects of old activated aNSCs (and
382 progeny) in the old brain.
383
384 We next sought to identify a molecular target to counter increased adhesion strength
385 observed in old aNSCs, as a way to restore age-related mobilization of old activated NSCs and
386 progeny out of the niche and subsequently improve neurogenesis in the old brain. Focal
387 adhesions are known to be regulated by several pathways, including via the Rho and Rho-
388 associated protein kinase (ROCK) pathway[6]. Indeed, Ingenuity Pathway Analysis (IPA)[74]
389 showed that the most enriched signaling pathway associated with the chromatin accessibility

390 changes in old aNSCs/NPCs was Gα 12/13 signaling (Fig. 4c, Supplementary Table 6), a
391 pathway that regulates cell adhesion in part via ROCK[6,75] (Fig. 4d).
392
393 To determine if the age-related increase in cell adhesion exhibited by old aNSCs could be
394 ameliorated via modulation of the ROCK pathway, we targeted ROCK with the small molecule
395 inhibitor Y-27632[7,59,76-82] in cultured aNSCs/NPCs. Quantification of force patterns at single-
396 molecule resolution using RGD molecular tension sensors revealed that treating old
397 aNSCs/NPCs with the ROCK inhibitor Y-27632 (ROCKi) eliminated force-producing adhesions
398 and decreased adhesion area (Fig. 4e,g, Extended Data Fig.10c,e) in both young and old
399 aNSCs/NPCs. ROCKi also decreased the proportion of cells with force-producing adhesions as
400 assessed by tension sensors (Fig. 4f) as well as focal adhesions (marked by PXN) in young and
401 old aNSCs/NPCs but had a greater effect on old aNSCs/NPCs (Fig. 4h-j, Extended Data Fig.
402 10i). In contrast, ROCKi did not affect the expression of ALCAM protein (Extended Data Fig.
403 10j), suggesting ROCKi acts downstream of some of the age-related adhesion gene expression
404 changes. Together, these results indicate that ROCK inhibition eliminates force-producing
405 adhesions and focal adhesions in aNSCs/NPCs.
406
407 **Inhibition of ROCK boosts migration speed in aNSCs/NPCs cultured from aged brains and**
408 **improves *in vivo* neurogenesis in old mice**
409
410 We asked if ROCK inhibition could improve the migration properties of old aNSCs *in*
411 *vitro*. In cultured aNSCs/NPCs, ROCKi treatment resulted in improved migration speed in both
412 young and old aNSCs/NPCs (Fig. 5a,b, Extended Data Fig. 10k, Supplementary Videos 1,2).

413 Furthermore, ROCKi rescued the age-related decline in old aNSC/NPC dispersion through
414 Matrigel but had no effect on young aNSC/NPC dispersion (Fig. 5c), consistent with the
415 observation that ROCKi had a more profound effect on decreasing focal adhesions in old
416 aNSCs/NPCs than in young counterparts (Fig. 4i,j). ROCKi induced cell morphological
417 changes[80] (Extended Data Fig. 10a) – consistent with its ability to improve cell migration – but it
418 did not overtly affect aNSC/NPC differentiation, proliferation, or survival under these culture
419 conditions (Extended Data Fig. 10b,l,m). Together, these results indicate that ROCK inhibition
420 boosts the migratory ability of aNSCs/NPCs cultured from old mice.
421
422 To determine how ROCKi treatment in the old neurogenic niche impacts the location of
423 cells in the niche and long-distance neurogenesis *in vivo*, we delivered ROCKi (or vehicle
424 control) via a mini-osmotic pump into the lateral ventricles of old mice, in close proximity to the
425 SVZ neurogenic niche (Fig. 5d). Seven days after ROCKi delivery, we injected old mice with
426 EdU and quantified EdU+ cells in the SVZ neurogenic niche, rostral migratory stream (RMS),
427 and olfactory bulb (OB), 4 hours or 7 days after EdU-injection (corresponding, respectively, to 7
428 and 14 days of ROCKi treatment) (Fig. 5d). We quantified both the location of aNSCs/NPCs in
429 the neurogenic niche in sagittal sections as well as the number of EdU+ cells in the niche and at
430 different locations along the neurogenic migration route (Fig. 5d), as we had previously done
431 (see Fig. 3). Interestingly, ROCKi delivery in the ventricles significantly increased aNSC/NPC
432 distance from the ventricle 14 days after treatment (7 days post-EdU injection) in old mice (Fig.
433 5e-g) – a feature associated with young neurogenic niches (see Fig. 3). These results suggest that
434 ROCK inhibition could restore at least in part the location of aNSCs/NPCs in the neurogenic
435 niche of old animals. While ROCKi did not affect the number of EdU+ cells in the SVZ

436 neurogenic niche or RMS (Fig. 5i,j), ROCKi delivery in the ventricles led to a significant
437 increase in EdU+ cells in the OB of old mice 7 days post-EdU injection (Fig. 5h,k). These EdU+
438 cells in the OB exhibited markers of neuroblasts and neurons (DCX, NeuN) (Fig. 5l).
439 Collectively, these results indicate that ROCK inhibition in the neurogenic niche restores the
440 age-related defects in location of old aNSCs/NPCs in the niche and boosts neurogenesis at a
441 distance in old brains.
442
443 Together with our observation that ROCK inhibition improves migration of old
444 aNSCs/NPCs in culture, these *in vivo* results are consistent with the possibility that defects in
445 adhesion and migration of activated NSCs (and progeny) during aging could underlie age-related
446 neurogenic decline (though other factors could also contribute). Thus, inhibition of the ROCK
447 pathway could be a strategy to improve the migratory property of old activated NSCs (and their
448 progeny) and to boost neurogenesis in old brains.
449
450 **Discussion**
451
452 Our study identifies genome-wide changes to the global chromatin landscape of five
453 freshly isolated cell types from the neurogenic niche of young and old animals. This analysis
454 uncovers previously uncharacterized opposing changes in chromatin dynamics in quiescent and
455 activated NSCs during aging *in vivo* – with some changes observed in activated NSCs preserved
456 in downstream progeny. Interestingly, many of these opposing chromatin changes in quiescent
457 and activated NSCs affect genes in adhesion and migration pathways and are accompanied by
458 corresponding expression changes in these genes. Functionally, quiescent and activated NSCs

459 exhibit opposing changes in adhesion and migration with age, with old quiescent NSCs
460 becoming less adherent (and more migratory) and activated NSCs – and downstream progenitors
461 – becoming more adherent (and less migratory) compared to young counterparts, and we further
462 identify some of the adhesion molecules involved in these age-dependent changes. By assessing
463 the force-producing ability of NSCs at the single molecule level using molecular tension sensors,
464 we observe increased force production in old activated NSCs – a phenotype that could explain at
465 least in part the migration defects of activated NSC with age. We also identify the ROCK
466 pathway as a potential target to revert the defects in adhesion and migration of old activated
467 NSCs. Indeed, a small molecule ROCK inhibitor could decrease force-production in old aNSCs
468 and restore part of their migration ability *in vitro*. *In vivo*, ROCK inhibitor injected in the
469 ventricles – in the vicinity of the neurogenic niche – reverses at least part of the age-dependent
470 changes in the location of NSCs (and progeny) within the niche and boosts neurogenesis in old
471 individuals. Our results have important implications for the role of NSC adhesion and migration
472 during aging and point to ROCK as a potential therapeutic target to restore age-dependent
473 defects that occur during NSC aging.
474
475 The chromatin landscape of quiescent NSCs becomes more closed with age whereas that
476 of activated NSCs becomes more open with age. The closing of chromatin regions with age in
477 quiescent NSCs is consistent with observations in cultured NSCs[33], hair follicle stem cells[83], and
478 with findings of increased repressive chromatin marks such as H3K27me3 in quiescent stem
479 cells from other niches[84], including muscle satellite cells[85,86] and hematopoietic stem cells[87]
480 during aging. In contrast, the chromatin landscape of activated NSCs generally becomes more
481 permissive with age, consistent with the observation that reducing the repressive 5-

482 hydroxymethylcytosine (5hmC) mark in hippocampal NPCs mimics age-dependent defects[28].
483 Interestingly, many of these age-related chromatin changes occur in regulatory regions of cell
484 adhesion and migration genes. The migratory properties of NSCs and neuroblasts has started to
485 be examined with age[55-59] and in the context of innervating distal tumors[88]. Recent live-cell
486 imaging of SVZ wholemounts showed that aNSC and NPC migration distance and speed
487 decreased with age[59]. However, the changes in migration and adhesion in quiescent NSCs during
488 aging have remained largely unknown. Adhesion molecules have been shown to play important
489 roles in both quiescent and activated stem cell function[31,60,61,89-92], and targeting some of the
490 adhesion pathways could be beneficial to counter age-dependent functional decline. Our study
491 reveals a dichotomy between changes to the adhesive and migratory properties of quiescent and
492 activated NSCs with age that could be a result of both intrinsic and extrinsic changes. While our
493 findings in cultured NSCs support the importance of intrinsic changes to cellular adhesion and
494 migration pathways with age, extrinsic changes likely also play a key role. Indeed, age-related
495 differences in the biomechanical properties of regenerative niches, such as stiffness, have been
496 shown to extrinsically induce age-related phenotypes[93]. It is also possible that the mechanical
497 memory of the *in vivo* niche could manifest in cell autonomous changes in cultured NSCs, as has
498 been observed with cultured mesenchymal stem cells[94,95] and epithelial cells[96] which retain
499 information from past physical environments. Given that mechanical cell deformations and niche
500 stiffness can affect chromatin states and promoter accessibility[83,97-99], epigenomic profiling might
501 be especially sensitive to identifying changes in the regulation of adhesion and migration in stem
502 cells and their progeny. Understanding the contribution of intrinsic and extrinsic responses, and
503 how they influence each other during aging, will be critical to identify strategies to boost
504 regeneration during aging.

505

506 Inhibiting Rho-associated kinase (ROCK) – a regulator of cytoskeletal dynamics[6] – with
507 the small molecule Y-27632 strikingly decreases force-producing adhesions in old activated
508 NSCs/NPCs and improves their motility *in vitro*. Inhibiting ROCK also restores some of the age-
509 dependent change in NSC/NPC location in the neurogenic niche and improves neurogenesis to
510 the olfactory bulb in old mice *in vivo*. ROCK inhibition is known to impact migration in a variety
511 of cells, including myoblasts, glioma cells, and microglia with different effects[100-107]. However,
512 the impact of ROCK inhibitor on aNSCs/NPCs and neurogenesis remains unclear and have not
513 been thoroughly tested during aging. Some studies indicate that ROCK inhibition causes
514 decreased migration speed in young NSCs[59], neuroblasts[108], and human embryonic NSCs[109]. On
515 the other hand, other studies show that ROCK inhibition increases NSC migration[80,110] and
516 hippocampal neurogenesis[76] in young animals. The effects of ROCK inhibition on NSC
517 migration may depend on context and age. In the future, leveraging lineage tracing approaches to
518 label and track stem cells as a function of space and time, coupled with *in vivo* imaging of the
519 niche[111], will be critical to better understand the specific effect of ROCK inhibition on
520 neurogenesis. While ROCK has pleiotropic roles in aspects other than migration (e.g. autophagy,
521 apoptosis, vesicle dynamics, etc.), this protein kinase may be a promising target in the aging
522 brain to restore aspects of migration notably in cases of injury and neurodegenerative disease[112].
523 ROCK inhibitors are well tolerated in humans and have begun to be studied in the context
524 neurodegenerative disease[112] and stroke[113,114], and could potentially be used to ameliorate other
525 age-dependent defects in the aging brain.

526

527

528 **Acknowledgements**

529 We thank D. Wagh from the Stanford Functional Genomics Facility for Illumina NextSeq
530 sequencing; the Stanford Shared FACS Facility for FACS use and support; K. Tsui and M.
531 Bassik for assistance and use of the Incucyte Live Cell Imaging system; M. T. Buckley, G. A.
532 Reeves, X. Zhao, P. P. Singh, C.-K. Hu, and K. Papsdorf for their feedback and reading of the
533 manuscript; M. T. Buckley, G. A. Reeves, P. P. Singh, and A. McKay for independently
534 checking scripts used in this study; J. Butterfield for help with mouse husbandry and genotyping;
535 and M. Bassik, J. Sage, and T. Wyss-Coray for guidance. This work was supported by
536 P01AG036695 (A.B.), R35GM130332 (A.R.D.), the Stanford Genome Training Program
537 (R.W.Y.), a Stanford Graduate Fellowship (R.W.Y.), a Genentech Foundation Pre-doctoral
538 Fellowship (R.W.Y.), and Stanford Medical Scientist Training Program grant T32GM007365
539 (O.Y.Z.). Figure schematics created using biorender.com.

540

541 **Authors contributions**

542 R.W.Y., O.Y.Z., and A.B. planned the study. R.W.Y. performed experiments for ATAC-seq, *in*
543 *vitro* migration assays, and EdU migration assays, and bioinformatically analyzed ATAC-seq
544 and single cell-RNA seq data. O.Y.Z. performed and analyzed experiments for *in vitro*
545 detachment assay, CRISPR-Cas9 perturbations, all immunofluorescent staining, and EdU
546 migration assays. B.L.Z. performed the RGD tension sensor experiments and analyzed the FRET
547 data supervised by A.R.D.. E.D.S. helped with single cell RNA-seq analyses. P.N.N. performed
548 the mini-osmotic pump implantations for *in vivo* ROCK inhibition and helped with single cell
549 RNA-seq. S.N. and M.S. generated the NSC deep learning model and performed motif
550 enrichment supervised by A.K.. T.R. assisted in the *in vivo* NSC migration study. M.W. helped

551 O.Y.Z. with staining experiments and quantification. A.K. and A.R.D. also provided intellectual
552 contribution. R.W.Y., O.Y.Z. and A.B. wrote the manuscript, and all authors provided
553 comments.
554
555 **Competing Interests**
556 The authors declare no competing interests.
557
558 **Data availability**
559 All raw sequencing reads and processed bam files for ATAC-seq libraries can be found under
560 BioProject PRJNA715736.
561
562 **Code availability**
563 The code used to analyze genomic data in the current study is available in the Github repository
564 for this paper (https://github.com/sunericd/Yeo_RW_NSC_ATACseq/). Code used to process
565 ATAC-seq data is available at https://github.com/kundajelab/atac_dnase_pipelines. Code used
566 for deep learning model training for transcription factor binding site identification is available at
567 https://github.com/kundajelab/retina-models.
568
569 **References**

570 1. Bond, A.M., Ming, G.L. & Song, H. Adult Mammalian Neural Stem Cells and
571 Neurogenesis: Five Decades Later. *Cell Stem Cell* **17**, 385-95 (2015).
572 2. Navarro Negredo, P., Yeo, R.W. & Brunet, A. Aging and Rejuvenation of Neural Stem
573 Cells and Their Niches. *Cell Stem Cell* **27**, 202-223 (2020).
574 3. Gage, F.H. & Temple, S. Neural stem cells: generating and regenerating the brain.
575 *Neuron* **80**, 588-601 (2013).

576 4. Silva-Vargas, V., Crouch, E.E. & Doetsch, F. Adult neural stem cells and their niche: a
577 dynamic duo during homeostasis, regeneration, and aging. *Curr Opin Neurobiol* **23**, 935-
578 42 (2013).
579 5. Denoth-Lippuner, A. & Jessberger, S. Formation and integration of new neurons in the
580 adult hippocampus. *Nat Rev Neurosci* **22**, 223-236 (2021).
581 6. Amano, M., Nakayama, M. & Kaibuchi, K. Rho-kinase/ROCK: A key regulator of the
582 cytoskeleton and cell polarity. *Cytoskeleton (Hoboken)* **67**, 545-54 (2010).
583 7. Ishizaki, T. *et al.* Pharmacological properties of Y-27632, a specific inhibitor of rho-
584 associated kinases. *Mol Pharmacol* **57**, 976-83 (2000).
585 8. Hattiangady, B., Rao, M.S. & Shetty, A.K. Plasticity of hippocampal stem/progenitor
586 cells to enhance neurogenesis in response to kainate-induced injury is lost by middle age.
587 *Aging Cell* **7**, 207-24 (2008).
588 9. Conover, J.C. & Shook, B.A. Aging of the subventricular zone neural stem cell niche.
589 *Aging Dis* **2**, 49-63 (2011).
590 10. Nicaise, A.M., Willis, C.M., Crocker, S.J. & Pluchino, S. Stem Cells of the Aging Brain.
591 *Front Aging Neurosci* **12**, 247 (2020).
592 11. Mirzadeh, Z., Merkle, F.T., Soriano-Navarro, M., Garcia-Verdugo, J.M. & Alvarez-
593 Buylla, A. Neural stem cells confer unique pinwheel architecture to the ventricular
594 surface in neurogenic regions of the adult brain. *Cell Stem Cell* **3**, 265-78 (2008).
595 12. Shen, Q. *et al.* Adult SVZ stem cells lie in a vascular niche: a quantitative analysis of
596 niche cell-cell interactions. *Cell Stem Cell* **3**, 289-300 (2008).
597 13. Tavazoie, M. *et al.* A specialized vascular niche for adult neural stem cells. *Cell Stem*
598 *Cell* **3**, 279-88 (2008).
599 14. Doetsch, F., Garcia-Verdugo, J.M. & Alvarez-Buylla, A. Cellular composition and three-
600 dimensional organization of the subventricular germinal zone in the adult mammalian
601 brain. *J Neurosci* **17**, 5046-61 (1997).
602 15. Kernie, S.G. & Parent, J.M. Forebrain neurogenesis after focal Ischemic and traumatic
603 brain injury. *Neurobiol Dis* **37**, 267-74 (2010).
604 16. Faiz, M. *et al.* Adult Neural Stem Cells from the Subventricular Zone Give Rise to
605 Reactive Astrocytes in the Cortex after Stroke. *Cell Stem Cell* **17**, 624-34 (2015).
606 17. Capilla-Gonzalez, V., Cebrian-Silla, A., Guerrero-Cazares, H., Garcia-Verdugo, J.M. &
607 Quinones-Hinojosa, A. Age-related changes in astrocytic and ependymal cells of the
608 subventricular zone. *Glia* **62**, 790-803 (2014).
609 18. Enwere, E. *et al.* Aging results in reduced epidermal growth factor receptor signaling,
610 diminished olfactory neurogenesis, and deficits in fine olfactory discrimination. *J*
611 *Neurosci* **24**, 8354-65 (2004).
612 19. Luo, J., Daniels, S.B., Lennington, J.B., Notti, R.Q. & Conover, J.C. The aging
613 neurogenic subventricular zone. *Aging Cell* **5**, 139-52 (2006).
614 20. Tropepe, V., Craig, C.G., Morshead, C.M. & van der Kooy, D. Transforming growth
615 factor-alpha null and senescent mice show decreased neural progenitor cell proliferation
616 in the forebrain subependyma. *J Neurosci* **17**, 7850-9 (1997).
617 21. Molofsky, A.V. *et al.* Increasing p16INK4a expression decreases forebrain progenitors
618 and neurogenesis during ageing. *Nature* **443**, 448-52 (2006).
619 22. Shi, Z. *et al.* Single-cell transcriptomics reveals gene signatures and alterations associated
620 with aging in distinct neural stem/progenitor cell subpopulations. *Protein Cell* **9**, 351-364
621 (2018).

622 23. Artegiani, B. *et al.* A Single-Cell RNA Sequencing Study Reveals Cellular and
623 Molecular Dynamics of the Hippocampal Neurogenic Niche. *Cell Rep* **21**, 3271-3284
624 (2017).
625 24. Dulken, B.W. *et al.* Single-cell analysis reveals T cell infiltration in old neurogenic
626 niches. *Nature* **571**, 205-210 (2019).
627 25. Kalamakis, G. *et al.* Quiescence Modulates Stem Cell Maintenance and Regenerative
628 Capacity in the Aging Brain. *Cell* **176**, 1407-1419 e14 (2019).
629 26. Klemm, S.L., Shipony, Z. & Greenleaf, W.J. Chromatin accessibility and the regulatory
630 epigenome. *Nat Rev Genet* **20**, 207-220 (2019).
631 27. Kane, A.E. & Sinclair, D.A. Epigenetic changes during aging and their reprogramming
632 potential. *Crit Rev Biochem Mol Biol* **54**, 61-83 (2019).
633 28. Gontier, G. *et al.* Tet2 Rescues Age-Related Regenerative Decline and Enhances
634 Cognitive Function in the Adult Mouse Brain. *Cell Rep* **22**, 1974-1981 (2018).
635 29. Benayoun, B.A. *et al.* Remodeling of epigenome and transcriptome landscapes with
636 aging in mice reveals widespread induction of inflammatory responses. *Genome Res* **29**,
637 697-709 (2019).
638 30. Berg, D.A. *et al.* A Common Embryonic Origin of Stem Cells Drives Developmental and
639 Adult Neurogenesis. *Cell* **177**, 654-668 e15 (2019).
640 31. Martynoga, B. *et al.* Epigenomic enhancer annotation reveals a key role for NFIX in
641 neural stem cell quiescence. *Genes Dev* **27**, 1769-86 (2013).
642 32. Lupo, G. *et al.* Molecular profiling of aged neural progenitors identifies Dbx2 as a
643 candidate regulator of age-associated neurogenic decline. *Aging Cell* **17**, e12745 (2018).
644 33. Maybury-Lewis, S.Y. *et al.* Changing and stable chromatin accessibility supports
645 transcriptional overhaul during neural stem cell activation and is altered with age. *Aging*
646 *Cell* **20**, e13499 (2021).
647 34. Zhuo, L. *et al.* Live astrocytes visualized by green fluorescent protein in transgenic mice.
648 *Dev Biol* **187**, 36-42 (1997).
649 35. Codega, P. *et al.* Prospective identification and purification of quiescent adult neural stem
650 cells from their in vivo niche. *Neuron* **82**, 545-59 (2014).
651 36. Leeman, D.S. *et al.* Lysosome activation clears aggregates and enhances quiescent neural
652 stem cell activation during aging. *Science* **359**, 1277-1283 (2018).
653 37. Buenrostro, J.D., Giresi, P.G., Zaba, L.C., Chang, H.Y. & Greenleaf, W.J. Transposition
654 of native chromatin for fast and sensitive epigenomic profiling of open chromatin, DNA-
655 binding proteins and nucleosome position. *Nat Methods* **10**, 1213-8 (2013).
656 38. Ucar, D. *et al.* The chromatin accessibility signature of human immune aging stems from
657 CD8(+) T cells. *J Exp Med* **214**, 3123-3144 (2017).
658 39. Shcherbina, A. *et al.* Dissecting Murine Muscle Stem Cell Aging through Regeneration
659 Using Integrative Genomic Analysis. *Cell Rep* **32**, 107964 (2020).
660 40. Koohy, H. *et al.* Genome organization and chromatin analysis identify transcriptional
661 downregulation of insulin-like growth factor signaling as a hallmark of aging in
662 developing B cells. *Genome Biol* **19**, 126 (2018).
663 41. Ge, Y. *et al.* The aging skin microenvironment dictates stem cell behavior. *Proc Natl*
664 *Acad Sci U S A* **117**, 5339-5350 (2020).
665 42. Guillemot, F. & Hassan, B.A. Beyond proneural: emerging functions and regulations of
666 proneural proteins. *Curr Opin Neurobiol* **42**, 93-101 (2017).

667 43. Buckley, M.T. *et al.* Cell type-specific aging clocks to quantify aging and rejuvenation in
668 regenerative regions of the brain. *bioRxiv* (2022).
669 44. Mira, H. *et al.* Signaling through BMPR-IA regulates quiescence and long-term activity
670 of neural stem cells in the adult hippocampus. *Cell Stem Cell* **7**, 78-89 (2010).
671 45. Jones, K.M. *et al.* CHD7 maintains neural stem cell quiescence and prevents premature
672 stem cell depletion in the adult hippocampus. *Stem Cells* **33**, 196-210 (2015).
673 46. Knobloch, M. *et al.* A Fatty Acid Oxidation-Dependent Metabolic Shift Regulates Adult
674 Neural Stem Cell Activity. *Cell Rep* **20**, 2144-2155 (2017).
675 47. Swart, G.W. Activated leukocyte cell adhesion molecule (CD166/ALCAM):
676 developmental and mechanistic aspects of cell clustering and cell migration. *Eur J Cell*
677 *Biol* **81**, 313-21 (2002).
678 48. Masedunskas, A. *et al.* Activated leukocyte cell adhesion molecule is a component of the
679 endothelial junction involved in transendothelial monocyte migration. *FEBS Lett* **580**,
680 2637-45 (2006).
681 49. Lunter, P.C. *et al.* Activated leukocyte cell adhesion molecule
682 (ALCAM/CD166/MEMD), a novel actor in invasive growth, controls matrix
683 metalloproteinase activity. *Cancer Research* **65**, 8801-8 (2005).
684 50. Schaller, M.D. Paxillin: a focal adhesion-associated adaptor protein. *Oncogene* **20**, 6459-
685 72 (2001).
686 51. Hu, Y.L. *et al.* FAK and paxillin dynamics at focal adhesions in the protrusions of
687 migrating cells. *Scientific Reports* **4**, 6024 (2014).
688 52. Brown, M.A. *et al.* The use of mild trypsinization conditions in the detachment of
689 endothelial cells to promote subsequent endothelialization on synthetic surfaces.
690 *Biomaterials* **28**, 3928-35 (2007).
691 53. Loffek, S. *et al.* Transmembrane collagen XVII modulates integrin dependent
692 keratinocyte migration via PI3K/Rac1 signaling. *PLoS One* **9**, e87263 (2014).
693 54. Mizrahi, A., Lu, J., Irving, R., Feng, G. & Katz, L.C. In vivo imaging of juxtaglomerular
694 neuron turnover in the mouse olfactory bulb. *Proc Natl Acad Sci U S A* **103**, 1912-7
695 (2006).
696 55. Mobley, A.S. *et al.* Age-dependent regional changes in the rostral migratory stream.
697 *Neurobiol Aging* **34**, 1873-81 (2013).
698 56. Shuboni-Mulligan, D.D. *et al.* In vivo serial MRI of age-dependent neural progenitor cell
699 migration in the rat brain. *Neuroimage* **199**, 153-159 (2019).
700 57. Capilla-Gonzalez, V., Cebrian-Silla, A., Guerrero-Cazares, H., Garcia-Verdugo, J.M. &
701 Quinones-Hinojosa, A. The generation of oligodendroglial cells is preserved in the rostral
702 migratory stream during aging. *Front Cell Neurosci* **7**, 147 (2013).
703 58. Fritze, J. *et al.* Loss of Cxcr5 alters neuroblast proliferation and migration in the aged
704 brain. *Stem Cells* **38**, 1175-1187 (2020).
705 59. Zhao, X. *et al.* 4D imaging analysis of the aging mouse neural stem cell niche reveals a
706 dramatic loss of progenitor cell dynamism regulated by the RHO-ROCK pathway. *Stem*
707 *Cell Reports* **17**, 245-258 (2022).
708 60. Morante-Redolat, J.M. & Porlan, E. Neural Stem Cell Regulation by Adhesion Molecules
709 Within the Subependymal Niche. *Front Cell Dev Biol* **7**, 102 (2019).
710 61. Kazanis, I. *et al.* Quiescence and activation of stem and precursor cell populations in the
711 subependymal zone of the mammalian brain are associated with distinct cellular and
712 extracellular matrix signals. *J Neurosci* **30**, 9771-81 (2010).

713 62. Kjell, J. *et al.* Defining the Adult Neural Stem Cell Niche Proteome Identifies Key
714 Regulators of Adult Neurogenesis. *Cell Stem Cell* **26**, 277-293 e8 (2020).
715 63. Luo, J., Shook, B.A., Daniels, S.B. & Conover, J.C. Subventricular zone-mediated
716 ependyma repair in the adult mammalian brain. *J Neurosci* **28**, 3804-13 (2008).
717 64. Boom, A. *et al.* Astrocytic calcium/zinc binding protein S100A6 over expression in
718 Alzheimer's disease and in PS1/APP transgenic mice models. *Biochim Biophys Acta*
719 **1742**, 161-8 (2004).
720 65. Hoyaux, D. *et al.* S100A6 overexpression within astrocytes associated with impaired
721 axons from both ALS mouse model and human patients. *J Neuropathol Exp Neurol* **61**,
722 736-44 (2002).
723 66. Gotz, M., Sirko, S., Beckers, J. & Irmler, M. Reactive astrocytes as neural stem or
724 progenitor cells: In vivo lineage, In vitro potential, and Genome-wide expression
725 analysis. *Glia* **63**, 1452-68 (2015).
726 67. Liddelow, S.A. & Barres, B.A. Reactive Astrocytes: Production, Function, and
727 Therapeutic Potential. *Immunity* **46**, 957-967 (2017).
728 68. Buffo, A. *et al.* Origin and progeny of reactive gliosis: A source of multipotent cells in
729 the injured brain. *Proc Natl Acad Sci U S A* **105**, 3581-6 (2008).
730 69. Liddelow, S.A. *et al.* Neurotoxic reactive astrocytes are induced by activated microglia.
731 *Nature* **541**, 481-487 (2017).
732 70. Das, S., Li, Z., Noori, A., Hyman, B.T. & Serrano-Pozo, A. Meta-analysis of mouse
733 transcriptomic studies supports a context-dependent astrocyte reaction in acute CNS
734 injury versus neurodegeneration. *J Neuroinflammation* **17**, 227 (2020).
735 71. Ahlenius, H., Visan, V., Kokaia, M., Lindvall, O. & Kokaia, Z. Neural stem and
736 progenitor cells retain their potential for proliferation and differentiation into functional
737 neurons despite lower number in aged brain. *J Neurosci* **29**, 4408-19 (2009).
738 72. Morimatsu, M., Mekhdjian, A.H., Adhikari, A.S. & Dunn, A.R. Molecular tension
739 sensors report forces generated by single integrin molecules in living cells. *Nano Lett* **13**,
740 3985-9 (2013).
741 73. Chang, A.C. *et al.* Single Molecule Force Measurements in Living Cells Reveal a
742 Minimally Tensioned Integrin State. *ACS Nano* **10**, 10745-10752 (2016).
743 74. Kramer, A., Green, J., Pollard, J., Jr. & Tugendreich, S. Causal analysis approaches in
744 Ingenuity Pathway Analysis. *Bioinformatics* **30**, 523-30 (2014).
745 75. Suzuki, N., Hajicek, N. & Kozasa, T. Regulation and physiological functions of G12/13-
746 mediated signaling pathways. *Neurosignals* **17**, 55-70 (2009).
747 76. Christie, K.J., Turbic, A. & Turnley, A.M. Adult hippocampal neurogenesis, Rho kinase
748 inhibition and enhancement of neuronal survival. *Neuroscience* **247**, 75-83 (2013).
749 77. Emre, N. *et al.* The ROCK inhibitor Y-27632 improves recovery of human embryonic
750 stem cells after fluorescence-activated cell sorting with multiple cell surface markers.
751 *PLoS One* **5**, e12148 (2010).
752 78. Uehata, M. *et al.* Calcium sensitization of smooth muscle mediated by a Rho-associated
753 protein kinase in hypertension. *Nature* **389**, 990-4 (1997).
754 79. Kim, J.E., Ryu, H.J., Kim, M.J. & Kang, T.C. LIM kinase-2 induces programmed
755 necrotic neuronal death via dysfunction of DRP1-mediated mitochondrial fission. *Cell*
756 *Death Differ* **21**, 1036-49 (2014).

757 80. Leong, S.Y., Faux, C.H., Turbic, A., Dixon, K.J. & Turnley, A.M. The Rho kinase
758 pathway regulates mouse adult neural precursor cell migration. *Stem Cells* **29**, 332-43
759 (2011).
760 81. Peh, G.S. *et al.* The effects of Rho-associated kinase inhibitor Y-27632 on primary
761 human corneal endothelial cells propagated using a dual media approach. *Sci Rep* **5**, 9167
762 (2015).
763 82. Narumiya, S., Ishizaki, T. & Uehata, M. Use and properties of ROCK-specific inhibitor
764 Y-27632. *Methods Enzymol* **325**, 273-84 (2000).
765 83. Koester, J. *et al.* Niche stiffening compromises hair follicle stem cell potential during
766 ageing by reducing bivalent promoter accessibility. *Nat Cell Biol* **23**, 771-781 (2021).
767 84. Tumpel, S. & Rudolph, K.L. Quiescence: Good and Bad of Stem Cell Aging. *Trends Cell*
768 *Biol* **29**, 672-685 (2019).
769 85. Liu, L. *et al.* Chromatin modifications as determinants of muscle stem cell quiescence
770 and chronological aging. *Cell Rep* **4**, 189-204 (2013).
771 86. Schworer, S. *et al.* Epigenetic stress responses induce muscle stem-cell ageing by Hoxa9
772 developmental signals. *Nature* **540**, 428-432 (2016).
773 87. Sun, D. *et al.* Epigenomic profiling of young and aged HSCs reveals concerted changes
774 during aging that reinforce self-renewal. *Cell Stem Cell* **14**, 673-88 (2014).
775 88. Mauffrey, P. *et al.* Progenitors from the central nervous system drive neurogenesis in
776 cancer. *Nature* **569**, 672-678 (2019).
777 89. Nascimento, M.A., Sorokin, L. & Coelho-Sampaio, T. Fractone Bulbs Derive from
778 Ependymal Cells and Their Laminin Composition Influence the Stem Cell Niche in the
779 Subventricular Zone. *J Neurosci* **38**, 3880-3889 (2018).
780 90. Sato, Y. *et al.* Ventricular-subventricular zone fractones are speckled basement
781 membranes that function as a neural stem cell niche. *Mol Biol Cell* **30**, 56-68 (2019).
782 91. Porlan, E. *et al.* MT5-MMP regulates adult neural stem cell functional quiescence
783 through the cleavage of N-cadherin. *Nat Cell Biol* **16**, 629-38 (2014).
784 92. Kokovay, E. *et al.* VCAM1 is essential to maintain the structure of the SVZ niche and
785 acts as an environmental sensor to regulate SVZ lineage progression. *Cell Stem Cell* **11**,
786 220-30 (2012).
787 93. Segel, M. *et al.* Niche stiffness underlies the ageing of central nervous system progenitor
788 cells. *Nature* **573**, 130-134 (2019).
789 94. Li, C.X. *et al.* MicroRNA-21 preserves the fibrotic mechanical memory of mesenchymal
790 stem cells. *Nat Mater* **16**, 379-389 (2017).
791 95. Yang, C., Tibbitt, M.W., Basta, L. & Anseth, K.S. Mechanical memory and dosing
792 influence stem cell fate. *Nat Mater* **13**, 645-52 (2014).
793 96. Nasrollahi, S. *et al.* Past matrix stiffness primes epithelial cells and regulates their future
794 collective migration through a mechanical memory. *Biomaterials* **146**, 146-155 (2017).
795 97. Miroshnikova, Y.A., Nava, M.M. & Wickstrom, S.A. Emerging roles of mechanical
796 forces in chromatin regulation. *J Cell Sci* **130**, 2243-2250 (2017).
797 98. Nava, M.M. *et al.* Heterochromatin-Driven Nuclear Softening Protects the Genome
798 against Mechanical Stress-Induced Damage. *Cell* **181**, 800-817 e22 (2020).
799 99. Jones, D.L. *et al.* ZNF416 is a pivotal transcriptional regulator of fibroblast
800 mechanoactivation. *J Cell Biol* **220**(2021).

100. Goetsch, K.P., Snyman, C., Myburgh, K.H. & Niesler, C.U. ROCK-2 is associated with focal adhesion maturation during myoblast migration. *J Cell Biochem* **115**, 1299-307 (2014).
101. Salhia, B. *et al.* Inhibition of Rho-kinase affects astrocytoma morphology, motility, and invasion through activation of Rac1. *Cancer Res* **65**, 8792-800 (2005).
102. Chen, Y., Chou, W.C., Ding, Y.M. & Wu, Y.C. Caffeine inhibits migration in glioma cells through the ROCK-FAK pathway. *Cell Physiol Biochem* **33**, 1888-98 (2014).
103. Fu, P.C. *et al.* The Rho-associated kinase inhibitors Y27632 and fasudil promote microglial migration in the spinal cord via the ERK signaling pathway. *Neural Regen Res* **13**, 677-683 (2018).
104. Piltti, J., Varjosalo, M., Qu, C., Hayrinen, J. & Lammi, M.J. Rho-kinase inhibitor Y-27632 increases cellular proliferation and migration in human foreskin fibroblast cells. *Proteomics* **15**, 2953-65 (2015).
105. Rudolph, J. *et al.* The JAK inhibitor ruxolitinib impairs dendritic cell migration via off-target inhibition of ROCK. *Leukemia* **30**, 2119-2123 (2016).
106. Srinivasan, S. *et al.* Blockade of ROCK inhibits migration of human primary keratinocytes and malignant epithelial skin cells by regulating actomyosin contractility. *Sci Rep* **9**, 19930 (2019).
107. Dyberg, C. *et al.* Inhibition of Rho-Associated Kinase Suppresses Medulloblastoma Growth. *Cancers (Basel)* **12**(2019).
108. Rolando, C. *et al.* Distinct roles of Nogo-a and Nogo receptor 1 in the homeostatic regulation of adult neural stem cell function and neuroblast migration. *J Neurosci* **32**, 17788-99 (2012).
109. Feng, J.F. *et al.* Guided migration of neural stem cells derived from human embryonic stem cells by an electric field. *Stem Cells* **30**, 349-55 (2012).
110. Galindo, L.T. *et al.* Chondroitin Sulfate Impairs Neural Stem Cell Migration Through ROCK Activation. *Mol Neurobiol* **55**, 3185-3195 (2018).
111. Gengatharan, A. *et al.* Adult neural stem cell activation in mice is regulated by the day/night cycle and intracellular calcium dynamics. *Cell* **184**, 709-722 e13 (2021).
112. Koch, J.C. *et al.* ROCK inhibition in models of neurodegeneration and its potential for clinical translation. *Pharmacol Ther* **189**, 1-21 (2018).
113. Rikitake, Y. *et al.* Inhibition of Rho kinase (ROCK) leads to increased cerebral blood flow and stroke protection. *Stroke* **36**, 2251-7 (2005).
114. Sladojevic, N., Yu, B. & Liao, J.K. ROCK as a therapeutic target for ischemic stroke. *Expert Rev Neurother* **17**, 1167-1177 (2017).

847 **Methods**

848

849 **Laboratory animals**

850 For *in vivo* ATAC-seq libraries, an equal number of male and female GFAP-GFP (FVB/N
851 background) mice[1] were pooled and used. GFAP-GFP transgenic mice express green fluorescent
852 protein (GFP) driven by the human promoter for glial fibrillary acidic protein (GFAP). For
853 ATAC-seq libraries generated from cultured NSCs, the SVZs from one male and one female
854 C57BL/6 mouse obtained from the NIA Aged Rodent colony were pooled and used. For gene
855 knockout experiments, male and female Rosa26-Cas9 knock-in mice[2] (C57BL/6 background)
856 were used (https://www.jax.org/strain/024858). The Rosa26-Cas9 mice constitutively express the
857 Cas9 endonuclease and an EGFP reporter under the control of a CAG promoter knocked into the
858 *Rosa26* locus. For immunohistochemistry of coronal brain sections, male and female GFAP-GFP
859 (FVB/N background) mice[1] were used. For all other experiments, male C57BL/6 mice obtained
860 from the NIA Aged Rodent colony were used. In all cases, mice were habituated for more than
861 one week at Stanford before use. At Stanford, all mice were housed in either the Comparative
862 Medicine Pavilion or the Neuro Vivarium, and their care was monitored by the Veterinary
863 Service Center at Stanford University under IACUC protocol 8661.

864

865 **ATAC-seq library generation from freshly isolated cells**

866 We used fluorescence-activated cell sorting (FACS) to freshly isolate populations of endothelial
867 cells, astrocytes, quiescent NSCs (qNSCs), activated NSCs (aNSCs), and neural progenitor cells
868 (NPCs) from GFAP-GFP (FVB/N background) animals[1], as previously described[3]. This GFAP-
869 GFP strain expresses GFP under the control of the human GFAP promoter and has been used to

870 isolate NSCs by FACS[3-6]. See also below *"Analysis of potential changes in FACS markers with*
871 *age"*.
872
873 Briefly, we micro-dissected and processed the subventricular zones from young (3-5 months old)
874 and old (20-24 months old) GFAP-GFP mice following a previously described protocol[4] with the
875 addition of negative gating for CD45 (hematopoietic lineage) and sorting of endothelial cells
876 (CD31+) as described[3] (see Extended Data Fig. 1a). All FACS sorting was performed at the
877 Stanford FACS facility on a BD Aria II sorter, using a 100-μm nozzle at 13.1 pounds/square inch
878 (psi), and Flowjo (v8) software was used for data analysis. Due to the rarity of NSC lineage cells,
879 we pooled sorted cells from 2 young male and 2 young female GFAP-GFP mice for the young
880 conditions (3-5 months old), and from 3 old male and 2-3 old female GFAP-GFP mice for the
881 old conditions (20-24 months old). For each respective library, we sorted either 2000 astrocytes
882 (CD45-/CD31-/GFAP-GFP+/PROM1-/EGFR-), 2000 qNSCs (CD45-/CD31-/GFAP-
883 GFP+/PROM1+/EGFR-) (with the exception of a single library which only had 1670 cells), 800-
884 1000 aNSCs (CD45-/CD31-/GFAP-GFP+/PROM1+/EGFR+), 2000 NPCs (CD45-/CD31-
885 /GFAP-GFP-/EGFR+), or 2000 endothelial cells (CD45-/CD31+) from GFAP-GFP animals for
886 ATAC-seq (see Supplementary Table 1). Young and old cells of the five cell types were sorted
887 into 150 μL of NeuroBasal-A medium (Gibco, 10888-022) with penicillin-streptomycin-
888 glutamine (Gibco, 10378-016) and 2% B27 minus vitamin A (Gibco, 12587-010) in a 96-well V-
889 bottomed plate (Costar, 3894) and spun down at 300g for 5 min at 4°C. Sorted cells were washed
890 with 100 μL ice-cold 1x PBS (Corning, 21-040-CV), male and female cells were pooled by age
891 and cell type, and then spun down at 300g for 5 min at 4°C. Next, 50 μL of lysis buffer (10 mM
892 Tris HCl pH 7.4 (Sigma, T2194), 10 mM NaCl, 3 mM $MgCl_2$ (Ambion, AM9530G), 0.10% NP-

893 40 (Thermo, 85124)) was added to each well (alternating between young and old wells) and was
894 immediately spun down at 500g for 10 min at 4°C. Lysis buffer was carefully aspirated and 5 μL
895 of transposition mix (2.5 μL 2x Tagment DNA (TD) buffer, 2.25 μL nuclease-free H_2O, 0.25 μL
896 Tn5 transposase (Illumina, FC-121-1030)) was added to each well and pipetted 6x to resuspend
897 nuclei. Cells were incubated for 30 min at 37°C in a sealed 96-well plate and then briefly spun
898 down at 500g for 1 min to account for evaporation. Transposed DNA was then purified using the
899 Zymo DNA Clean & Concentrator kit (Zymo, D4014) and eluted in 20 μL of nuclease-free H_2O.
900 PCR amplification and subsequent qPCR monitoring was performed as previously described in
901 the original ATAC-seq protocol[7]. ATAC-seq libraries from young and old cells were amplified
902 with 11-14 PCR cycles and then purified using the Zymo DNA Clean & Concentrator kit (Zymo,
903 D4014) and eluted in 15 μL of nuclease-free H_2O. See below "*Library sequencing and ATAC-*
904 *seq quality control of in vivo and cultured NSCs*" for details on sequencing of ATAC-seq
905 libraries.
906
907 **Analysis of potential changes in FACS markers with age**
908 To assess whether the protein levels of the FACS markers used to freshly isolate NSCs from the
909 SVZ neurogenic niche changed with age, we used the same sorted cell populations from young
910 and old GFAP-GFP animals described above in "*ATAC-seq library generation from freshly*
911 *isolated cells*" and used Flowjo (v10.7.1) to export the compensated scaled fluorescence values
912 for NSC markers (GFAP-GFP, PROM1, EGFR) from all propidium iodide-negative (live) cells,
913 quiescent NSCs (CD45-/CD31-/GFAP-GFP+/PROM1+/EGFR-), and activated NSCs (CD45-
914 /CD31-/GFAP-GFP+/PROM1+/EGFR+) freshly isolated from the SVZ. Fluorescence values for
915 these three channels were normalized to the young mean for an experiment and the means for

916 each animal were then visualized using box plots with R (v3.5.2). Statistical comparisons
917 between sample means was performed in R using a two-tailed Mann-Whitney test.
918
919 For all live cells, there was a significant increase in EGFR and PROM1 expression with age and
920 a significant decrease in GFAP expression with age (Extended Data Fig. 1b), likely reflecting
921 changes in cell type composition with age in the SVZ neurogenic niche[8-11]. Despite the
922 significant decrease in GFAP expression in all live cells, we are still able to gate and FACS-
923 purify cells with high GFAP expression (Extended Data Fig. 1a). For FACS-purified quiescent
924 NSCs, there was no age-related change in EGFR, GFAP, or PROM1 expression (Extended Data
925 Fig. 1c). As quiescent NSCs do not express EGFR, raw fluorescence values for this marker were
926 very low compared to fluorescence values for other markers. For FACS-purified activated NSCs,
927 there was no change in GFAP or PROM1 expression, but a slight increase in EGFR expression
928 with age (Extended Data Fig. 1d).
929
930 In previous studies, we verified that young and old FACS-isolated SVZ astrocytes, qNSCs,
931 aNSCs, and NPCs expressed well-established cell type markers (validated by RT-qPCR) and
932 showed expected cell cycle characteristics[3]. In addition, we found that NSCs isolated using this
933 GFAP-GFP FACS scheme in young animals were similar to NSCs isolated with a different
934 FACS scheme using the marker GLAST[5]. We also confirmed cell adhesion and migration
935 molecular signatures observed by ATAC-seq by single cell RNA-seq datasets (Fig. 2a-d;
936 Extended Data Fig. 5). While we cannot completely rule out that other cells could be present in
937 the populations isolated with this FACS scheme, especially from old mice, it is unlikely that
938 these other cells would strongly impact the results.

939 **Primary NSC cell culture**

940 To obtain primary cultures of quiescent and activated NSCs from young and old mice for
941 ATAC-seq, we used a previously described primary culture protocol[12], which does not depend
942 on FACS to isolate NSCs. We micro-dissected and pooled SVZs from pairs of male and female
943 C57BL/6 animals at a young age (3 months old) or an old age (23 months old) obtained from the
944 NIA Aged Rodent colony. To obtain primary cultures of quiescent and activated NSCs from
945 young and old mice for immunofluorescence staining, detachment assays, migration assays, and
946 tension sensor assays, we used the same protocol, but cells were isolated from SVZs from a
947 single young C57BL/6 male (2.5-4 months old) or a single old C57BL/6 male (20-25 months
948 old) animal obtained from the NIA Aged Rodent colony (see Source Data). To obtain primary
949 cultures for CRISPR-Cas9 experiments, SVZs from a single young male or female (3.3-5.2
950 months old) or old male or female (21.8 – 25.3 months old) Rosa26-Cas9[2] (C57BL/6
951 background) mice were used (see Source Data). In all cases, micro-dissected SVZs were finely
952 minced, suspended in 5 mL of 1x PBS +0.1% Gentamicin (Thermo Fisher, 15710064) and spun
953 down at 300g for 5 min at room temperature. We then dissociated SVZs by enzymatic digestion
954 using 5 mL of HBSS (Corning, 21-021-CVR) with 1% penicillin-streptomycin-glutamine
955 (Gibco, 10378-016), 1 U/mL Dispase II (STEMCELL Technologies, 07913), 2.5 U/mL Papain
956 (Worthington Biochemical, LS003126), and 250 U/mL DNAse I (D4527, Sigma-Aldrich),
957 vortexed briefly, and left at 37°C for 40 min on a rotator. Following digestion, the samples were
958 spun down at 300g for 5 min at room temperature and resuspended in 5 mL of NeuroBasal-A
959 medium (Gibco, 10888-022) with 1% penicillin-streptomycin-glutamine (Gibco, 10378-016) and
960 2% B27 minus vitamin A (Gibco, 12587-010) and triturated repeatedly (20x) with 2-3 washes.
961 Single-cell suspensions were then resuspended in "complete activated media": Neurobasal-A

962 (Gibco, 10888-022) supplemented with 2% B27 minus vitamin A (Gibco, 12587-010), 1%
963 penicillin–streptomycin–glutamine (Gibco, 10378-016), 20 ng/mL of EGF (Peprotech, AF-100-
964 15), and 20 ng/mL of bFGF (Peprotech, 100-18B). For passaging, cells were dissociated with 1
965 mL Accutase (STEMCELL Technologies, 07920) for 5 min at 37°C, washed once with 5 mL 1x
966 PBS, and resuspended in "complete activated media" for expansion of activated NSCs/NPCs
967 (aNSCs/NPCs). For quiescent NSCs (qNSCs), quiescence was induced over 5-10 days by
968 replacing "complete activated media" with "complete quiescent media": Neurobasal-A (Gibco,
969 10888-022) supplemented with 2% B27 minus vitamin A (Gibco, 12587-010), 1% penicillin–
970 streptomycin–glutamine (Gibco, 10378-016), 50 ng/mL of BMP4 (Biolegend 94073), and 20
971 ng/mL of bFGF (Peprotech, 100-18B). For adherent cultures of both qNSCs and aNSCs/NPCs,
972 we coated plates with Poly-D-Lysine (PDL) (Sigma-Aldrich, P6407, diluted 1:20 in 1x PBS) for
973 30-120 min at 37°C, and washed plates 4x with 1x PBS prior to plating cells at the appropriate
974 density. All cell counting was performed using the Countess II FL Automated Cell Counter (Life
975 Technologies, AMQAF1000).
976
977 **ATAC-seq library generation from primary NSC cultures**
978 To establish individual primary NSC cultures for ATAC-seq, we dissected and pooled the SVZs
979 from one male and one female C57BL/6 NIA mouse from either a young cohort (3 months old)
980 or an old cohort (23 months old). We dissociated and cultured NSCs as described above (in the
981 section "*Primary NSC cell culture*") to generate 4 young and 4 old biological replicates. At
982 passage 5, NSCs were plated at a density of 1.2 million cells per 6cm PDL-coated plate in
983 complete quiescent media for 8 days prior to sorting. At passage 7, NSCs from the same culture
984 were plated at a density of 1.5 million cells per 6cm plate onto PDL-coated plates in complete

985 activated media for 24 hours prior to sorting to synchronize quiescent and activated sorting
986 experiments. Plates were washed 3x with 1x PBS. Adherent qNSCs were lifted from the plate
987 using 1 mL of Accutase (STEMCELL Technologies, 07920) incubated for 15 min at 37°C and
988 adherent aNSCs/NPCs were lifted from the plate using 1 mL of Accutase (STEMCELL
989 Technologies, 07920) incubated for 5 min at 37°C. The Accutase (STEMCELL Technologies,
990 07920) cell suspension was diluted with 10 mL of 1x PBS, cells were spun down at 300g for 5
991 min, then resuspended in 200 μL of Neurobasal-A (Gibco, 10888-022) supplemented with 2%
992 B27 minus vitamin A (Gibco, 12587-010), 1% penicillin–streptomycin–glutamine (Gibco,
993 10378-016) with propidium iodide (BioLegend, 421301, 1:5000) for live/dead staining. Cells
994 were kept on ice during all subsequent steps.
995
996 Due to concern about differing levels of dead cells in the young vs. old cultures as well as the
997 contaminating influence of dead cells on ATAC-seq libraries, all samples were sorted using
998 fluorescence-activated cell sorting (FACS) based on the live gate (propidium iodide).
999 Specifically, 10,000-15,000 live cultured qNSCs and aNSCs/NPCs (see Supplementary Table 1)
1000 were respectively sorted into 100 μL of NeuroBasal-A medium (Gibco, 10888-022) with
1001 penicillin-streptomycin-glutamine (Gibco, 10378-016) and 2% B27 minus vitamin A (Gibco,
1002 12587-010) in a 96-well V-bottomed plate (Costar, 3894) and spun down at 300g for 5 min at
1003 4°C. Sorted cells were washed with 100 μL ice-cold 1x PBS (Corning, 21-040-CV), and spun
1004 down at 300g for 5 min at 4°C. 50 μL of lysis buffer (10mM Tris HCl pH 7.4 (Sigma, T2194),
1005 10mM NaCl, 3mM $MgCl_2$ (Ambion, AM9530G), 0.10% NP-40 (Thermo, 85124)) was added to
1006 each well (alternating between young and old wells) which were immediately spun down at 500g
1007 for 10 min at 4°C. Lysis buffer was carefully aspirated and 50 μL of transposition mix (12.5 μL

1008 4x Tagment DNA (TD) buffer (gift from the Chang Lab), 35 μL nuclease-free H_2O, 2.5 μL Tn5
1009 (gift from the Chang Lab)) was added to each well and pipetted 6x to resuspend nuclei. Cells
1010 were incubated for 30 min at 37°C in a sealed 96-well plate and then briefly spun down at 500g
1011 for 1 min to account for evaporation. Transposed DNA was then purified using the Zymo DNA
1012 Clean & Concentrator kit (Zymo, D4014) and eluted in 20 μL of nuclease-free H_2O. PCR
1013 amplification and subsequent qPCR monitoring was performed as previously described in the
1014 original ATAC-seq protocol[7]. All libraries were amplified for 5 PCR cycles, and then an
1015 additional 4 PCR cycles (based off of qPCR amplification curves), and then purified using the
1016 Zymo DNA Clean & Concentrator kit (Zymo, D4014) and eluted in 15 μL of nuclease-free H_2O.
1017

1018 **Library sequencing and ATAC-seq quality control of *in vivo* and cultured NSCs**

1019 We quantified individual library concentrations using a Bioanalyzer (High Sensitivity) and
1020 pooled at a concentration of 5 nM for sequencing. Multiplexed libraries were sequenced using
1021 NextSeq (400M) by the Stanford Functional Genomics Facility. To assess individual library
1022 quality, individual library paired-end FASTQ files were processed using the Kundaje Lab's
1023 ATAC-seq Pipeline (https://github.com/kundajelab/atac_dnase_pipelines) with default
1024 parameters (using "-species mm10" and including "-auto_detect_adapter").
1025 For *in vivo* ATAC-seq libraries generated from freshly isolated SVZ cells, libraries were
1026 excluded based on insufficient read coverage (<10 million unique reads) or low peak calling
1027 (<=20,000 peaks). In general, endothelial cell libraries were of worse quality than the other four
1028 sorted cell types and we additionally censored one endothelial library with low bowtie alignment
1029 (~92%) since all other libraries had a bowtie alignment of >= 95%. The high-quality libraries

1030 were sequenced to a mean read depth of 29,187,427 unique reads (ranging from ~10-69 million
1031 reads per library) (see Supplementary Table 1).
1032
1033 In general, ATAC-seq library quality was better for cultured NSCs than freshly isolated NSCs,
1034 so we used a different set of metrics for quality control. For cultured NSCs, 1 library (out of 4)
1035 from each condition was excluded to due to poor quality, defined as the library with the lowest
1036 transcription start site (TSS) enrichment (<20 in all cases). Additionally, both young and old
1037 quiescent cultures had one library that appeared highly anomalous (~2-fold greater fraction of
1038 reads in peaks (FRiP) and TSS enrichment compared to every other library) so they were
1039 additionally excluded to not confound results. The remaining 2-3 high-quality libraries per
1040 condition were sequenced to a mean read depth of 26,271,688 unique reads (ranging from ~18-
1041 42 million reads per library) (see Supplementary Table 1).
1042
1043 **ATAC-seq pipeline and processing**
1044 Libraries that passed quality control were re-processed using the Kundaje Lab's ATAC-seq
1045 Pipeline (https://github.com/kundajelab/atac_dnase_pipelines) starting from de-duplicated BAM
1046 files to call peaks per multi-replicate condition. De-duplicated, Tn5-shifted tagAlign files for
1047 each replicate were converted to BAM files (using bedToBam (v2.29.2)) and sorted (using
1048 samtools sort (v1.10)) for downstream analysis. Peaks per multi-replicate condition were
1049 selected using "overlap > optimal set" resulting in approximately 20,000-90,000 peaks per *in*
1050 *vivo* condition (with a mean peakset size of 65,243 peaks) and approximately 90,000-150,000
1051 peaks per cultured NSC condition (with a mean peakset size of 118,987 peaks). To generate
1052 pooled read libraries, the 2-3 high-quality filtered, de-duplicated BAM files for each condition

1053 were merged (using samtools merge (v1.10)), sorted (using samtools sort (v1.10)), Tn5-shifted
1054 (using deepTools alignmentSieve (v3.4.3)), and indexed (using samtools index (v1.10)). All
1055 analysis was performed using the *mm10* mouse genome
1056 ("TxDb.Mmusculus.UCSC.mm10.knownGene").
1057
1058 **Transcription start site (TSS) enrichment**
1059 Transcription start site (TSS) enrichment heatmaps were generated with ngsplot.R (v2.6.1)[13]
1060 using pooled, Tn5-shifted, sorted BAM files as inputs for each of the 10 conditions. All analysis
1061 was performed using the *mm10* mouse genome ("TxDb.Mmusculus.UCSC.mm10.knownGene").
1062
1063 **Generating consensus peaksets and count matrices**
1064 To generate consensus peaksets for downstream analysis, BAM files and multi-replicate peak
1065 files were loaded into a Large DBA object using Diffbind (v2.10.0)[14,15] "dba.count" with
1066 parameters "minOverlap=0" and "score=DBA_SCORE_READS". We annotated peaks in the
1067 consensus count matrices using the "annotatePeak" function of the package ChIPSeeker
1068 (v1.18.0)[16] with parameters "tssREgion=c(-3000,3000)".
1069
1070 **Functional enrichment of genetic elements within global peaksets**
1071 The "annotatePeak" function of ChIPSeeker (v1.18.0)[16] was used to identify the genetic element
1072 identity of each chromatin peak within the multi-replicate peakset for each condition with
1073 parameters (tssRegion=c(-3000, 3000), annoDb="org.Mm.eg.db"), and the annotation statistics
1074 were extracted using "@annoStat". The different promoter terms "Promoter (<=1kb)",

1075 “Promoter (1-2kb)”, and “Promoter (2-3kb)” were manually grouped together under “Promoter”,
1076 and the two intron terms were manually grouped under “Intron”.
1077
1078 **Principal Component Analysis (PCA)**
1079 DESeq2 (v1.22.2)[17] was used to calculate dispersion estimates from raw consensus count
1080 matrices and then variance stabilizing transformations were applied prior to visualization by
1081 principal component analysis.
1082
1083 For *in vivo* ATAC-seq libraries generated from freshly isolated SVZ cells, PCA on all chromatin
1084 peaks was generated using the global consensus peakset of 141,970 peaks. PCA consisting of all
1085 young and old qNSC and aNSC libraries was generated using the count matrix consisting of
1086 these 87,796 peaks. Based on peak annotations, the NSC consensus peakset was sub-divided into
1087 a distal+intronic peakset (60,231 peaks), a distal peakset (31,660 peaks), an intronic peakset
1088 (28,571 peaks), and a promoter peakset (20,633 peaks)). For ATAC-seq libraries generated from
1089 cultured NSCs, PCA was generated from the consensus peakset with 121,497 peaks. To compare
1090 how cultured NSCs compared to NSCs freshly isolated from the SVZ, we performed PCA on the
1091 count matrix consisting of the 11 freshly isolated NSC libraries and the 10 cultured NSC libraries
1092 (156,963 peaks).
1093
1094 **PCA with ATAC-seq peaks with enhancer marks**
1095 To identify ATAC-seq peaks that have enhancer marks, we downloaded FASTQ files for
1096 chromatin immunoprecipitation followed by sequencing (ChIP-seq) datasets for histone H3
1097 acetylated lysine 27 (H3K27ac) and p300 – two marks of active enhancers – obtained from

1098 cultured quiescent NSCs and proliferative (activated) NSCs[12]. We then processed these datasets
1099 using the standard ENCODE ChIP-seq pipelines. ATAC-seq peaksets that overlap with both
1100 H3K27ac and p300 marks were generated for qNSCs and aNSCs using "bedtools intersect -wa -
1101 u" resulting in subsetted peaksets of size 5401 and 3875 respectively. The resulting peak files
1102 were used to generate an accessibility count matrix (6644 peaks) which was used for PCA as
1103 described above.
1104
1105 **Clustering ATAC-seq libraries from freshly isolated cells for heatmap visualization**
1106 To cluster and visualize all ATAC-seq libraries from freshly isolated SVZ cell populations
1107 together, we generated a heatmap from the global consensus peakset (141,970 peaks) with
1108 "cor()" using the default Pearson's correlation with the R library "pheatmap" (v1.0.12).
1109
1110 **Correlating ATAC-seq promoter accessibility and single cell RNA-seq expression**
1111 For the five cell populations freshly isolated from the SVZ of young and old mice for ATAC-
1112 seq, the average (VST-normalized) chromatin accessibility value of each gene's promoter peak
1113 was associated with the average single cell RNA-seq[11] log-normalized expression value for that
1114 gene. Promoters were binned in deciles based on promoter accessibility in ATAC-seq, and the
1115 association between promoter chromatin accessibility and associated gene expression was plotted
1116 as boxplots of deciles using R (v3.5.2).
1117
1118 **Chromatin signal track visualization for freshly isolated NSCs**
1119 Alignment tracks were visualized using IGV (v2.4.19). For each condition, the BAM file for a
1120 single representative library (see Supplementary Table 1) was normalized by Reads per Kilobase

1121 per Million mapped reads (RPKM-normalization) and converted to a bigwig file using deepTools
1122 (v3.4.3) with the following parameters: "--extendReads 100 --normalizeUsing RPKM --binSize
1123 10".
1124
1125 **Differential peak calling with Diffbind v2**
1126 To identify differentially accessible peaks that change with age for each cell type, count matrices
1127 consisting of young and old replicates within a single cell type were generated using Diffbind
1128 (v2.10.0)[14,15] as described above (see "*Generating consensus peaksets and count matrices*").
1129 Differential peak calling was accomplished using EdgeR (v3.24.3)[18,19] with the following
1130 parameters for "dba.analyze": bCorPlot=FALSE, bParallel=TRUE, bTagwise=FALSE,
1131 bFullLibrarySize=TRUE, bReduceObjects=FALSE,method=DBA_EDGER". For all
1132 comparisons, differential peaks were obtained using a false discovery rate (FDR) threshold of
1133 0.05 (see Supplementary Table 2). Differential peaks were annotated and associated with their
1134 closest gene using the "annotatePeak" function of the package ChIPSeeker (v1.18.0)[16] with
1135 parameters "tssREgion=c(-3000,3000)". For the differential peaks that change with age in the
1136 freshly isolated qNSC and aNSC libraries respectively, differential peaks were aligned to the
1137 *mm10* chromosomes using the "covplot()" function in ChIPSeeker (v1.18.0)[16] for ease of
1138 visualization.
1139
1140 During the course of this study, the Diffbind package was significantly updated leading to
1141 changes in differential peak calling (Diffbind v3). Using EdgeR with Diffbind v3, similar
1142 differential peaksets to those called by Diffbind v2 can be obtained with the settings
1143 "DBA$config$design <- FALSE". We also tested another differential peak caller using Diffbind

1144 v3 (DESeq2), which could not call differential peaks in our samples at FDR<0.05, possibly due
1145 to the low cell number used as input and the resulting relatively shallow sequencing depth. Due
1146 to this discrepancy, we verified that the original differential peaksets had clean signal pileups
1147 (Extended Data Fig. 3i, see "*Global signal pileup analysis of chromatin accessibility in NSCs*"
1148 below) and that the FDR values of the original differential peaksets (called by EdgeR using
1149 Diffbind v2) correlated well with the *P*-values of DESeq2 peaks (using Diffbind v3) (Extended
1150 Data Fig. 3l,m).
1151
1152 **Functional enrichment of genetic elements within differential NSC peaksets**
1153 The differentially accessible peaks that change with age in the freshly isolated qNSC and aNSC
1154 conditions, respectively, were separated into sets that close with age or open with age and were
1155 annotated with the "annotatePeak" function of ChIPSeeker (v1.18.0)[16] with parameters
1156 (tssRegion=c(-3000, 3000), annoDb="org.Mm.eg.db"). The annotation statistics from
1157 "@annoStat" were manually grouped into 4 categories: "Distal Intergenic", "Intron",
1158 "Promoter", and "Other".
1159
1160 **Nucleosome peak calling**
1161 To identify whether the chromatin landscapes of young and old freshly isolated qNSCs and
1162 aNSCs had different levels of heterochromatin-associated nucleosomes, we used the package
1163 NucleoATAC (v0.2.1)[20]. We called nucleosome peaks from our ATAC-seq data using
1164 "nucleoatac run" with parameters: "--bed" the multi-replicate peak files for each condition, "--
1165 bam" pooled, down-sampled (to 30 million unique reads), Tn5-shifted BAM files, and "--fasta"

1166 the mm10 Mus musculus UCSC genome. The number of nucleosome peaks for each condition
1167 were taken from the "*.nucmap_combined.bed" files and plotted with R (v3.5.2).
1168
1169 **Global signal pileup analysis of chromatin accessibility in NSCs**
1170 We plotted the smoothed signal using the "fc.signal.bigwig" tracks outputted by the ENCODE
1171 ATAC-seq pipeline for each of the tracks within differential peaks output by EdgeR for young
1172 and old aNSCs and qNSCs and subsampled common peaks for aNSC and qNSC separately.
1173
1174 **Gene Ontology (GO) Biological Pathway Enrichment of differentially accessible chromatin**
1175 **peaks**
1176 Differentially accessible peaks were associated with nearby genes using the ChIPSeeker
1177 (v1.18.0)[16] function "annotatePeak". Gene lists were uploaded to the online tool EnrichR[21,22] and
1178 top ranked GO terms from "GO Biological Process 2018" were extracted for pathways that
1179 change with age (see Supplementary Table 3). Selected GO terms were ranked by *P*-value and
1180 plotted for visualization in R (v3.5.2).
1181
1182 In most cases, there was a direct correlation between chromatin changes and transcriptional
1183 (transcriptional upregulation of genes in a GO term found to enriched in differentially accessible
1184 chromatin peaks with age). Exceptions to this include the GO term "Cell-cell adhesion (plasma
1185 membrane)" (Fig. 1g) which opened in old qNSCs but is transcriptionally downregulated with
1186 age (Extended Data Fig. 5e), "Adherens Junction Organization" which opened in old aNSCs but
1187 showed no significant transcriptional change with age (Extended Data Fig. 5b), and "Response to
1188 Forskolin" which opened in young qNSCs but showed no significant transcriptional change with

1189 age (Extended Data Fig. 5c). For GO enrichment of differentially accessible peaks derived from
1190 cultured NSCs (Fig. 2f), the GO term "Heterophilic cell-cell adhesion (plasma membrane)"
1191 whose chromatin opened in old cultured qNSCs is transcriptionally downregulated with age and
1192 the GO term "Negative Chemotaxis" which opened in old qNSCs does not show a significant
1193 transcriptional change with age.
1194
1195 **Gene Ontology (GO) Biological Pathway Enrichment of genes driving PC axes**
1196 To identify what biological processes were associated with peaks driving the principal
1197 components (PCs) in the PCA of young and old freshly isolated qNSCs and aNSCs, the top 1000
1198 peaks driving the principal components (either negatively or positively) were extracted and
1199 associated with genes (see Supplementary Table 4). The genes (under header "Symbol")
1200 associated with these peaks were uploaded to EnrichR to identify top ranked GO terms from
1201 "GO Biological Process 2018" (see Supplementary Table 5). The top 6 GO terms for PC2
1202 negative peaks (grouping old qNSCs and young aNSCs) and PC2 positive peaks (grouping
1203 young qNSCs and old aNSCs) were ranked by *P*-value and plotted in R (v3.5.2) for
1204 visualization.
1205
1206 **Chromatin peak heatmaps within cell adhesion pathways**
1207 To visualize how aging affects chromatin peak accessibility associated with cell adhesion and
1208 migration, genes associated with differential peaks that change with age in either freshly isolated
1209 qNSCs or aNSCs respectively were intersected with the "Cell Adhesion" GO gene list
1210 (GO:0007155) or the "Negative Regulation of Cell Migration" GO gene list (GO:0030336)

1211 (http://www.informatics.jax.org). Differential peak accessibility levels were plotted as heatmaps
1212 using "pheatmap" (v1.0.12) in R (v3.5.2) (TMM-normalized read counts, scaled row-wise).
1213
1214 **Venn diagrams of cell adhesion genes with dynamically accessible chromatin peaks**
1215 To visualize whether the opposing chromatin changes during aging in qNSCs and aNSCs
1216 involved shared adhesion genes, we used Venn diagrams to visualize the number of cell adhesion
1217 genes (from the "Cell Adhesion" GO gene list (GO:0007155)) with nearby chromatin peaks
1218 (annotated by ChIPSeeker (v1.18.0)[16]) that were differentially open in young qNSCs (compared
1219 to old qNSCs) and open in old aNSCs (compared young aNSCs). We also used a Venn diagram
1220 to visualize the overlap of cell adhesion genes with nearby chromatin peaks that open with age in
1221 both aNSCs and NPCs.
1222
1223 ***De novo* transcription factor binding patterns using a deep learning model and TF-**
1224 **MoDISco**
1225 To identify transcription factor binding patterns, ATAC-seq peaks for *in vivo* quiescent or
1226 activated NSCs isolated from young and old mice were separately converted to BigWig tracks of
1227 base-resolution Tn5 insertion sites with an +4/-4 shift to account for Tn5 shift. For each cell type,
1228 in addition to the peak regions, we selected an equal number of non-peak regions that were
1229 matched for GC content in their peaks. We then trained cell type-specific BPNet models to
1230 predict the log counts and base-resolution Tn5 insertion profiles as previously reported[23,24].
1231 Briefly, the BPNet model takes as input a 2,114 bp one-hot encoded input sequence and predicts
1232 the ATAC-seq profile and log counts in a 1,000 bp window centered at the input sequence.
1233 Following BPNet formulation, we used a multinomial negative log likelihood (MNLL) for the

1234 profile output of the model and a mean square error (MSE) loss for the log counts output of the
1235 model. The relative loss weight used for the counts loss was 0.1 times the mean total counts per
1236 region. During each epoch, training examples were jittered by up to 500 bp on either side and a
1237 random half of the sequences were reverse complemented. Each batch contained a 10:1 ratio of
1238 peaks to non-peak regions. Model training was performed using Keras/Tensorflow 2. Code used
1239 for model training is available at https://github.com/kundajelab/retina-models.
1240
1241 We computed importance scores for the counts output using the DeepSHAP[25] implementation of
1242 DeepLIFT algorithm[26]. We next ran the TF-MoDISco algorithm[27] to perform *de novo* motif
1243 discovery in each cell type. We mapped the discovered motifs to position weight matrices
1244 (PWMs) from HOCOMOCO[28] using TomTom[29] (Extended Data Fig. 8a). For each cell type, we
1245 computed the relative fraction of TF-MoDISco seqlets attributed to each motif (Extended Data
1246 Fig. 8a).
1247
1248 **Single cell RNA-seq expression values for cell adhesion and migration pathways**
1249 Single cell RNA-seq datasets from young and old SVZ neurogenic niches[11], consisting of 14,685
1250 cells (8,884 cells from young and 5,801 cells from old), were used to identify how gene
1251 expression of specific molecular signatures and genes involved in cell adhesion and migration
1252 differs by cell type and age at single-cell resolution.
1253
1254 Cell types were clustered and annotated as described previously[11] with Seurat[30]. In brief, we
1255 performed t-SNE clustering using Seurat[30] with the first 15 principal components and performed
1256 principal component analysis (PCA) on the 4,125 most variable genes. Significant clusters and

1257 marker genes for each significant cluster were found using the Seurat functions FindClusters()
1258 and FindAllMarkers(). This identified 11 different cell types (qNSCs/astrocytes – which cluster
1259 together, aNSCs/NPCs – which cluster together, neuroblasts, neurons, oligodendrocytes,
1260 progenitor cells, oligodendrocytes, endothelial cells, mural cells, microglia, macrophages, and T-
1261 cells) which were annotated using a combination of marker genes identified from literature and
1262 gene ontology for cell types using EnrichR (http://amp.pharm.mssm.edu/Enrichr/). Single cell
1263 gene expression values for three cell types – qNSCs/astrocytes (which cluster together),
1264 aNSCs/NPCs (which cluster together), and neuroblasts – were extracted and subset based on
1265 genes from Gene Ontology lists of cell adhesion and migration pathways. For each single cell
1266 within a cell population, the expression levels of cell adhesion/migration genes were summed.
1267 The cumulative expression level of adhesion genes comparing young qNSCs/astrocytes,
1268 aNSCs/NPCs, and neuroblasts was visualized using violin plots with R (v3.5.2). Statistical
1269 comparisons between conditions was performed in R using a two-tailed Mann-Whitney test. We
1270 also performed a Welch-corrected t-test and results were similar. A two-tailed Mann-Whitney
1271 test was chosen for reporting because it does not require data to be normally distributed and is
1272 commonly used to make comparisons for single gene expression values[31,32].
1273

1274 **Differentially accessible chromatin peaks of specific cell adhesion genes that change with**
1275 **age**

1276 For specific "Cell Adhesion" genes (GO:007155) (*Alcam, Ctnnd2, Itgb8, Lsamp, Ntm*), TMM-
1277 normalized accessibility values for differential peaks that change with age were obtained from
1278 the output of EdgeR (Diffbind v2) (Supplementary Table 2) and visualized using boxplots with R

1279 (v4.1.0). When there were multiple chromatin peaks associated with the same gene that change
1280 with age, the peak upstream of, and closest to the TSS was chosen.
1281
1282 **Single cell RNA-seq expression values for specific cell adhesion genes**
1283 Using the same single cell RNA-seq dataset as above[11], we used the FindMarkers function from
1284 Seurat (v4.0.5) and tested if specific "Cell Adhesion" genes (GO:007155) (*Alcam, Ctnnd2, Itgb8,*
1285 *Lsamp, Ntm*) whose chromatin changed with age in qNSCs and aNSCs (see "*Differentially*
1286 *accessible chromatin peaks of specific cell adhesion genes that change with age*") also showed
1287 transcriptional changes. Statistical comparisons between conditions was performed in R using a
1288 two-tailed Mann-Whitney test. We validated these differentially expressed genes in two other
1289 single cell RNA-seq datasets of SVZ neurogenic niches from mice at different ages[33,34]. We
1290 picked three representative genes that were significantly downregulated with age in
1291 qNSCs/astrocytes in at least two of the three single cell RNA-seq datasets and three
1292 representative genes that were significantly upregulated with age in aNSCs/NPCs in at least two
1293 of the three single cell RNA-seq datasets. Expression values were log-normalized counts per
1294 10,000 transcripts and were visualized using violin plots with R (v3.5.2). Data shown is from
1295 same dataset[11] described above.
1296
1297 **Gene expression trajectory of specific cell adhesion genes during aging time course**
1298 Gene expression trajectories as a function of age were derived from single cell gene expression
1299 data of the SVZ of 28 mice, tiling ages from young to old (3.3 months to 29 months)[33].
1300 Expression values were log-normalized counts per 10,000 transcripts. Each dot represents gene

1301 expression value per mouse. Shaded region corresponds to 95% confidence interval. Line is a
1302 smoothed fit using geom_smooth with method="loess" (ggplot2 v3.3.5).
1303
1304 **Assessing cell cycle heterogeneity and cell adhesion pathways using single cell RNA-seq**
1305 Using single cell RNA-seq dataset from young and old SVZ neurogenic niches[11], we investigated
1306 the heterogeneity in cell cycle and cell adhesion pathways (Extended Data Fig. 6a). Using Seurat
1307 package (v3.1.5)[30], single cells were assigned to different cell cycle stages (G0/G1, G2/M, and S
1308 phase) and assigned a continuous "G2/M score" and "S phase score" based on the expression
1309 levels of G2/M phase marker genes and S phase marker genes, respectively, by the Seurat
1310 CellCycleScoring() function. Low "S phase score" indicate that cells express low levels of S
1311 phase marker genes. The proportion of single cells from young and old SVZ neurogenic niches
1312 that belong to these three different cell cycle stages was then plotted as barplots (Extended Data
1313 Fig. 6b).
1314
1315 We plotted the relationship between Seurat's "S phase score" and the cumulative expression of
1316 genes from the "Cell Adhesion" GO gene list (GO:0007155) in young and old qNSCs/astrocytes,
1317 aNSCs/NPCs, and neuroblasts (Extended Data Fig. 6c). For this analysis, each young cell
1318 population was downsampled to the number of old cells (480 qNSCs/astrocytes, 82
1319 aNSCs/NPCs, and 146 neuroblasts). We found that some activated NSCs became more
1320 "quiescent-like" with age (Extended Data Fig. 6b,c). However, adhesion and proliferation could
1321 also be uncoupled, as some old activated NSCs can exhibit adhesion changes without exhibiting
1322 proliferation changes (Extended Data Fig. 6c). Although a subpopulation of old aNSCs/NPCs are
1323 more quiescent and could contribute to the changes in cell adhesion and migration, this

1324 subpopulation is unlikely to explain all adhesion changes with age, and age-dependent adhesion
1325 changes also occur at the single cell level.
1326
1327 **Immunofluorescence staining of young and old primary NSC cultures**
1328 NSCs were cultured as described above (see "*Primary NSC cell culture*") in complete activated
1329 media until Passage 2-4 and then passaged with Accutase (STEMCELL Technologies, 07920)
1330 and seeded at a density of 5,000 cells per well in Matrigel (Corning, 354230, Lot #0062012,
1331 diluted [1:100] in cold DMEM/F12 (Thermo Fisher Scientific, 11320033))-coated coverslips in
1332 24-well plates with complete activated or quiescent media. After 48 hours, adherent
1333 aNSCs/NPCs were washed 1x with PBS, then fixed with 4% paraformaldehyde (Electron
1334 Microscopy Sciences, 15714) for 15 min at room temperature. Wells were washed 4x with PBS
1335 and then stored in PBS, wrapped in parafilm, at 4°C until immunofluorescence staining.
1336 Quiescent media was replaced every other day for 7 days and then adherent qNSCs were fixed
1337 with 4% paraformaldehyde (Electron Microscopy Sciences, 15714) for 15 min at room
1338 temperature, washed 4x with PBS, and then stored in PBS, wrapped in parafilm, at 4°C until
1339 immunofluorescence staining.
1340
1341 For immunostaining, cells were permeabilized with 0.1% Triton X-100 (Fisher Scientific,
1342 BP151) for 10 min at room temperature, and then washed 2x with PBS. Blocking was performed
1343 for 30 min with 1% BSA (Sigma, A7979) in 1x PBS. Primary staining was conducted for 1-1.5
1344 hour at room temperature with phalloidin (Invitrogen, A12379, 665217, [1:500]),
1345 ALCAM/CD166 (Bio-techne, AF1172-SP, [1:40]), paxillin (Abcam, ab32084, [1:200]), or
1346 cleaved-caspase3 (Cell Signaling Technology, 9664T, [1:1000]) resuspended in 1% BSA

1347 (Sigma, A7979). Wells were then washed 4x with 1x PBS and secondary staining was performed
1348 for 1 hour at room temperature with Donkey anti-Rabbit Alexa 568 (Invitrogen, A10042,
1349 [1:500]) or Donkey anti-Goat Alexa 647 (Invitrogen, A21447, [1:500]) resuspended in 1% BSA
1350 (Sigma, A7979). DAPI (ThermoFisher, 62248 [1:500]) was added during secondary antibody
1351 staining. Wells were washed 4x with 1x PBS+0.2% TWEEN 20 (Sigma-Aldrich, P1379-1L),
1352 then 4x with 1x PBS. Coverslips were mounted onto glass slides with ProLong Gold Antifade
1353 Mountant with DAPI (ThermoFisher, P36931) and visualized with a Nikon Eclipse Ti confocal
1354 microscope equipped with a Zyla sCMOS camera (Andor) and NIS- Elements software (AR
1355 4.30.02, 64-bit). Quantification of immunofluorescence staining of ALCAM was done using a
1356 custom pipeline in Fiji (v2)[35]. A mask was created using the phalloidin channel to create a cell
1357 mask and overlaid onto ALCAM channel. The sum of pixel intensity within the cell mask
1358 (RawIntDen) was then used to determine fluorescence intensity for each cell, normalized by cell
1359 size. For each experiment, values were normalized by dividing each cell's fluorescence intensity
1360 by the mean fluorescence intensity of all cells in the young condition for aNSCs/NPCs and the
1361 old condition for qNSCs and the same threshold settings were used to create the phalloidin cell
1362 mask for all images within one experiment. For focal adhesion quantification, paxillin channel
1363 was used. Images were converted to 8-bit and background subtracted (rolling=5 sliding),
1364 threshold was set (kept the same for all images taken within one experiment, see Source Data for
1365 thresholding information), a region of interest (ROI) was drawn around cell periphery, and
1366 number of focal adhesions counted ("Analyze Particles", size=0.5-infinity). For cleaved-
1367 caspase3 quantification, CellProfiler (v4.2.1) was used to identify and count nuclei (DAPI) using
1368 the IdentifyPrimaryObject function and cleaved-caspase3-positive cells using the
1369 IdentifySecondaryObjects function. Staining, imaging, and analysis was performed in a blinded

1370 manner. *P*-values were calculated with a two-tailed Mann-Whitney test comparing sample
1371 means. For immunofluorescence images (Fig. 2h,k, Extended Data Fig. 7e), brightness and
1372 contrast were adjusted in Fiji (v2) to enhance visualization. These adjustments were performed
1373 after all data quantification was complete. The same settings were applied to all images shown
1374 for each experiment.
1375
1376 We have also tested antibodies for a number of other cell adhesion proteins (ITGB1 (abcam,
1377 ab24693), ITGA6 (abcam, ab181551), EFNB2 (Invitrogen, PA5-106933), PLPP3 (Sigma,
1378 HPA072751), N-Cadherin (Cell Signaling Technology, 13116T), VE-Cadherin (Santa Cruz, sc-
1379 9989), E-Cadherin (Cell Signaling Technology, 3195T), NRXN1 (abcam, ab222806), ATDC
1380 (Santa Cruz, sc-166707), and talin (Sigma-Aldrich, T3287), but the antibodies for did not work
1381 well for immunostaining or FACS on cultured NSCs due to non-specific staining or lack of
1382 signal. PTPRD (Bioworld, BS71853) showed a trending, but not significant increase with age in
1383 qNSCs and aNSCs/NPCs.
1384
1385 We used immunostaining instead of FACS for quantification, because of the potential concern
1386 that the proteolytic enzymes used to dissociate cells into single cell suspension for FACS could
1387 affect the localization, endocytosis, or cleavage of membrane proteins involved in cell adhesion.
1388
1389 **Detachment assay of cultured qNSCs and aNSCs/NPCs**
1390 For the cell detachment assay, aNSCs/NPCs were cultured in complete activated media until
1391 Passage 2-6 and then seeded at a density of 30,000 cells per well in PDL-coated 96-well plates
1392 (Falcon, 353072) with complete activated media. After 16-24 hours, media on adherent

1393 aNSCs/NPCs was replaced with complete activated media containing 10 nM Syto64 (Invitrogen,
1394 S11346, Lot #8344573) to visualize the cells and incubated for 1-2 hours. Media was replaced
1395 with complete activated media to remove excess Syto64. The plates were immediately brought to
1396 the Incucyte S3 system and imaged with the 4x objective for whole-well imaging with the red
1397 image channel. Each well was visually inspected for appropriate cell density, no cell clumping,
1398 and even distribution of cells. After imaging, media was removed and replaced with 100 μL of
1399 Accutase (STEMCELL Technologies, 07920) and incubated at room temperature for 5 min to lift
1400 the cells. Accutase (STEMCELL Technologies, 07920) was then removed and wells were
1401 washed once with 1x PBS and 100 μL of complete activated media was added to the plates. The
1402 plates were immediately imaged with Incucyte S3 4x objective for whole-well imaging with the
1403 red image channel. For analysis, well quantification area was restricted by 250 pixels using
1404 Incucyte's built-in analysis software to decrease noise from cell debris accumulating at edges of
1405 well. Cell count was calculated using Incucyte's built-in analysis software and percent cells
1406 remaining was calculated as 100*(amount of cells after Accutase/amount of cells before
1407 Accutase).
1408
1409 For cell detachment assay on quiescent NSCs, aNSCs/NPCs were first cultured in complete
1410 activated media until Passage 2-6 and then seeded at a density of 10,000 cells per well in PDL-
1411 coated 96-well plates with complete quiescent media. Complete quiescent media was replaced
1412 every other day for 7 days to induce quiescence. Next, qNSCs were incubated with Syto64,
1413 imaged, and analyzed as described above for aNSCs/NPCs with the following change: as qNSCs
1414 are more adhesive than aNSCs/NPCs, they were treated with Trypsin-EDTA (0.25%) phenol red
1415 (Thermo Fisher Scientific 25200114) (instead of Accutase) for 15 min at room temperature to lift

1416 the cells. *P*-values were calculated using a two-tailed Mann-Whitney test on the average of 2-4
1417 technical replicates for each biological replicate. Experiments were not performed in a blinded
1418 manner; however, quantification of percent cells remaining was done in an automated manner
1419 using Incucyte's analysis software for cell counting.
1420
1421 **NFIC CRISPR-Cas9 gene knockout in young and old cultured aNSCs/NPCs**
1422 *Selection of gene to knockout*
1423 To knockout a transcription factor family involved in the program of genes identified to change
1424 with age in aNSCs, we used the following criteria: 1) Transcription factor identified in chromatin
1425 accessibility to change with age in aNSCs, 2) Transcription factor expressed in aNSC (using
1426 single cell RNA-seq), 3) Transcription factor known to be implicated in cell adhesion and
1427 migration. The NFI family of transcription factors (NFIA, NFIB, NFIC and NFIX) met these
1428 criteria. Among these 4 family members, we focused on NFIC because our pilot studies targeting
1429 this isoform were the most promising.
1430
1431 *Cloning of sgRNAs*
1432 To knockout NFIC, we used a CRISPR/Cas9 approach, using aNSCs/NPCs cells microdissected
1433 from SVZs of young and old Cas9-expressing mice (Rosa26-Cas9[2]) and delivered guide RNAs
1434 to these cells using a lentivirus system. To deliver NFIC or Safe targeting control guide RNAs
1435 that target a safe harbor locus, we used the sgRNA-expressing plasmid MCB320 (gift from Mike
1436 Bassik Lab) (https://www.addgene.org/89359/) and subcloned sgRNAs of interest. This plasmid
1437 contains a puromycin resistance gene and mCherry reporter for selection. See Supplementary
1438 Table 7 for all primers used for cloning and sequencing. The MCB320 plasmid was digested

1439 with the Blp1 and BstXI restriction enzymes and the gel-extracted, purified band was used for
1440 ligation reaction with a double-stranded oligonucleotide containing the sgRNA sequence. For the
1441 forward oligonucleotide of each sgRNA sequence, we added the following cloning adapter
1442 sequences: 5'-ttgg and 3'- gtttaagagc. For the reverse complement oligonucleotide of each
1443 sgRNA sequence, we used the reverse complement of the sgRNA sequence and added 5'-
1444 ttagctcttaaac and 3' -ccaacaag. Each pair of oligonucleotides (IDT, standard desalting) (1 μM
1445 each of forward and reverse) was annealed in 98 μL of nuclease free duplex buffer (IDT, 11-05-
1446 03-01) for 5 min at 95°C and then gradually cooled to room temperature. Then, 1 μL of a 1:20
1447 dilution (in nuclease free duplex buffer (IDT, 11-05-03-01)) and was ligated with 500 ng of the
1448 purified digested plasmid band and then transformed in NEB stable competent cells (New
1449 England BioLabs, C3050H). Successful ligation of the guide was confirmed by Sanger
1450 sequencing using a mU6 sequencing primer (Supplementary Table 7).
1451
1452 *Lentivirus production*
1453 For lentivirus production, human embryonic kidney 293T cells (HEK293T) were cultured in
1454 DMEM (Gibco, 11965092) + 10% FBS (Gibco, 10099-141) + 1% penicillin–streptomycin–
1455 glutamine (Gibco, 10378-016) (complete DMEM). HEK293T cells were plated at a density of 5
1456 million cells per 10 cm plate (Greiner Bio-One, 664-160) in 10 mL of complete DMEM
1457 media.16 hours after plating, media was replaced on HEK293T cells with fresh complete
1458 DMEM. 3-4 hours later, HEK293T cells were transfected using polyethylenimine (PEI)
1459 (Polysciences, 23966-2, 1 mg/mL) and 3rd generation lentivirus packaging vectors (pMDLg,
1460 pRSV, and pVSVG; gift from Mike Bassik lab). Per transfection, 50 μL of PEI was added to 900
1461 μL of antibiotic and FBS free DMEM (Gibco, 11965092) and incubated at room temperature for

1462 10 min. 0.5 μg of each packaging vector (pMDLg, pRSV, and pVSVG) was combined with 10
1463 μg of MCB320 lentiviral plasmid containing guide of interest into a final volume of 50 μL. This
1464 DNA mix was then added to the DMEM-PEI mixture and incubated at room temperature for 20
1465 min. PEI-DNA mixture was then added dropwise to HEK293T cells. 24 hours later, media was
1466 replaced with plain Neurobasal-A (Gibco, 10888-022) (no growth factors or B-27). Supernatant
1467 (10 mL) was collected 24 hours later and the media was replaced for another collection 48 hours
1468 after transfection. Supernatants were combined, centrifuged at 3000 rcf for 5 min, and then
1469 filtered through a 0.45 μm filter (EMD Millipore, SE1M003M00). Filtered supernatant was then
1470 flash frozen into 1.5 mL aliquots and stored at -80°C until ready for use. Multiple guide
1471 sequences were evaluated for knockout efficiency. Guides with high knockout efficiency was
1472 subsequently used for all experiments.
1473
1474 *Infection of aNSCs/NPCs*
1475 Activated NSCs/NPCs were cultured from young and old mixed-sex Rosa26-Cas9[2] knock-in
1476 mice as described in "*Primary NSC cell Culture*". For infection, 1 million aNSCs/NPCs per well
1477 were plated onto PDL-coated 6-well plates in 1 mL of complete activated media. 24 hours later,
1478 media was removed from adherent aNSCs/NPCs. 0.75 mL of filtered viral supernatant was
1479 combined with 0.25 mL of complete activated media, supplemented with 4x growth factors and
1480 B-27 (final volume of growth factors and B-27 is 1x) and added to adherent aNSCs/NPCs. After
1481 24 hours, media was replaced with 0.75 mL of filtered viral supernatant and 0.25 mL of
1482 completed activated media, supplemented with 4x growth factors and B-27 for a second round of
1483 infection. After 24 hours, media was changed to complete activated media. Two days later,
1484 successful infection was verified by microscopy using the mCherry reporter. Once mCherry

1485 expression was confirmed, 0.5 μg/mL of puromycin (Sigma-Aldrich, P8833) was added to the
1486 culture media to select for cells that had been successfully infected. When all uninfected control
1487 aNSCs/NPCs died from puromycin selection (approximately 2-3 days later), adherent
1488 aNSCs/NPCs were washed with complete activated media to remove puromycin and allowed to
1489 expand for 24-48 hours as adherent cultures. aNSCs/NPCs were then passaged and plated onto
1490 PDL-coated 96-well plates for detachment assay. All remaining cells (usually 250,000 –
1491 400,000) were plated onto PDL-coated 24-well plates for genomic DNA collection for
1492 verification of the knockout (see below). If there were not enough cells to perform the
1493 detachment assay and genomic DNA collection, cells were expanded as neurospheres for an
1494 additional 2-3 days. If cultures failed to recover from lentiviral transduction (continued slow
1495 growth), they were not used for subsequent experiments. 16-24 hours after plating cells, we
1496 performed the detachment assay as described above (see "*Detachment assay of cultured qNSCs*
1497 *and aNSCs/NPCs*") except cells were incubated with Accutase for 3 min instead of 5 min. All
1498 experiments were performed in a paired-manner (paired young and old). *P*-values were
1499 calculated using a Wilcoxon Matched-Pairs Signed Ranks Tests comparing sample means. To
1500 take into account the paired-manner of the experiment, the difference in percent cells remaining
1501 (Old aNSC/NPC – Young aNSC/NPC) was also calculated. Difference in percent cells remaining
1502 greater than 0 indicates old cells are more adhesive than young cells. *P*-values comparing
1503 difference in percent cells remaining were calculated using a two-tailed Mann-Whitney test.
1504
1505 *Verification of knockout efficacy*
1506 For genomic DNA isolation, aNSCs/NPCs were plated at a density of 250,000 – 400,000 cells
1507 per well of a PDL-coated 24-well plate at the same time as cells were plated for the detachment

1508 assay. After 16-24 hours, genomic DNA was harvested (same day as detachment assay). Cells
1509 were washed with 500 μL cold PBS and then lysed with 100 μL DirectPCR Lysis Reagent
1510 (Viagen Biotech, 102-T) with 1% Proteinase K (Fisher Scientific, 25-530-049) for 10 min at
1511 room temperature. Supernatant was pipetted repeatedly to lift cells and then transferred to PCR
1512 tubes and incubated at 65°C for 25 min and then 95°C for 15 min in a thermocycler. PCR was
1513 performed to amplify the region targeted by sgRNA and Sanger sequenced (see primers in
1514 Supplementary Table 7). Knockout efficiency was evaluated using Synthego ICE analysis tool
1515 (https://ice.synthego.com/#/)[36]. With this tool, a score of 50 indicates 50% of the population
1516 sequenced was unedited (contains wild-type sequence). With this protocol, we achieved editing
1517 efficiencies of 58-84 (Safe targeting control guide, one guide sequence that edits a region of the
1518 genome that is considered "neutral"[37]) and 56-79 (*NFIC* targeting guide, one guide sequence that
1519 edits *NFIC*).
1520
1521 **Migration assay of cultured qNSCs and aNSCs/NPCs using live cell imaging**
1522 aNSCs/NPCs were cultured in complete activated media until Passage 2-4 and then seeded at a
1523 density of 200,000 cells per well in a PDL-coated 12-well plate with complete activated media
1524 treated with vehicle (H_2O) or 10 μM Y-27632 (dissolved in H_2O) (Tocris, 1254). After 48 hours,
1525 adherent aNSCs/NPCs were passaged with 500 μL of Accutase (STEMCELL Technologies,
1526 07920), and resuspended in in Neurobasal-A (Gibco, 10888-022) supplemented with 2% B27
1527 minus vitamin A (Gibco, 12587-010) and 1% penicillin–streptomycin–glutamine (Gibco, 10378-
1528 016) with propidium iodide (BioLegend, 421301, 1:5000) for live/dead staining. 1000 live (PI-)
1529 cells per well were sorted with flow cytometry using the BD PICI onto PDL-coated Incucyte
1530 ImageLock 96-well plates (Essen BioScience, 4379) containing 100 μL of complete activated

1531 media with 10 nM Syto64 (Invitrogen, S11346, Lot #8344573) and either vehicle (H_2O) or 10
1532 μM Y-27632 (dissolved in H_2O) (Tocris, 1254). The ImageLock plate was immediately brought
1533 to the Incucyte Zoom or Incucyte S3 live imaging system to image (with Phase and red image
1534 channels) at 37°C every 30 min for 20 hours with the 20X objective. After 20 hours, the cell
1535 media was washed 2x with PBS and then replaced with 100 μL of complete quiescent media.
1536 Media was changed every other day for 7 days to induce quiescence. The media was then
1537 replaced with complete quiescent media supplemented with 10 nM Syto64 (Invitrogen, S11346,
1538 Lot #8344573) prior to imaging. Wells were imaged (with Phase and red image channels) using
1539 either the Incucyte S3 or Incucyte Zoom system with the 20X objective every hour for 20 hours
1540 at 37°C. Three images (from different parts of the well) at each timepoint were taken for each
1541 well and tracked cell metrics were summed across these three images. This 20 hour window
1542 includes time needed for cells to adhere to the plate (early time points) in addition to migration
1543 (later time points). Cell migration tracking was performed in an automated manner using Imaris
1544 (v9.3.0). Every image stack was manually inspected to ensure that cell tracking was correctly
1545 performed (e.g. that automated cell tracking was not incorrectly labelling debris and that cell
1546 tracks accurately follow individual cells). "Track Velocity" was output for visualization with
1547 Prism (v8) and *P*-values were calculated with a two-tailed Mann-Whitney test comparing both
1548 single cell values as well as sample mean values (where single cell velocities were averaged by
1549 animal). Experiments were not performed in a blinded manner; however, quantification of cell
1550 migration velocity was performed in an automated manner using Imaris (v9.3.0).
1551
1552
1553

1554 **Matrigel dispersion assay**

1555 For Matrigel dispersion assays, aNSCs/NPCs were cultured in complete activated media until
1556 Passage 4-6, passaged with Accutase (STEMCELL Technologies, 07920), and resuspended in
1557 complete activated media at a concentration of 100,000 cells/μL. Note that this assay integrates
1558 cell migration, as well as other factors (e.g. cell proliferation, survival, etc.). Matrigel (Corning,
1559 354230, Lot #8344573 for experiments with young and old aNSCs/NPCs in Fig. 2 and Lot
1560 #9028255 for experiments with ROCKi in Fig. 4) was diluted 1:2 in cold F12:DMEM (Gibco,
1561 11-330-057) while on ice to prevent solidification, and 50 μL was immediately added per well to
1562 a 96-well plate. We note that there are lot to lot variations in quantify of extracellular matrix
1563 proteins present in Matrigel which likely affect activated NSC's ability to disperse through the
1564 material. The 96-well plate was moved to the 37°C incubator for 3 hours prior to spotting 50,000
1565 cells (in a volume of 0.5 μL) directly to the center of the Matrigel-coated well. The plate was
1566 returned to the 37°C incubator for 15-30 min to allow for cells to adhere. Next, 150 μL of
1567 complete activated media (treated with vehicle (H_2O) or 10 μM Y-27632 (dissolved in H_2O)
1568 (Tocris, 1254)) was very carefully added to each well (for the ROCKi experiments), and the 96-
1569 well plate was placed in either the Incucyte Zoom or Incucyte S3 live imaging system to image
1570 every 6 hours for 48 hours using the 4x objective to image the entire well. For each biological
1571 replicate, 1-4 technical replicates were quantified to account for difficulties in spotting 0.5 μL
1572 volumes, and the distances migrated at each timepoint were averaged among technical replicates.
1573 We manually quantified dispersion distance, defined as the maximum distance from the initial
1574 spotting perimeter to the outermost cell body, using Fiji (v2)[35]. Neither imaging nor analysis was
1575 performed in a blinded manner. *P*-values were calculated with a two-tailed Mann-Whitney test at

1576 each 12-hour timepoint. At early time points, cell proliferation/survival are less likely to be
1577 strong contributing factors in the Matrigel assay than at later time points.
1578
1579 ***In vitro* EdU pulse assay of cultured aNSCs/NPCs**
1580 Cultured aNSCs/NPCs from young and old male C57BL/6 mice were plated onto PDL-coated
1581 coverslips in 24-well plates with complete activated media with or without 10 μM ROCK
1582 inhibitor (ROCKi) compound Y-27632 (dissolved in H_2O) (Tocris, 1254). Forty-eight hours after
1583 plating, 10 μM of EdU (Thermo Fisher Scientific, C10086) was added to adherent aNSCs/NPCs
1584 culture. Two hours later, aNSCs/NPCs were washed once with 1x PBS and then fixed with 4%
1585 paraformaldehyde and processed for immunostaining as previously described (see
1586 "*Immunofluorescence staining of young and old cultured NSCs*"), except in this case CliCK-IT
1587 EdU Alexa Fluor 488 imaging protocol (Thermo Fisher Scientific, C10337) was performed,
1588 according to the manufacturer's instruction, for 30 min at room temperature prior to blocking.
1589 Samples were imaged at 20x with a Nikon Eclipse Ti confocal microscope equipped with a Zyla
1590 sCMOS camera (Andor) and NIS- Elements software (AR 4.30.02, 64-bit). CellProfiler (v4.2.1)
1591 was used to identify and count nuclei (DAPI) using the IdentifyPrimaryObjects function and
1592 EdU-positive nuclei using the IdentifySecondaryObjects function. Staining, imaging, and
1593 analysis was performed in a blinded manner. *P*-values were calculated with a two-tailed Mann-
1594 Whitney test comparing sample means.
1595
1596
1597

1598 **Immunofluorescence staining of SVZ coronal sections to measure distance of quiescent and**
1599 **activated NSCs relative to the ventricle**
1600 For immunofluorescence staining of SVZ coronal sections to measure distance of quiescent and
1601 activated NSCs relative to the ventricle, four young (4 months old) and four old (18-26 months
1602 old) GFAP-GFP animals of both sexes (2 male and 2 female animals per age condition),
1603 combined over two experiments, were subjected to intracardiac perfusion with 4%
1604 paraformaldehyde (Electron Microscopy Sciences, 15714) in 1x PBS. We used male and female
1605 GFAP-GFP mice for these experiments, similar to what was used for generating ATAC-seq
1606 libraries from freshly isolated cells from neurogenic niches (Fig. 1), see "*ATAC-seq library*
1607 *generation from freshly isolated cells*". Brains were post-fixed overnight in 4%
1608 paraformaldehyde (Electron Microscopy Sciences, 15714) and then dehydrated in 30% sucrose
1609 (Sigma-Aldrich, S3929) for 72 hours. Brains were embedded in Tissue-Tek optimal cutting
1610 temperature (O.C.T.) compound (Electron Microscopy Sciences, 62550), sectioned in 16 μm
1611 coronal sections using a cryostat (Leica CM3050S), and then mounted on electrostatic glass
1612 slides (Fisher Scientific, 12-550-15). To ensure a similar anatomic region of the lateral ventricle
1613 was being immunostained and analyzed in each animal, the corpus callosum was first identified
1614 in the coronal sections as an anatomical landmark. For these experiments, 6 serial coronal
1615 sections spaced approximately 100 μm apart were selected for immunostaining. These serial
1616 coronal sections correspond to images 42 – 47 from the Allen Institute Coronal Brain Atlas
1617 (https://mouse.brain-map.org/static/atlas). The 3 more anterior serial coronal sections were
1618 stained with antibodies to GFAP, Ki67, Vinculin, and with DAPI and the 3 more posterior serial
1619 coronal sections were stained with antibodies to S100a6, Ki67, ARL13b, and with DAPI (see
1620 below).

1621

1622 To perform immunofluorescence staining, coronal sections were washed with 1x PBS and then
1623 permeabilized with ice-cold methanol + 0.1% Triton X-100 (Fisher Scientific, BP151) for 15
1624 min at room temperature. Slides were washed 3x with 1x PBS for 5 min. Antigen retrieval was
1625 performed in 10 mM sodium citrate buffer (pH 6.0) (2.94 g Tri-sodium citrate dihydrate (Sigma-
1626 Aldrich, S1804) in 1000 mL milliQ H_2O adjusted to pH 6.0 with 1N HCl) + 0.05% TWEEN 20
1627 (Sigma-Aldrich, P1379-1L) in a 85°C water bath for 2 hours. Slides were then cooled to room
1628 temperature for 20 min (in antigen retrieval buffer), and coronal sections were blocked with 5%
1629 Normal Donkey Serum (NDS) (ImmunoReagents Inc., SP-072-VX10) and 1% BSA (Sigma,
1630 A7979) in 1x PBS for 30 min at room temperature. Primary antibody staining was performed
1631 overnight at 4°C in 5% Normal Donkey Serum and 1% BSA in 1x PBS. Primary antibodies used
1632 were the following: Ki67 (Invitrogen, Clone SolA15, 14-5698-82, [1:200]), GFAP (Abcam,
1633 ab53554, [1:500]), Vinculin (Abcam, ab129002, [1:200]), S100a6 (Abcam, ab181975, [1:500]),
1634 and ARL13b (Abcam, ab136648, [1:500]). Vinculin (cell adhesion protein) and ARL13b (ciliary
1635 marker) were used to demarcate ventricle border, for GFAP staining and S100a6 staining,
1636 respectively. Different antibodies were used to mark the ventricular wall because of species
1637 compatibility for the staining panel. Coronal sections were then washed 3x with 1x PBS and
1638 0.2% TWEEN 20 for 10 min at room temperature followed by two 1x PBS washes for 15 min.
1639 Secondary antibody staining was performed at room temperature for 2 hours in 5% NDS and 1%
1640 BSA in 1x PBS. Secondary antibodies used were the following: Donkey anti-Goat 488 (Sigma
1641 Aldrich, SAB460032-250UL [1:1000]), Donkey anti-Rat 594 (Life Technologies, A21209
1642 [1:1000]), Donkey anti-Mouse 488 (Life Technologies, A21202, [1:1000]), Donkey anti-Goat
1643 488 (Invitrogen, A11055, [1:1000]), Donkey anti-Rabbit 568 (Invitrogen, A10042, [1:1000]),

1644 and/or Donkey anti-Rat 647 (Invitrogen, A48272, [1:1000]). DAPI (ThermoFisher, 62248
1645 [1:500]) was added during secondary antibody staining. Sections were washed 3x for with 1x
1646 PBS and 0.2% TWEEN 20 for 10 min at room temperature followed by 3 1x PBS washes for 5
1647 min. Coronal sections were mounted with ProLong Gold Antifade Mountant with DAPI
1648 (ThermoFisher, P36931). Multiple Z-stacks using the 60x objective of a Nikon Eclipse Ti
1649 confocal microscope equipped with a Zyla sCMOS camera (Andor) and NIS- Elements software
1650 (AR 4.30.02, 64-bit) were captured to image the entire length of the SVZ from one hemisphere
1651 per section (3 sections per animal for GFAP staining and 3 sections per animal for S100a6
1652 staining). For immunofluorescence images (Fig. 3c, Extended Data Fig. 9a,b) brightness and
1653 contrast were adjusted in Fiji (v2) to enhance visualization. These adjustments were performed
1654 after all data quantification was complete and the same settings were applied to all images shown
1655 for each experiment.
1656
1657 **Quantification of the location of quiescent and activated NSCs with respect to the ventricle**
1658 **in coronal sections**
1659 For quantification of the location of quiescent and activated NSCs with respect to the ventricle in
1660 coronal sections, captured Z-stacks (30 slices per stack for GFAP staining and 15 slices per stack
1661 for S100a6 staining) were transformed into a Z-projection (sum slices) and quantified using a
1662 custom pipeline. Analysis was restricted to the region that is 200 μm from ventricle wall to not
1663 include striatal astrocytes (though the vast majority of cells were less than 50 μm away from the
1664 ventricle wall) (Fig. 3c, Extended Data Fig. 9a,b).
1665

1666 GFAP and S100a6 were used as NSC markers. For staining with GFAP, GFAP+/Ki67- cells
1667 were identified as qNSCs/astrocytes and GFAP+/Ki67+ cells were identified as aNSCs. For
1668 staining with S100a6, S100a6+/Ki67- cells were identified as qNSCs and S100a6+/Ki67+ cells
1669 were identified as aNSCs. See also below, *"Single cell RNA-seq to detect potential ependymal-*
1670 *repairing SVZ astrocytes and reactive astrocytes"*. NSCs directly lining blood vessels were
1671 censored in the analysis because they were considered to be localized to a blood vessel rather
1672 than the niche lining the ventricle wall. The center of each NSC nuclei was chosen as a
1673 consistent fixed point to assess cell location within the niche. Distances from the ventricle were
1674 calculated by measuring Euclidean distance from the center of the nucleus of each cell of interest
1675 to the ventricle border in Fiji (v2). Neither imaging nor cell type annotation was performed in a
1676 blinded manner; however, distance quantification was performed in an automated manner. *P*-
1677 values were calculated with a two-tailed Mann-Whitney test comparing sample means.
1678

1679 **Immunofluorescence staining of SVZ sagittal sections for distance of quiescent and**
1680 **activated NSCs and neuroblasts relative to the ventricle**

1681 For immunofluorescence staining of SVZ sagittal sections for distance of quiescent and activated
1682 NSCs and neuroblasts relative to the ventricle, 5 young male (2-3 months) and 5 old male (21
1683 months) C57BL/6 mice were used (combined over 2 independent experiments) (note that these
1684 animals were the same as those used in the 4 hour time point in "*In vivo EdU-labelling to follow*
1685 *location of cells in subventricular zone, rostral migratory stream, and olfactory bulb*", see
1686 below). Mice were intraperitoneally injected with 5-ethynyl-2'-deoxyuridine (EdU) (Fisher
1687 Scientific, A10044) (resuspended in PBS at 5 mg/mL) at a dose of 50 mg/kg 4 hours prior to

1688 intracardiac perfusion with 4% paraformaldehyde (PFA) (Electron Microscopy Sciences, 15714)
1689 in PBS.
1690
1691 Brains were processed and immunostained in a similar manner as coronal sections (see above
1692 "*Immunofluorescence staining of SVZ coronal sections to measure distance of quiescent and*
1693 *activated NSCs relative to the ventricle*"), except they were sectioned in 16 µm sagittal sections
1694 rather than coronal. Sagittal sections corresponding approximately to image 14 from the Allen
1695 Institute Sagittal Brain Atlas (https://mouse.brain-map.org/static/atlas) were stained and imaged
1696 as described in "*Immunofluorescence staining of SVZ coronal sections for distance of NSCs*
1697 *relative to the ventricle*" with the antibodies described below.
1698
1699 For immunostaining for quiescent NSCs/astrocytes and activated NSCs in sagittal sections,
1700 primary antibodies used were the following: Ki67 (Invitrogen, Clone SolA15, 14-5698-82,
1701 [1:200]), GFAP (Abcam, ab53554, [1:500]), and Vinculin (Abcam, ab129002, [1:200]).
1702 Secondary antibodies used were the following: Donkey anti-Goat 488 (Sigma Aldrich,
1703 SAB460032-250UL [1:1000]), Donkey anti-Rabbit 568 (Invitrogen, A10042, [1:1000]), and
1704 Donkey anti-Rat 647 (Invitrogen, A48272, [1:1000]). DAPI (ThermoFisher, 62248 [1:500]) was
1705 added during secondary antibody staining.
1706
1707 For immunostaining for EdU+ activated NSCs/NPCs and neuroblasts, the CliCK-IT EdU Alexa
1708 Fluor 488 imaging protocol (Thermo Fisher Scientific, C10337) was performed for 30 min at
1709 room temperature prior to blocking, according to the manufacturer's instructions. The following
1710 primary antibodies were used: Ki67 (Invitrogen, Clone SolA15, 14-5698-82, [1:200]) and DCX

1711 (Cell Signaling Technologies, 4604 [1:500]). The following secondary antibodies were used:
1712 Donkey anti-Rabbit Alexa 568 (Invitrogen, A10042 [1:500]) and Goat anti-Rat Alexa 647
1713 (Invitrogen, A21247 [1:500]). DAPI (1 mg/mL) (Thermo Fisher, 62248) was included at a
1714 concentration of 1:500 with the secondary antibody mix.
1715
1716 Multiple images tiling the entire length of the ventricle from one sagittal section per animal were
1717 captured with a 20x objective using a Zeiss LSM 900 confocal microscope equipped with Zeiss
1718 ZEN Blue 3.0 software. Images were automatically stitched together using the Zeiss ZEN Blue
1719 3.0 software to create a single image containing the entire SVZ. For immunofluorescence
1720 images (Fig. 3f), brightness and contrast were adjusted in Fiji (v2) to enhance visualization.
1721 These adjustments were performed after all data quantification was complete and the same
1722 settings were applied to all images shown for each experiment.
1723
1724 **Quantification of the location of quiescent and activated NSCs and neuroblasts with**
1725 **respect to the ventricle in sagittal sections**
1726 For quantification of the location of quiescent and activated NSCs and EdU+ aNSCs/NPCs and
1727 EdU+ neuroblasts with respect to the ventricle in sagittal sections, one section containing the
1728 entire rostral migratory stream (RMS) was used for quantification to ensure consistency in the
1729 region being analyzed from animal to animal. Analysis of the SVZ was restricted to the region
1730 that is 200 μm from ventricle wall to not include striatal astrocytes (though the vast majority of
1731 cells were less than 50 μm away from the ventricle wall) (Fig. 3f).
1732

1733 In the staining panel with DAPI, GFAP, Ki67, and Vinculin, GFAP+/Ki67- cells were
1734 considered qNSCs/astrocytes and GFAP+/Ki67+ were considered aNSCs. In staining panel with
1735 DAPI, EdU, Ki67, and DCX, EdU+ cells were classified as aNSCs/NPCs if they were
1736 Ki67+/DCX- and as neuroblasts if they were DCX+ (and either Ki67+ or Ki67-). Quantification
1737 and analysis of distance of qNSCs/astrocytes, aNSCs, EdU+ aNSCs/NPCs, and EdU+
1738 neuroblasts to the ventricle was performed as described above ("*Quantification of the location of*
1739 *quiescent and activated NSCs with respect to the ventricle in coronal sections*").
1740
1741 **Single cell RNA-seq to detect potential ependymal-repairing SVZ astrocytes and reactive**
1742 **astrocytes**
1743 *Ependymal-repairing SVZ astrocytes*
1744 SVZ astrocytes that intercalate into the ependymal lining are GFAP+ and proliferative and can
1745 take on ependymal markers[38,39]. To test if old aNSC populations could contain ependymal-
1746 repairing astrocytes, we performed UMAP analysis on cells from the SVZ neurogenic niche as
1747 previously described[33] on single cell gene expression data of 21,458 single cell transcriptomes of
1748 cells[33] from the SVZ neurogenic niches of 28 mice, tiling ages from young to old using the
1749 Seurat package (v4.0.5)[30]. We examined this dataset first because it contains many ependymal
1750 cells. We filtered for cells expressing markers of ependymal-repairing SVZ astrocytes (*Gfap,*
1751 *S100b, Cd24a,* and *Ctnnb1*)[38,39] using FeaturePlot(min.cutoff = "q10", max.cutoff = "q90")
1752 (Seurat v4.0.5). This identified 4 cells that expressed these 4 markers. All 4 of these cells
1753 clustered with ependymal cells. The presence of these cells did not appear to be dependent on old
1754 age, as these 4 cells were from animals that were, respectively, 4.7, 5.4, 16.83, and 18.87 months
1755 old. We also examined the presence of ependymal-repairing astrocytes in our other single cell

1756 RNA-seq dataset[11] (which has very few ependymal cells), and we also only observed 2 cells
1757 exhibiting markers of ependymal-repairing SVZ astrocytes (out of 14,685 cells), 1 from young
1758 and 1 from old animals. Together, these data suggest that ependymal-repairing SVZ astrocytes
1759 are present but not numerous in the SVZ neurogenic niche of old animals.
1760
1761 *Reactive astrocytes*
1762 To test if any cells in our single cell datasets from the SVZ neurogenic niches of 28 mice[33] or
1763 from young and old SVZ neurogenic niches[11] (described above) expressed markers of reactive
1764 astrocytes, we performed similar UMAP analysis. We used markers of A1 reactive astrocytes
1765 (produced in response to neuroinflammation)[40], A2 reactive astrocytes (produced in response to
1766 ischemia)[40], and pan-injury reactive astrocytes (identified from meta-analysis of 15
1767 transcriptomic reactive astrocyte datasets)[41](see Supplementary Table 8 for full list of gene
1768 markers). We did not detect any cell in either dataset (out of 21,458 cells in one dataset[33] and
1769 14,685 cells in another dataset[11]) that expressed these types of reactive astrocyte markers[40,41]. In
1770 addition, the ependymal-repairing SVZ astrocytes we identified above did not express these
1771 markers.
1772
1773 ***In vivo* EdU-labelling to follow location of cells in subventricular zone, rostral migratory**
1774 **stream, and olfactory bulb**
1775 For these experiments, 12 young (2-3 months) and 12 old (21 months) male C57BL/6 animals
1776 (combined over 2 independent experiments) were intraperitoneally injected with 5-ethynyl-2'-
1777 deoxyuridine (EdU) (Fisher Scientific, A10044) (resuspended in PBS at 5 mg/mL) at a dose of
1778 50 mg/kg either 4 hours, 2 days, or 7 days prior to intracardiac perfusion with 4%

1779 paraformaldehyde (PFA) (Electron Microscopy Sciences, 15714) in PBS. The 5 young (2-3
1780 months) and 5 old (21 months) male C57BL/6 that were intraperitoneally injected with EdU 4
1781 hours before intracardiac perfusion used here were the same as the animals used above in
1782 "*Immunofluorescence staining of SVZ sagittal sections for distance of quiescent and activated*
1783 *NSCs and neuroblasts relative to the ventricle*" and "*Quantification of distance of EdU-positive*
1784 *aNSCs/NPCs and neuroblasts from the ventricle in sagittal sections*". Brains were processed and
1785 immunofluorescence staining of sagittal sections was performed as described above (see
1786 "*Immunofluorescence staining of SVZ sagittal sections for distance of quiescent and activated*
1787 *NSCs and neuroblasts relative to the ventricle*").
1788
1789 Multiple sections per brain, corresponding approximately to image 14 from the Allen Institute
1790 Sagittal Brain Atlas (https://mouse.brain-map.org/static/atlas) were stained and imaged. Sagittal
1791 sections were selected for quantification based on presence of an intact RMS as visualized by a
1792 stream of DCX-positive cells connecting the SVZ to the OB. Very few sections contained a fully
1793 intact RMS and one young 7-day post-injection replicate from the second experiment was
1794 censored due to lack of high-quality sections at the appropriate depth. Images of sagittal sections
1795 were captured using a 5x objective, and 9x3 images (for a total of 27) were automatically
1796 stitched together using the Zeiss ZEN Blue 3.0 software. For quantification, EdU-labelled nuclei
1797 were counted using Fiji (v2)[35]. Every image was converted to 8-bit, the threshold was adjusted
1798 ((90,255) for replicate 1 and (70,255) for replicate 2), watershed was applied to the image and
1799 EdU-labelled nuclei were counted in an automated fashion with "Analyze Particles (size
1800 (micron^2): (20-infinity) for replicate 1 and 2, and circularity: (0.2-1.00) for replicate 1)". EdU-
1801 labelled nuclei were quantified in three regions (along the entire length of the ventricle for SVZ,

1802 the entire length of the RMS, and the entire OB), which were manually defined using a hand-
1803 drawn region of interest (ROI) for each section. Neither imaging nor analysis was performed in a
1804 blinded manner; however, cell counting was performed in an automated manner with the same
1805 thresholding for all images for each replicate. *P*-values were calculated with a two-tailed Mann-
1806 Whitney test. For immunofluorescence images (Fig. 3i,j, Extended Data Fig. 9j), brightness and
1807 contrast were adjusted in Fiji (v2) to enhance visualization. These adjustments were performed
1808 after all data quantification was complete and the same settings were applied to all images shown
1809 for each experiment.
1810
1811 **Quantification of efficiency of EdU incorporation**
1812 We used the same sagittal section images that were quantified above for EdU localization to
1813 SVZ, RMS, and OB (see "*In vivo EdU-labelling to follow location of cells in subventricular*
1814 *zone, rostral migratory stream, and olfactory bulb*"). To calculate EdU labelling efficiency, we
1815 analyzed the number of EdU-labeled nuclei in the SVZ 4 hours after EdU injection. Number of
1816 EdU-labelled nuclei in the SVZ was quantified as described above using Fiji (v2). The number of
1817 Ki67+ cells was quantified in the same region using the same pipeline as counting EdU-labelled
1818 nuclei. See Source Data for thresholding information. The same threshold was applied to all
1819 images captured the same day. To calculate EdU labeling efficiency 4 hours after EdU injection,
1820 the number of EdU+ cells was divided by the total number of Ki67+ in the SVZ in each image.
1821 Neither imaging nor analysis was performed in a blinded manner; however, cell counting was
1822 performed in an automated manner with the same thresholding for all images for each replicate.
1823 *P*-values were calculated with a two-tailed Mann-Whitney test.
1824

1825 **Ingenuity Pathway Analysis (IPA)**

1826 Genes associated with differentially accessible peaks (FDR<0.05) that open in old aNSCs freshly
1827 isolated from the SVZ were uploaded to Ingenuity Pathway Analysis (IPA) (v1.16)[42] (QIAGEN
1828 Inc., https://www.qiagenbioinformatics.com/products/ingenuitypathway-analysis) to identify
1829 age-related regulatory changes (see Supplementary Table 6). For each peak-associated gene, we
1830 uploaded the log fold-change, p-value, and FDR (q-value) and based the IPA analysis on FDR.
1831 Statistical enrichment of pathways was reported with *P*-values calculated by IPA using Fisher's
1832 Exact Test.

1833

1834 **RGD molecular tension sensor FRET measurements of cultured NSCs**

1835 Sensors containing a minimal RGD sequence derived from fibronectin
1836 (TVYAVTGRGDSPASSAA) were expressed, purified, and labeled with AlexaFluor-546 and -
1837 647, and coverslips passivated with maleimide polyethylene glycol (PEG) succinimidyl
1838 carboxymethyl ester (JenKem Technology, A5003-1) were prepared as previously described[43,44].
1839 Flow chambers for imaging were prepared as described[44] with slight modifications. 8-well flow
1840 chambers (Grace BioLabs, #622505, ~55 μL channel volume) were attached to PEGylated
1841 coverslips as previously described[45]. Chambers were incubated with 300 nM double-labeled
1842 sensor at room temperature for 45 min. The chambers were then washed with 150 μL of 1x PBS
1843 for 1 min to prevent non-specific cell attachment. 60 μL of cell suspensions at a density of
1844 300,000-400,000 cells/mL were added to the channels, and the chambers were incubated for 3
1845 hours at 37°C and 5% CO2 in complete activation media to allow time for cells to spread.
1846 Chambers were then washed with 150 μL of warm media, and brightfield and FRET
1847 measurements were made immediately after and acquired with an objective heater (Bioptechs)

1848 set to 37°C. For measurements on cells treated with the ROCK inhibitor Y-27632, complete
1849 activated media was supplemented with 10 μM Y-27632 (dissolved in H_2O) (Tocris, 1254)) for
1850 cell suspensions and media washes.
1851
1852 We limited our measurements and analysis to individual cells that looked well-spread in
1853 brightfield and cell clusters of no more than 5 cells in which cell outlines could be clearly
1854 distinguished. Under conditions used, the vast majority of cells fulfilled the criteria of being
1855 "well-spread in brightfield with cell clusters of no more than 5 cells". FRET fluorescence
1856 measurements were performed with objective-type total internal reflection fluorescence (TIRF)
1857 microscopy on an inverted microscope (Nikon TiE) with an Apo TIRF 100× oil objective lens,
1858 numerical aperture 1.49 (Nikon) as described previously[43] and controlled using Micromanager[46].
1859 Samples were excited with 532-nm (Crystalaser) or 635-nm (Blue Sky Research) lasers. Emitted
1860 light passed through a quad-edge laser-flat dichroic with center/bandwidths of 405/60 nm,
1861 488/100 nm, 532/100 nm, and 635/100 nm from Semrock Inc. (Di01-R405/488/532/635-25×36)
1862 and corresponding quad-pass filter with center/bandwidths of 446/37 nm, 510/20 nm, 581/70 nm,
1863 703/88 nm band-pass filter (FF01-446/510/581/703-25). Donor and acceptor images were taken
1864 through separate additional cubes stacked into the light path (donor: 550 nm long-pass; acceptor:
1865 679/41 nm and 700/75 nm) and recorded on a Hamamatsu Orca Flash 4.0 camera.
1866
1867 Images were prepared in Fiji (v2)[35] and analyzed using custom MATLAB scripts, in which
1868 FRET efficiencies were computed and thresholded to identify adhesions and quantify forces
1869 within adhesions. Adhesions were identified based on FRET values measured using the RGD
1870 tension sensor. FRET efficiencies were computed for each pixel in each image, and regions

1871 exceeding specific FRET efficiencies and area cutoffs were identified as adhesions using a
1872 Watershed algorithm. Forces at adhesions were substantially greater than any signal beneath the
1873 cell body, which is similar to background, consistent with previous force measurements at focal
1874 adhesions[43] (Extended Data Fig. 10g,h).
1875
1876 **Immunofluorescence staining of cultured NSCs treated with ROCK inhibitor**
1877 aNSCs/NPCs were cultured as described above (see *Primary NSC cell culture*) until Passage 2-4
1878 and then passaged with Accutase (STEMCELL Technologies, 07920) and seeded at a density of
1879 5,000 cells per well on Matrigel (Corning, 354230, Lot #0062012, diluted 1:100 in DMEM/F12
1880 (Thermo Fisher Scientific, 11320033))-coated coverslips in 24-well plates with complete
1881 activated or quiescent media with or without 10 μM Y-27632 (dissolved in H_2O) (Tocris, 1254).
1882 After 48 hours, adherent aNSCs/NPCs (with or without 10 μM Y-27632 (dissolved in H_2O)
1883 (Tocris, 1254)) were washed 1x with 1x PBS, then fixed with 4% paraformaldehyde (Electron
1884 Microscopy Sciences, 15714) for 15 min at room temperature. Wells were washed 4x with 1x
1885 PBS and then stored, wrapped in parafilm, at 4°C until immunofluorescence staining. For
1886 quiescent NSCs, cells were plated at the density of 5,000 cells per well in a Matrigel (Corning,
1887 354230, Lot #0062012, diluted 1:100 in DMEM/F12 (Thermo Fisher Scientific, 11320033))-
1888 coated 24-well plate in quiescent media (with or without 10 μM Y-27632). The quiescent media
1889 (with or without 10 μM Y-27632) was replaced every other day for 7 days and qNSCs were then
1890 fixed with 4% paraformaldehyde as described above. Staining and quantification for ALCAM,
1891 focal adhesions (paxillin), and cleaved-caspase3 was performed in the same manner as described
1892 above (see "*Immunofluorescence staining of young and old cultured NSCs*"). Staining for DCX
1893 was performed in the same manner as for ALCAM, paxillin, and cleaved-caspase3.

1894 Quantification for DCX+ cells was performed using CellProfiler (v4.2.1). The function
1895 IdentifyPrimaryObjects was used to identify and count nuclei (DAPI) which served as a seed for
1896 IdentifySecondaryObjects to identify and count cells that were DCX-positive. Antibodies used
1897 were phalloidin (Invitrogen, A12379, 665217, [1:500]), ALCAM/CD166 (Bio-techne, AF1172-
1898 SP, [1:40]), paxillin (Abcam, ab32084, [1:200]), and DCX (Cell Signaling Technologies, 4604
1899 [1:500]) resuspended in 1% BSA (Sigma, A7979). Staining, imaging, and analysis was
1900 performed in a blinded manner. *P*-values were calculated with a two-tailed Mann-Whitney test
1901 comparing sample means. For immunofluorescence images (Fig. 4h), brightness and contrast
1902 were adjusted in Fiji (v2) to enhance visualization. These adjustments were performed after all
1903 data quantification was complete. The same settings were applied to all images shown for each
1904 experiment.
1905
1906 **Osmotic pump surgery for *in vivo* intracerebroventricular delivery of ROCK inhibitor in**
1907 **old mice**
1908 For delivery of ROCK inhibitor in the lateral ventricle of old mice, Y-27632 (ROCKi) (Tocris,
1909 1254) was diluted in artificial CSF (Tocris, 3525) in a total volume of 200 μL to a final
1910 concentration of 100 μM. A concentration of 100 μM was chosen based on a previous study[47].
1911 The diluted Y-27632 or vehicle control (artificial CSF only) were loaded into 200 μL osmotic
1912 pumps (ALZET/Durect, model 2002) with a 14-day infusion rate of 0.5 μL per hour and pumps
1913 were allowed to equilibrate in PBS in a 37°C water bath overnight. Before surgery, mice were
1914 anaesthetized with isofluorane and received post-surgical buprenorphine and saline. Osmotic
1915 pumps were connected to a cannula (ALZET, Brain infusion kit III) and inserted by stereotactic
1916 surgery at +1 mm lateral, −0.3 mm anterior–posterior, and −3mm deep relative to bregma in

1917 order to target the right lateral ventricle of old (20-22 months old) male C57BL/6 mice (8-10
1918 mice per condition (vehicle control or ROCKi), combined over two independent experiments).
1919 The pump connected to the cannula was then placed subcutaneously along the back of the
1920 mouse. Mice were randomized to either the control or the Y-27632 group (ROCKi) prior to
1921 surgery. The day before surgery, mice were singly-housed and cage-mates were separated across
1922 experimental conditions. We alternated performing the surgery between control and Y-27632
1923 mice to avoid batch effect.
1924
1925 One week after start of drug delivery, mice were intraperitoneally injected with 5-ethynyl-2'-
1926 deoxyuridine (EdU) (Fisher Scientific, A10044) (resuspended in 1x PBS at 5 mg/mL) at a dose
1927 of 50 mg/kg either 4 hours or 7 days prior to intracardiac perfusion with 4% paraformaldehyde
1928 (PFA) (Electron Microscopy Sciences, 15714) in PBS.
1929
1930 **Quantification of distance of NSCs relative to ventricle and of location of EdU+ cells in**
1931 **different locations in old mice treated with ROCK inhibitor**
1932 Quantification of sagittal distance of aNSCs/NPCs was performed as described above in
1933 "*Quantification of the location of quiescent and activated NSCs and neuroblasts with respect to*
1934 *the ventricle in sagittal sections*", except that all Ki67+/DCX- cells were counted as
1935 aNSCs/NPCs (rather than filtering first by cells that are EdU-positive) and images were captured
1936 with the 60x objective of a Nikon Eclipse Ti confocal microscope equipped with a Zyla sCMOS
1937 camera (Andor) and NIS- Elements software (AR 4.30.02, 64-bit). *P*-values were calculated with
1938 a two-tailed Mann-Whitney test comparing sample means.
1939

1940 For quantification of number of EdU cells in the entire SVZ (along the entire ventricle), entire
1941 length of the RMS, and entire OB, sagittal sections were immunostained, imaged, and analyzed
1942 as described above in "*In vivo EdU-labelling to follow location of cells in SVZ, RMS, and OB*"
1943 except analysis of EdU-positive cell localization (in SVZ, RMS, or OB) was performed in a
1944 blinded manner.
1945
1946 Brain sections adjacent to the ones used for quantification of number of EdU cells in the entire
1947 SVZ, entire RMS, and entire OB were immunostained as described above in
1948 "*Immunofluorescence staining of SVZ sagittal sections for distance of quiescent and activated*
1949 *NSCs and neuroblasts relative to the ventricle*". The following primary antibodies were used:
1950 DCX (Cell Signaling Technologies, 4604 [1:500]) and NeuN (Millipore, Clone A60, MAB377,
1951 2919670 [1:500]). The following secondary antibodies were used: Donkey anti-Rabbit Alexa 647
1952 (Invitrogen, A31573 [1:500]) and Donkey anti-Mouse Alexa 568 (Invitrogen, A10037 [1:500]).
1953 DAPI (1 mg/mL) (Thermo Fisher, 62248) was included at a concentration of 1:500 with the
1954 secondary antibody mix. Images of EdU-positive cells in the OB were captured with the 60x
1955 objective of a Nikon Eclipse Ti confocal microscope equipped with a Zyla sCMOS camera
1956 (Andor) and NIS- Elements software (AR 4.30.02, 64-bit). For immunofluorescence images (Fig.
1957 5e,h,l), brightness and contrast were adjusted in Fiji (v2) to enhance visualization. These
1958 adjustments were performed after all data quantification was complete and the same settings
1959 were applied to all images shown for each experiment.
1960
1961
1962

1963 **Statistical analyses**

1964 For all experiments, young and old conditions were processed in an alternate manner rather than
1965 in two large groups, to minimize the group effect. We did not perform power analyses, though
1966 we did take into account previous experiments to determine the number of animals needed. To
1967 calculate statistical significance for experiments, all tests were two-sided Mann-Whitney tests
1968 (with the exception of Fisher's Exact Tests and Wilcoxon Matched-Pairs Signed Ranks Tests
1969 which are noted in Figure Legends). Results from individual experiments and all statistical
1970 analyses are included in Source Data.

1971

1972

1973 **References**

1974

1975 1. Zhuo, L. *et al.* Live astrocytes visualized by green fluorescent protein in transgenic mice.
1976 *Dev Biol* **187**, 36-42 (1997).
1977 2. Platt, R.J. *et al.* CRISPR-Cas9 knockin mice for genome editing and cancer modeling.
1978 *Cell* **159**, 440-55 (2014).
1979 3. Leeman, D.S. *et al.* Lysosome activation clears aggregates and enhances quiescent neural
1980 stem cell activation during aging. *Science* **359**, 1277-1283 (2018).
1981 4. Codega, P. *et al.* Prospective identification and purification of quiescent adult neural stem
1982 cells from their in vivo niche. *Neuron* **82**, 545-59 (2014).
1983 5. Dulken, B.W., Leeman, D.S., Boutet, S.C., Hebestreit, K. & Brunet, A. Single-Cell
1984 Transcriptomic Analysis Defines Heterogeneity and Transcriptional Dynamics in the
1985 Adult Neural Stem Cell Lineage. *Cell Rep* **18**, 777-790 (2017).
1986 6. Beckervordersandforth, R. *et al.* In vivo fate mapping and expression analysis reveals
1987 molecular hallmarks of prospectively isolated adult neural stem cells. *Cell Stem Cell* **7**,
1988 744-58 (2010).
1989 7. Buenrostro, J.D., Giresi, P.G., Zaba, L.C., Chang, H.Y. & Greenleaf, W.J. Transposition
1990 of native chromatin for fast and sensitive epigenomic profiling of open chromatin, DNA-
1991 binding proteins and nucleosome position. *Nat Methods* **10**, 1213-8 (2013).
1992 8. Conover, J.C. & Shook, B.A. Aging of the subventricular zone neural stem cell niche.
1993 *Aging Dis* **2**, 49-63 (2011).

9. Maslov, A.Y., Barone, T.A., Plunkett, R.J. & Pruitt, S.C. Neural stem cell detection, characterization, and age-related changes in the subventricular zone of mice. *J Neurosci* **24**, 1726-33 (2004).
10. Kalamakis, G. *et al.* Quiescence Modulates Stem Cell Maintenance and Regenerative Capacity in the Aging Brain. *Cell* **176**, 1407-1419 e14 (2019).
11. Dulken, B.W. *et al.* Single-cell analysis reveals T cell infiltration in old neurogenic niches. *Nature* **571**, 205-210 (2019).
12. Martynoga, B. *et al.* Epigenomic enhancer annotation reveals a key role for NFIX in neural stem cell quiescence. *Genes Dev* **27**, 1769-86 (2013).
13. Shen, L., Shao, N., Liu, X. & Nestler, E. ngs.plot: Quick mining and visualization of next-generation sequencing data by integrating genomic databases. *BMC Genomics* **15**, 284 (2014).
14. Stark, R.B., G.D. DiffBind: differential binding analysis of ChIP-seq peak data. *Bioconductor* (2011).
15. Ross-Innes, C.S. *et al.* Differential oestrogen receptor binding is associated with clinical outcome in breast cancer. *Nature* **481**, 389-93 (2012).
16. Yu, G., Wang, L.G. & He, Q.Y. ChIPseeker: an R/Bioconductor package for ChIP peak annotation, comparison and visualization. *Bioinformatics* **31**, 2382-3 (2015).
17. Love, M.I., Huber, W. & Anders, S. Moderated estimation of fold change and dispersion for RNA-seq data with DESeq2. *Genome Biol* **15**, 550 (2014).
18. Robinson, M.D., McCarthy, D.J. & Smyth, G.K. edgeR: a Bioconductor package for differential expression analysis of digital gene expression data. *Bioinformatics* **26**, 139-40 (2010).
19. McCarthy, D.J., Chen, Y. & Smyth, G.K. Differential expression analysis of multifactor RNA-Seq experiments with respect to biological variation. *Nucleic Acids Res* **40**, 4288-97 (2012).
20. Schep, A.N. *et al.* Structured nucleosome fingerprints enable high-resolution mapping of chromatin architecture within regulatory regions. *Genome Res* **25**, 1757-70 (2015).
21. Chen, E.Y. *et al.* Enrichr: interactive and collaborative HTML5 gene list enrichment analysis tool. *BMC Bioinformatics* **14**, 128 (2013).
22. Kuleshov, M.V. *et al.* Enrichr: a comprehensive gene set enrichment analysis web server 2016 update. *Nucleic Acids Res* **44**, W90-7 (2016).
23. Avsec, Z. *et al.* Base-resolution models of transcription-factor binding reveal soft motif syntax. *Nat Genet* **53**, 354-366 (2021).
24. Trevino, A.E. *et al.* Chromatin and gene-regulatory dynamics of the developing human cerebral cortex at single-cell resolution. *Cell* **184**, 5053-5069 e23 (2021).
25. Lundberg, S. & Lee, S. A Unified Approach to Interpreting Model Predictions. *arxiv*, arXiv:1705.07874 (2017).
26. Shrikumar, A., Greenside, P. & Kundaje, A. Learning Important Features Through Propagating Activation Differences. in *Proceedings of the 34th International Conference on Machine Learning* Vol. 70 (eds Doina, P. & Yee Whye, T.) 3145--3153 (PMLR, Proceedings of Machine Learning Research, 2017).
27. Shrikumar, A. *et al.* Technical Note on Transcription Factor Motif Discovery from Importance Scores (TF-MoDISco) version 0.5.6.5. arXiv:1811.00416 (2018).

2038 28. Kulakovskiy, I.V. *et al.* HOCOMOCO: towards a complete collection of transcription
2039 factor binding models for human and mouse via large-scale ChIP-Seq analysis. *Nucleic*
2040 *Acids Res* **46**, D252-D259 (2018).
2041 29. Gupta, S., Stamatoyannopoulos, J.A., Bailey, T.L. & Noble, W.S. Quantifying similarity
2042 between motifs. *Genome Biol* **8**, R24 (2007).
2043 30. Stuart, T. *et al.* Comprehensive Integration of Single-Cell Data. *Cell* **177**, 1888-1902 e21
2044 (2019).
2045 31. Dominguez Conde, C. *et al.* Cross-tissue immune cell analysis reveals tissue-specific
2046 features in humans. *Science* **376**, eabl5197 (2022).
2047 32. Tabula Muris, C. A single-cell transcriptomic atlas characterizes ageing tissues in the
2048 mouse. *Nature* **583**, 590-595 (2020).
2049 33. Buckley, M.T. *et al.* Cell type-specific aging clocks to quantify aging and rejuvenation in
2050 regenerative regions of the brain. *bioRxiv* (2022).
2051 34. Liu, L. *et al.* Exercise reprograms the inflammatory landscape of multiple stem cell
2052 compartments during mammalian aging. *bioRxiv* (2022).
2053 35. Schindelin, J. *et al.* Fiji: an open-source platform for biological-image analysis. *Nat*
2054 *Methods* **9**, 676-82 (2012).
2055 36. Conant, D. *et al.* Inference of CRISPR Edits from Sanger Trace Data. *CRISPR J* **5**, 123-
2056 130 (2022).
2057 37. Morgens, D.W. *et al.* Genome-scale measurement of off-target activity using Cas9
2058 toxicity in high-throughput screens. *Nat Commun* **8**, 15178 (2017).
2059 38. Luo, J., Shook, B.A., Daniels, S.B. & Conover, J.C. Subventricular zone-mediated
2060 ependyma repair in the adult mammalian brain. *J Neurosci* **28**, 3804-13 (2008).
2061 39. Luo, J., Daniels, S.B., Lennington, J.B., Notti, R.Q. & Conover, J.C. The aging
2062 neurogenic subventricular zone. *Aging Cell* **5**, 139-52 (2006).
2063 40. Liddelow, S.A. & Barres, B.A. Reactive Astrocytes: Production, Function, and
2064 Therapeutic Potential. *Immunity* **46**, 957-967 (2017).
2065 41. Das, S., Li, Z., Noori, A., Hyman, B.T. & Serrano-Pozo, A. Meta-analysis of mouse
2066 transcriptomic studies supports a context-dependent astrocyte reaction in acute CNS
2067 injury versus neurodegeneration. *J Neuroinflammation* **17**, 227 (2020).
2068 42. Kramer, A., Green, J., Pollard, J., Jr. & Tugendreich, S. Causal analysis approaches in
2069 Ingenuity Pathway Analysis. *Bioinformatics* **30**, 523-30 (2014).
2070 43. Chang, A.C. *et al.* Single Molecule Force Measurements in Living Cells Reveal a
2071 Minimally Tensioned Integrin State. *ACS Nano* **10**, 10745-10752 (2016).
2072 44. Tan, S.J. *et al.* Regulation and dynamics of force transmission at individual cell-matrix
2073 adhesion bonds. *Sci Adv* **6**, eaax0317 (2020).
2074 45. Morimatsu, M., Mekhdjian, A.H., Chang, A.C., Tan, S.J. & Dunn, A.R. Visualizing the
2075 interior architecture of focal adhesions with high-resolution traction maps. *Nano Lett* **15**,
2076 2220-8 (2015).
2077 46. Edelstein, A.D. *et al.* Advanced methods of microscope control using muManager
2078 software. *J Biol Methods* **1**(2014).
2079 47. Leong, S.Y., Faux, C.H., Turbic, A., Dixon, K.J. & Turnley, A.M. The Rho kinase
2080 pathway regulates mouse adult neural precursor cell migration. *Stem Cells* **29**, 332-43
2081 (2011).
2082

Figure 1

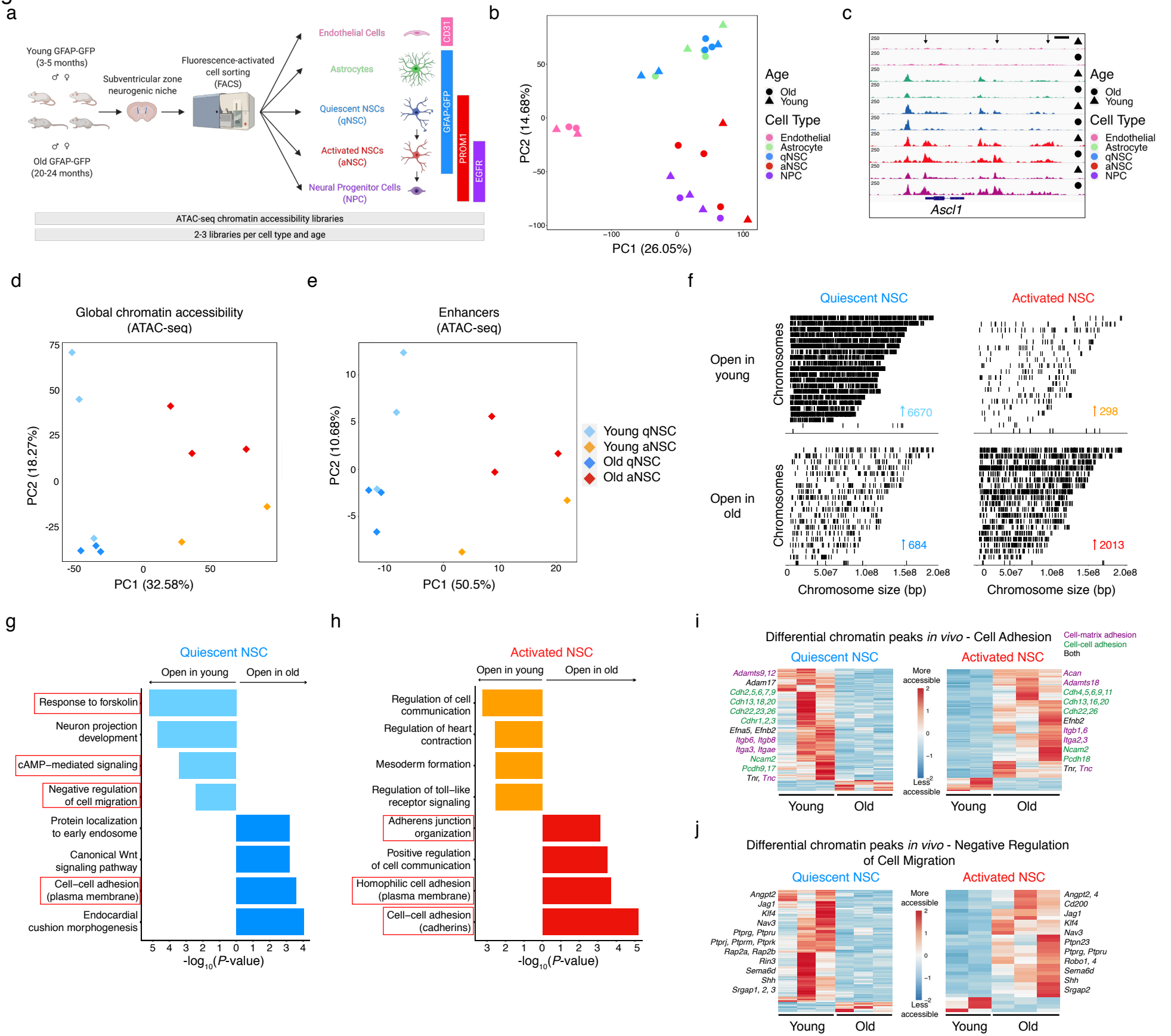
a
Young GFAP-GFP
(3-5 months)
Subventricular zone
neurogenic niche
Fluorescence-activated
cell sorting
(FACS)
Old GFAP-GFP
(20-24 months)
Endothelial Cells
Astrocytes
Quiescent NSCs
(qNSC)
Activated NSCs
(aNSC)
Neural Progenitor Cells
(NPC)
CD31
GFAP-GFP
PROM1
EGFR
ATAC-seq chromatin accessibility libraries
2-3 libraries per cell type and age
b
PC2 (14.68%)
PC1 (26.05%)
Age
Old
Young
Cell Type
Endothelial
Astrocyte
qNSC
aNSC
NPC
c
Ascl1
Age
Old
Young
Cell Type
Endothelial
Astrocyte
qNSC
aNSC
NPC
d
Global chromatin accessibility
(ATAC-seq)
PC2 (18.27%)
PC1 (32.58%)
e
Enhancers
(ATAC-seq)
PC2 (10.68%)
PC1 (50.5%)
Young qNSC
Young aNSC
Old qNSC
Old aNSC
f
Quiescent NSC
Activated NSC
Open in young
Open in old
Chromosomes
6670
298
684
2013
Chromosome size (bp)
g
Quiescent NSC
Open in young
Open in old
Response to forskolin
Neuron projection development
cAMP–mediated signaling
Negative regulation of cell migration
Protein localization to early endosome
Canonical Wnt signaling pathway
Cell–cell adhesion (plasma membrane)
Endocardial cushion morphogenesis
-log10(P-value)
h
Activated NSC
Open in young
Open in old
Regulation of cell communication
Regulation of heart contraction
Mesoderm formation
Regulation of toll–like receptor signaling
Adherens junction organization
Positive regulation of cell communication
Homophilic cell adhesion (plasma membrane)
Cell–cell adhesion (cadherins)
-log10(P-value)
i
Differential chromatin peaks in vivo - Cell Adhesion
Cell-matrix adhesion
Cell-cell adhesion
Both
Quiescent NSC
Activated NSC
Adamts9,12
Adam17
Cdh2,5,6,7,9
Cdh13,18,20
Cdh22,23,26
Cdhr1,2,3
Efna5, Efnb2
Itgb6, Itgb8
Itga3, Itgae
Ncam2
Pcdh9,17
Tnr, Tnc
More accessible
Less accessible
Acan
Adamts18
Cdh4,5,6,9,11
Cdh13,16,20
Cdh22,26
Efnb2
Itgb1,6
Itga2,3
Ncam2
Pcdh18
Tnr, Tnc
Young
Old
j
Differential chromatin peaks in vivo - Negative Regulation of Cell Migration
Quiescent NSC
Activated NSC
Angpt2
Jag1
Klf4
Nav3
Ptprg, Ptpru
Ptprj, Ptprm, Ptprk
Rap2a, Rap2b
Rin3
Sema6d
Shh
Srgap1, 2, 3
More accessible
Less accessible
Angpt2, 4
Cd200
Jag1
Klf4
Nav3
Ptpn23
Ptprg, Ptpru
Robo1, 4
Sema6d
Shh
Srgap2
Young
Old

Figure 1: Chromatin profiling of five cell types freshly isolated from the SVZ neurogenic region reveals opposing changes with age in quiescent and activated NSCs involving cell adhesion and migration pathways

a, Experimental design for freshly isolating cells from the subventricular zone (SVZ) neurogenic niche in young (3-5 months) and old (20-24 months) GFAP-GFP mice. For each library, 800-2000 cells were pooled from male and female GFAP-GFP mice using fluorescence-activated cell sorted (FACS) with different markers (see Methods). qNSC, quiescent neural stem cell. aNSC, activated neural stem cell. NPC, neural progenitor cell. GFAP, glial fibrillary acidic protein. PROM1, Prominin-1. EGFR, epidermal growth factor receptor. CD31, endothelial cell marker. **b,** Principal Component Analysis (PCA) on all chromatin peaks from endothelial cells, astrocytes, quiescent NSCs (qNSC), activated NSCs (aNSC), and neural progenitor cells (NPC) freshly isolated from the SVZ of young (triangle) and old (round) GFAP-GFP mice where each dot represents a single ATAC-seq library. PCA was generated using the variance stabilizing transformation (VST)-normalized global consensus count matrix. PC, principal component. **c,** Genome browser (IGV) view of chromatin accessibility signal tracks from representative RPKM-normalized libraries of all SVZ niche cell types around the *Ascl1* loci. Black arrows represent sites of differentially accessible peaks that open in young aNSCs when compared to young qNSCs. *Ascl1*, Achaete-Scute Family bHLH Transcription Factor 1. Scale bar, 1kb. **d,** PCA on all genome-wide chromatin peaks from qNSCs and aNSCs freshly isolated from the young and old SVZ where each dot represents a single sequencing library (PC1 vs. PC2). PCA was generated using variance stabilizing transformation (VST)-normalized read counts. PC, principal component. **e,** PCA on chromatin peaks that overlap with marks of enhancers (H3K27ac and p300 binding) from qNSCs and aNSCs freshly isolated from the young and old SVZ where each dot represents a single ATAC-seq library (PC1 vs. PC2). PCA was generated using the variance stabilizing transformation (VST)-normalized NSC consensus count matrix. PC, principal component. **f,** Chromosome-level visualization of differentially accessible ATAC-seq peaks (FDR<0.05) that change with age in quiescent NSC (left) and activated NSC (right) respectively. Each vertical bar represents a dynamic ATAC-seq peak aligned to mouse chromosomes (*mm10* version of the mouse genome) that is differentially open in young (top) or old (bottom) NSCs. **g,h,** Selected GO terms for genes associated with differentially accessible ATAC-seq peaks (FDR<0.05) that change with age in quiescent **(g)** and activated **(h)** NSCs generated by EnrichR and ranked by *P*-value. ATAC-seq peaks were annotated with their nearest gene using ChIPSeeker (v1.18.0). Red boxes indicate GO terms associated with adhesion and migration. **i,** Heatmap showing accessibility levels of differential ATAC-seq peaks associated with the "Cell Adhesion" GO category (GO:0007155) that change with age in quiescent NSC (left) and activated NSC (right) respectively. Selected gene names with associated differentially accessible peaks are displayed. TMM-normalized read counts (by EdgeR), scaled row-wise. Genes names colored according to their classification on AmiGO as cell-matrix adhesion genes (purple), cell-cell adhesion genes (green), or both (black). **j,** Heatmap showing accessibility levels of differential ATAC-seq peaks associated with the "Negative Regulation of Cell Migration" GO category (GO:0030336) that change with age in quiescent NSC (left) and activated NSC (right) respectively. Selected gene names with associated differentially accessible peaks are displayed. TMM-normalized read counts (by EdgeR), scaled row-wise.

Figure 2

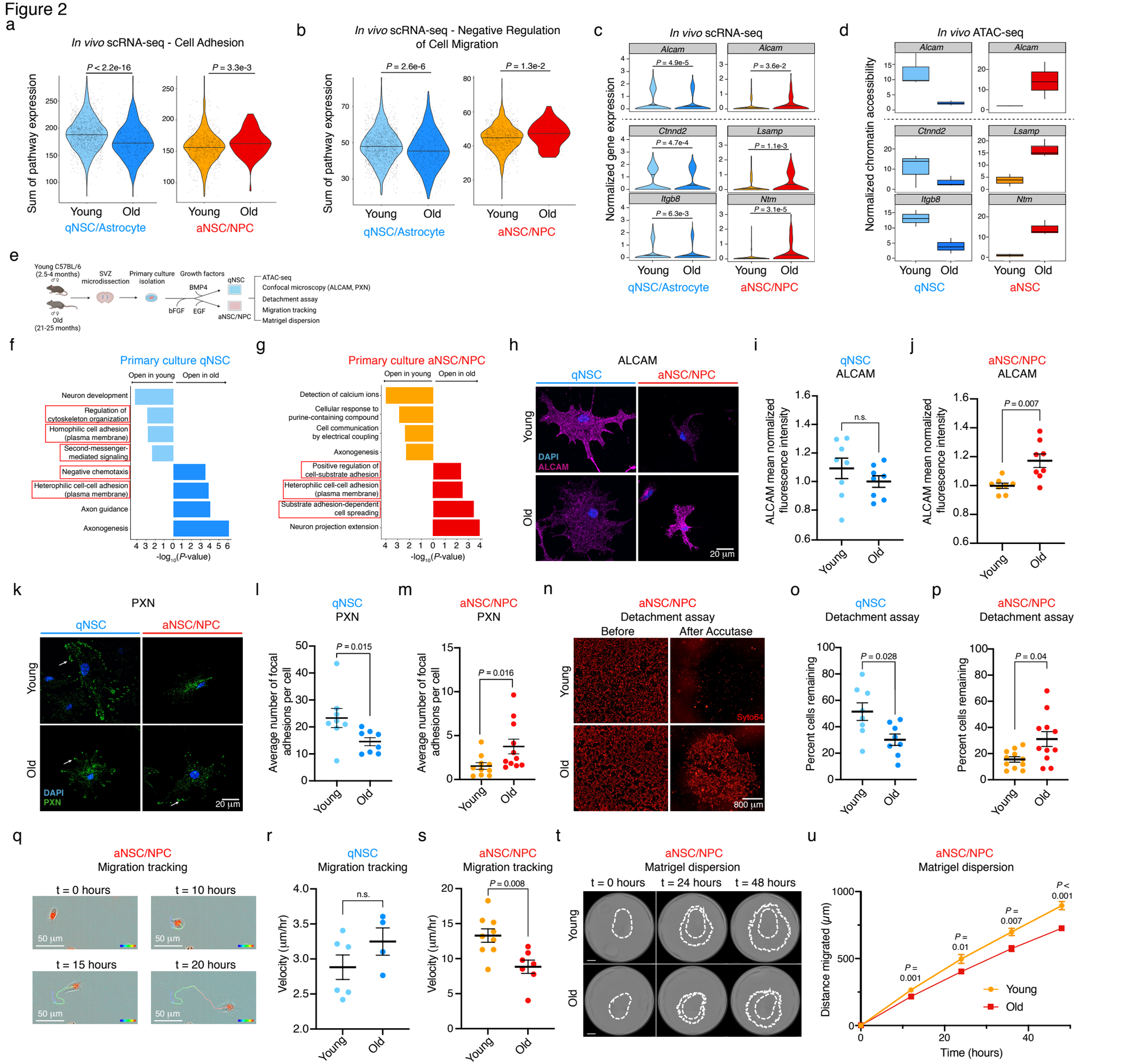
a
In vivo scRNA-seq - Cell Adhesion
P < 2.2e-16
P = 3.3e-3
Sum of pathway expression
Young
Old
qNSC/Astrocyte
aNSC/NPC
b
In vivo scRNA-seq - Negative Regulation of Cell Migration
P = 2.6e-6
P = 1.3e-2
c
In vivo scRNA-seq
Alcam
Ctnnd2
Itgb8
Lsamp
Ntm
P = 4.9e-5
P = 3.6e-2
P = 4.7e-4
P = 1.1e-3
P = 6.3e-3
P = 3.1e-5
Normalized gene expression
d
In vivo ATAC-seq
Normalized chromatin accessibility
qNSC
aNSC
e
Young C57BL/6 (2.5-4 months)
Old (21-25 months)
SVZ microdissection
Primary culture isolation
Growth factors
BMP4
bFGF
EGF
ATAC-seq
Confocal microscopy (ALCAM, PXN)
Detachment assay
Migration tracking
Matrigel dispersion
f
Primary culture qNSC
Open in young
Open in old
Neuron development
Regulation of cytoskeleton organization
Homophilic cell adhesion (plasma membrane)
Second-messenger-mediated signaling
Negative chemotaxis
Heterophilic cell-cell adhesion (plasma membrane)
Axon guidance
Axonogenesis
-log10(P-value)
g
Primary culture aNSC/NPC
Detection of calcium ions
Cellular response to purine-containing compound
Cell communication by electrical coupling
Axonogenesis
Positive regulation of cell-substrate adhesion
Heterophilic cell-cell adhesion (plasma membrane)
Substrate adhesion-dependent cell spreading
Neuron projection extension
h
ALCAM
DAPI
ALCAM
20 µm
i
qNSC
ALCAM
ALCAM mean normalized fluorescence intensity
n.s.
j
aNSC/NPC
ALCAM
P = 0.007
k
PXN
DAPI
PXN
20 µm
l
qNSC
PXN
Average number of focal adhesions per cell
P = 0.015
m
aNSC/NPC
PXN
P = 0.016
n
aNSC/NPC
Detachment assay
Before
After Accutase
Syto64
800 µm
o
qNSC
Detachment assay
Percent cells remaining
P = 0.028
p
aNSC/NPC
Detachment assay
P = 0.04
q
aNSC/NPC
Migration tracking
t = 0 hours
t = 10 hours
t = 15 hours
t = 20 hours
50 µm
r
qNSC
Migration tracking
Velocity (µm/hr)
n.s.
s
aNSC/NPC
Migration tracking
P = 0.008
t
aNSC/NPC
Matrigel dispersion
t = 0 hours
t = 24 hours
t = 48 hours
u
aNSC/NPC
Matrigel dispersion
Distance migrated (µm)
P = 0.001
P = 0.01
P = 0.007
P < 0.001
Time (hours)

Figure 2: Opposing chromatin changes in quiescent and activated NSCs during aging are associated with gene expression changes and functional defects in cell adhesion and migration
a,b, Violin plots of the distribution of single cell cumulative expression profiles of genes within the "Cell Adhesion" GO category (GO:0007155) **(a)** and "Negative Regulation of Cell Migration" GO category (GO:0030336) **(b)** for young and old qNSCs/Astrocytes (left) and aNSCs/NPCs (right) from single cell RNA-seq data (see Methods). Each dot represents the cumulative expression of genes within the GO category in a single cell. *P*-values were calculated using a two-tailed Mann-Whitney test. **c,** Violin plots of select cell adhesion gene expression profiles that change with age for young and old qNSCs/Astrocytes (left) and aNSCs/NPCs (right) from single cell RNA-seq data (see Methods). Gene above dotted line is example of gene that is shared between qNSCs/Astrocytes and aNSCs/NPCs and genes below dotted line are examples of genes that are not shared between qNSCs/Astrocytes and aNSCs/NPCs. *P*-values were calculated using a two-tailed Mann-Whitney test. **d,** Boxplots of TMM-normalized chromatin accessibility changes in differentially accessible peaks near cell adhesion genes from (c) for young and old qNSCs/Astrocytes (left) and aNSCs/NPCs (right) freshly isolated from the SVZ. Gene above dotted line is example of gene that is shared between qNSCs/Astrocytes and aNSCs/NPCs and genes below dotted line are examples of genes that are not shared between qNSCs/Astrocytes and aNSCs/NPCs. Boxplot displays median and lower and upper quartile values. **e,** Schematic for experiments in primary cultures of qNSCs and aNSCs/NPCs. Young (2.5-4 months) and old (21-25 months) C57BL/6 SVZs were microdissected and processed for primary NSC culture. Cultures were maintained and expanded as aNSCs/NPCs with bFGF and EGF growth factors (low passage) and quiescence (for qNSCs) was induced with bFGF and BMP4 growth factors for 5-10 days for all *in vitro* experiments (ATAC-seq, confocal microscopy, detachment assay, and live-cell migration tracking). Mixed male and female mice were used for ATAC-seq experiments on primary NSC culture (similar to the animals used for the *in vivo* design, Fig. 1a). Male mice were used for other primary NSC culture experiments. **f,g,** Selected GO terms for genes associated with differentially accessible ATAC-seq peaks (FDR<0.05) that change with age in primary cultures of qNSCs **(f)** and aNSCs/NPCs **(g)** generated by EnrichR and ranked by *P*-value. Red boxes indicate GO terms associated with cell adhesion and cell migration. **h,** Representative images of immunofluorescence staining for ALCAM of young (2.5-3 months) and old (21-22.1 months) qNSCs (left) and aNSCs/NPCs (right) cultured on Matrigel. Purple, ALCAM (transmembrane glycoprotein involved in cell-cell adhesion); Blue, DAPI (nuclei). Scale bar, 20 μm. **i,j,** Quantification of ALCAM mean normalized fluorescence intensity of young (2.5-3 months) and old (21-22.1 months) qNSCs **(i)** and aNSCs/NPCs **(j)** on Matrigel. Each dot represents mean normalized fluorescence intensity of 30 fields (each containing 1-3 cells) in a primary culture derived from an individual mouse, normalized by experiment and cell size. $n = 8$ young male mice, and $n = 8$ old male mice, combined over 2 (qNSCs) or 3 (aNSCs/NPCs) independent experiments. Data are mean ± SEM. *P*-values were calculated using a two-tailed Mann-Whitney test. Data from independent experiments are in Source Data. **k,** Representative images of immunofluorescence staining for paxillin (PXN) of young (2.5-3 months) and old (21-22.1 months) qNSCs (left) and aNSCs/NPCs (right) cultured on Matrigel. Green, paxillin (PXN, focal adhesions); Blue, DAPI (nuclei). White arrow indicates localization of PXN to peripheral focal adhesions. Scale bar, 20 μm. **l,m,** Quantification of PXN immunostaining of young (2.5-3 months) and old (22.1-22.1 months) qNSCs **(l)** and aNSCs/NPCs **(m)** cultured on Matrigel. Each dot represents average number of focal adhesions per cell (28-32 cells per dot) in a primary culture derived from an individual mouse. $n = 8$ young male mice, and $n = 8$ old male mice (qNSCs), $n = 10$ young male mice, and $n = 11$ old male mice (aNSCs/NPCs), combined over 2 (qNSC) or 3 (aNSCs/NPCs) independent experiments. Data are mean ± SEM. *P*-values were calculated using a two-tailed Mann-

Whitney test. Data from independent experiments are in Source Data. **n,** Representative images of young (3 months) and old (21 months) aNSCs/NPCs in the presence of cell-permeant red fluorescent nucleic acid stain Syto64 cultured on Poly-D-Lysine taken before (left) and after (right) a 5 minute incubation with Accutase and wash with 1x PBS. The Incucyte S3 system was used for 4x whole-well imaging. Incucyte S3 built-in analysis software was used for cell counts for percent cells remaining after Accutase (or Trypsin for qNSCs) treatment. Scale bar, 800 μm. **o,** Quantification of percent cells remaining of young (3-4 months) and old (21-25 months) qNSCs cultured on Poly-D-Lysine after a 15 minute incubation with trypsin and wash with 1x PBS. Each dot represents average percent cells remaining after trypsin treatment of 2-4 technical replicates (each plated at a density of 10,000 cells) per primary culture derived from an individual mouse. $n = 8$ young male mice and $n = 8$ old male mice combined over 2 independent experiments. Data are mean ± SEM. *P*-values were calculated using a two-tailed Mann-Whitney test. Data from independent experiments are in Source Data. **p,** Percent cells remaining of young (2.5-4 months) and old (21-22.1 months) aNSCs/NPCs cultured on Poly-D-Lysine after 5 minute incubation with Accutase and wash with 1x PBS. Each dot represents average percent cells remaining after Accutase treatment of 2-4 technical replicates (each plated at a density of 30,000 cells) per primary culture derived from an individual mouse. $n = 11$ young male mice, and $n = 11$ old male mice, combined over 6 experiments. Data are mean ± SEM. *P*-values were calculated using a two-tailed Mann-Whitney test. Data from independent experiments are in Source Data. **q,** Representative images of a young (3-4 months) aNSC/NPC taken at t = 0, 10, 15, and 20 hours after plating onto Poly-D-Lysine. The Incucyte system was used for 20x imaging and migration tracks were determined using Imaris (v9.3.0). Color gradient bar represents the passage of time from 0 (blue) to 20 (red) hours. Scale bar, 50 μm. **r,** Migration speed of young (3-4 months) and old (23-24 months) qNSCs on Poly-D-Lysine. Each dot represents the average velocity over a 20-hour period of 5-42 cells in a primary culture derived from an individual mouse. $n = 6$ young male mice and $n = 4$ old male mice, combined over 2 independent experiments. Data are mean ± SEM. *P*-values were calculated using a two-tailed Mann-Whitney test. Data from independent experiments are in Source Data. **s,** Migration speed of young (3-4 months) and old (21-24 months) aNSCs/NPCs on Poly-D-Lysine. Each dot represents the average velocity per mouse over a 20-hour period of 6-28 cells. $n = 9$ young male mice and $n = 7$ old male mice, combined over 3 independent experiments. Data are mean ± SEM. *P*-values were calculated using a two-tailed Mann-Whitney test. Data from independent experiments are in Source Data. **t,** Representative images of young (top) and old (bottom) aNSC/NPC dispersion through Matrigel taken 0, 24, and 48 hours after plating aNSCs/NPCs. The dotted white outline represents the outermost extent of invasion and the inner dotted white line represents the initial extent of the cells after plating (t = 0 hours). Scale bar, 800 μm. **u,** Migration distance timecourse of young (3-4 months) and old (21-24 months) aNSC/NPC dispersion through Matrigel over 48 hours with 12-hour intervals. At each timepoint, dispersion distance of aNSC cultures was averaged over 1-4 technical replicates (each seeded with 50,000 cells) from a primary culture derived from an individual mouse. $n = 7$ young male mice, and $n = 10$ old male mice, combined over 2 independent experiments. Data are mean ± SEM. *P*-values were calculated at each timepoint using a two-tailed Mann-Whitney test. Data from independent experiments are in Source Data.

Figure 3

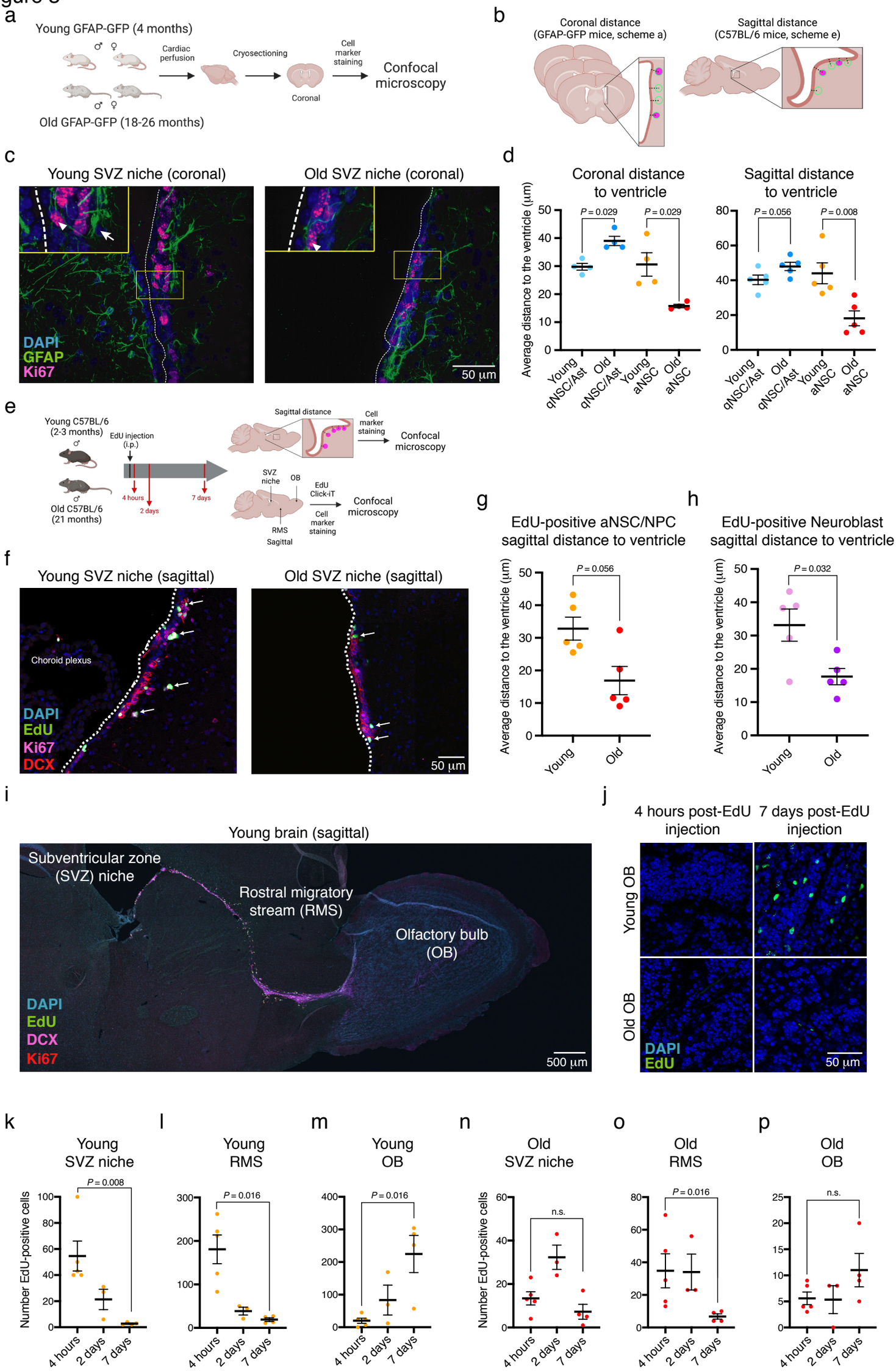
a
Young GFAP-GFP (4 months)
Cardiac perfusion
Cryosectioning
Cell marker staining
Confocal microscopy
Coronal
Old GFAP-GFP (18-26 months)
b
Coronal distance (GFAP-GFP mice, scheme a)
Sagittal distance (C57BL/6 mice, scheme e)
c
Young SVZ niche (coronal)
Old SVZ niche (coronal)
DAPI
GFAP
Ki67
50 µm
d
Coronal distance to ventricle
Sagittal distance to ventricle
Average distance to the ventricle (µm)
P = 0.029
P = 0.029
P = 0.056
P = 0.008
Young qNSC/Ast
Old qNSC/Ast
Young aNSC
Old aNSC
e
Young C57BL/6 (2-3 months)
EdU injection (i.p.)
4 hours
2 days
7 days
Old C57BL/6 (21 months)
Sagittal distance
Cell marker staining
Confocal microscopy
SVZ niche
OB
RMS
Sagittal
EdU Click-iT
Cell marker staining
Confocal microscopy
f
Young SVZ niche (sagittal)
Old SVZ niche (sagittal)
Choroid plexus
DAPI
EdU
Ki67
DCX
50 µm
g
EdU-positive aNSC/NPC sagittal distance to ventricle
Average distance to the ventricle (µm)
P = 0.056
Young
Old
h
EdU-positive Neuroblast sagittal distance to ventricle
Average distance to the ventricle (µm)
P = 0.032
Young
Old
i
Young brain (sagittal)
Subventricular zone (SVZ) niche
Rostral migratory stream (RMS)
Olfactory bulb (OB)
DAPI
EdU
DCX
Ki67
500 µm
j
4 hours post-EdU injection
7 days post-EdU injection
Young OB
Old OB
DAPI
EdU
50 µm
k
Young SVZ niche
Number EdU-positive cells
P = 0.008
4 hours
2 days
7 days
l
Young RMS
P = 0.016
m
Young OB
P = 0.016
n
Old SVZ niche
Number EdU-positive cells
n.s.
o
Old RMS
P = 0.016
p
Old OB
n.s.

Figure 3: Age-dependent location defects of quiescent and activated NSCs and progeny *in vivo* in the niche, the rostral migratory stream, and the olfactory bulb

a, Design of immunofluorescence experiments for quantifying the location of qNSCs/astrocytes and aNSCs *in vivo* during aging in coronal brain sections. Young (4 months) and old (18-26 months) mixed-sex GFAP-GFP animals were perfused with 4% PFA, brains were cryosectioned at a thickness of 16 μm and stained for cell markers prior to quantification with confocal microscopy. **b,** Schematic depicting how coronal (a) and sagittal (e) distance of cells to the ventricle were quantified. For coronal sections, three serial coronal sections from GFAP-GFP mice were used per animal, and distance was measured from center of nuclei of cell type of interest to ventricle wall (demarcated by vinculin staining for coronal sections stained with GFAP). The corpus callosum was used as an anatomical landmark for coronal sections to ensure correspondence among sections. For sagittal sections, one sagittal section from C57BL/6 animal containing the rostral migratory stream (RMS) was used to quantify sagittal distance of cell types of interest. Only cells within 200 μm of the ventricle wall were quantified as to include only niche cells (see Methods). **c,** Representative images of immunofluorescence staining of coronal SVZ sections from young (4 months) (left) and old (25 months) (right) GFAP-GFP mice. Yellow box denotes inset containing qNSCs and niche astrocytes (GFAP+/Ki67-) and aNSC (GFAP+/Ki67+) indicated with white arrows and arrowheads, respectively. The ventricular lining is indicated by a dotted white line (see Extended Data Fig. 9a for demarcation of ventricle wall with vinculin). Green, GFAP (astrocyte/NSC marker); Pink, Ki67 (proliferation marker); Blue, DAPI (nuclei). Scale bar, 50 μm. **d,** Quantification of NSC distance to the ventricle for qNSCs and niche astrocytes (Ast) (GFAP+/Ki67-) and aNSCs (GFAP+/Ki67+) in coronal sections (left, a) of young (4 months) and old (18-26 months) SVZs from mixed sex GFAP-GFP mice and sagittal sections (right, e) of young (2-3 months) and old (21 months) SVZs from male C57BL/6 mice. Each dot represents the mean distance from the ventricle of 19 - 231 cells in 3-7 fields per section (3 sections for coronal sections or 1 section for sagittal section) per individual mouse. Coronal sections: $n = 4$ young, and $n = 4$ old mixed-sex GFAP-GFP mice, combined over 2 independent experiments. Sagittal sections: $n = 5$ young male mice, and $n = 5$ old male C57BL/6 mice combined over 2 independent experiments. Data are mean ± SEM. *P*-values were calculated using a two-tailed Mann-Whitney test. Data from independent experiments are in Source Data. **e,** Design of immunofluorescence experiments to assess both the location of quiescent and activated NSCs, NPCs, and neuroblasts in the SVZ neurogenic niche (d,f-h) and EdU-labelled NSC localization along migratory path *in vivo* (i-p). Young (2-3 months) and old (21 months) C57/BL6 male mice were intraperitoneally injected with EdU, and then sacrificed, and perfused with 4% PFA after a time interval of 4 hours, 2 days, or 7 days after EdU injection. Perfused brains were sagittally cryosectioned at a thickness of 16 μm and stained for EdU and cell markers prior to quantification with confocal microscopy. EdU, 5-Ethynyl-2'-deoxyuridine. i.p., intraperitoneal. SVZ, subventricular zone niche. RMS, rostral migratory stream. OB, olfactory bulb. **f,** Representative images of immunofluorescence staining of sagittal SVZ sections of young (2-3 months) (left) and old (21 months) (right) male C57BL/6 mice 4 hours after intraperitoneal EdU injection. Green, EdU (proliferation marker); Pink, Ki67 (aNSC/NPC/neuroblast marker); Red, DCX (neuroblast marker); Blue, DAPI (nuclei). Dotted white line indicates ventricle wall and white arrows indicate EdU-positive cells. Scale bar, 50 μm. EdU, 5-Ethynyl-2'-deoxyuridine. **g,** Distance to the ventricle was calculated for EdU+ aNSCs/NPCs (Ki67+/DCX-) in sagittal sections of young (2-3 months) and old (21 months) SVZs 4 hours after EdU injection. Each dot represents the mean aNSC/NPC distance from the ventricle of 2-35 cells from 1 section per individual mouse. $n = 5$ young male mice, and $n = 5$ old male mice, combined over 2 experiments. Data are mean ± SEM. *P*-values were calculated using a two-tailed Mann-Whitney test. Data from independent experiments are in

Source Data. **h,** Distance to the ventricle was calculated for EdU+ neuroblasts (DCX+) in sagittal sections of young (2-3 months) and old (21 months) SVZs 4 hours after EdU injection. Each dot represents the mean neuroblast distance from the ventricle of 3-25 cells from 1 section per individual mouse. n = 5 young male mice, and n = 5 old male mice, combined over 2 experiments. Data are mean ± SEM. P-values were calculated using a two-tailed Mann-Whitney test. Data from independent experiments are in Source Data. **i,** Representative immunofluorescence staining of sagittal section of young brain encompassing the subventricular zone (SVZ) niche, rostral migratory stream (RMS), and olfactory bulb (OB) of a young (2-3 months) male C57BL/6 mouse 4 hours after intraperitoneal EdU injection. Green, EdU (proliferation marker); Red, Ki67 (aNSC/NPC/neuroblast marker); Pink, DCX (neuroblast marker); Blue, DAPI (nuclei). Scale bar, 500 μm. **j,** Representative images of immunofluorescence staining in sagittal sections of the olfactory bulb from a young (2-3 months) (top) or old (21 months) (bottom) male C57BL/6 mouse 4 hours (left) or 7 days (right) after intraperitoneal EdU injection. Green, EdU (proliferation marker); Blue, DAPI (nuclei). Scale bar, 50 μm. **k-m,** Quantification of EdU+ cells from young (2-3 months) sagittal sections 4 hours, 2 days, and 7 days post-injection of EdU. Each colored dot represents the total number of EdU+ cells counted in the SVZ (along the entire length of the ventricle **(k)**, along the entire length of the RMS **(l)**, and in the entire OB **(m)** of one sagittal section from an individual mouse. n = 5 young male mice 4 hours post-injection, n = 3 young male mice 2 days post-injection, and n = 4 young male mice 7 days post-injection, combined over 2 experiments. Data are mean ± SEM. P-values were calculated using a two-tailed Mann-Whitney test. Data from independent experiments are in Source Data. **n-p,** Quantification of EdU+ cells from old (21 months) sagittal sections 4 hours, 2 days, and 7 days post-injection of EdU. Each colored dot represents the total number of EdU+ cells counted in the SVZ (along the entire length of the ventricle **(n)**, along the entire length of the RMS **(o)**, and in the entire OB **(p)** in one sagittal section from an individual mouse. n = 5 old male mice 4 hours post-injection, n = 3 old male mice 2 days post-injection, and n = 4 old male mice 7 days post-injection, combined over 2 experiments. Data are mean ± SEM. P-values were calculated using a two-tailed Mann-Whitney test. Data from independent experiments are in Source Data.

Figure 4

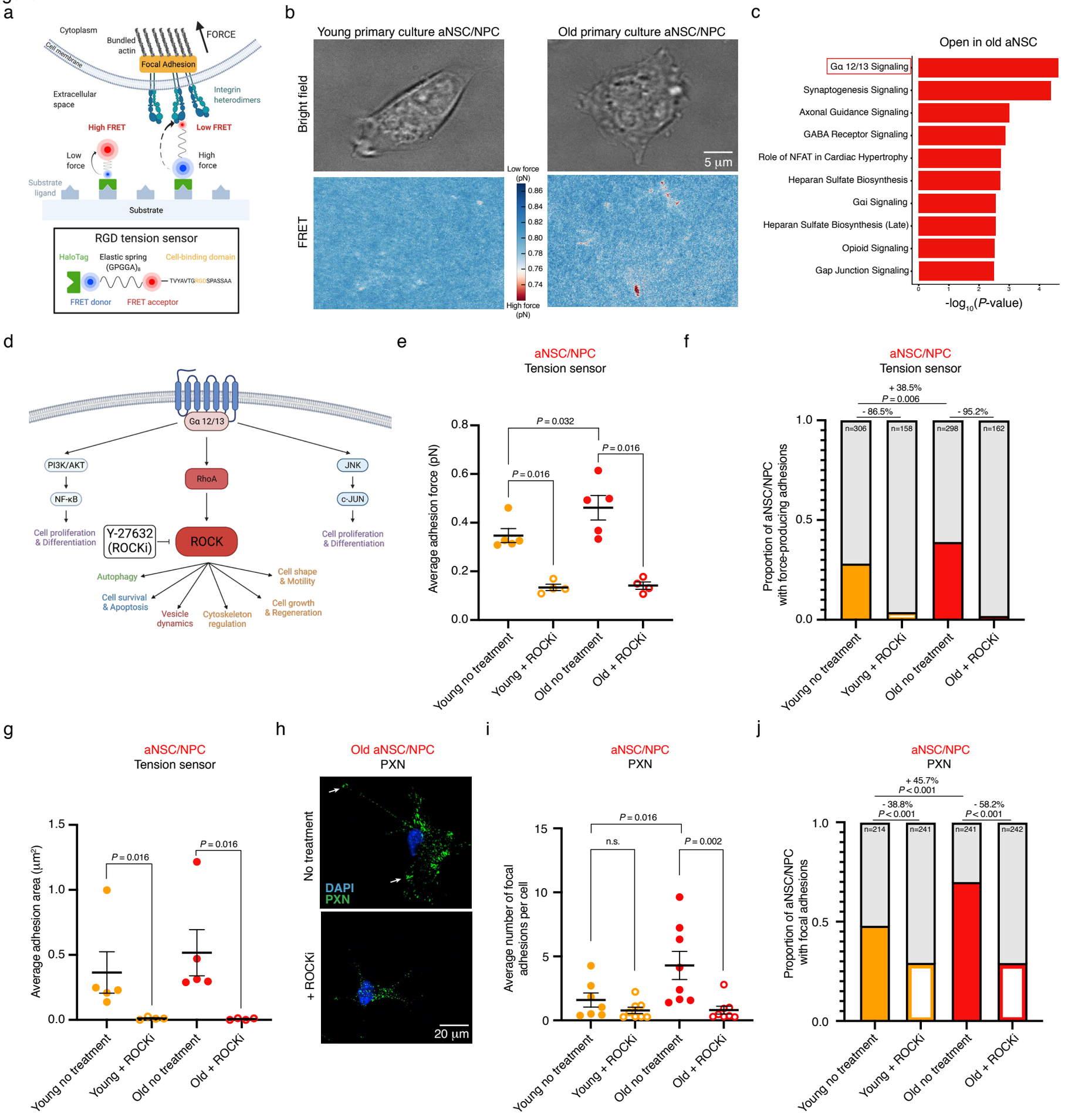
a
Cytoplasm
Bundled actin
FORCE
Cell membrane
Focal Adhesion
Extracellular space
Integrin heterodimers
High FRET
Low FRET
Low force
High force
Substrate ligand
Substrate
RGD tension sensor
HaloTag
Elastic spring (GPGGA)8
Cell-binding domain
TVYAVTGRGDSPASSAA
FRET donor
FRET acceptor
b
Young primary culture aNSC/NPC
Old primary culture aNSC/NPC
Bright field
FRET
Low force (pN)
0.86
0.84
0.82
0.80
0.78
0.76
0.74
High force (pN)
5 µm
c
Open in old aNSC
Gα 12/13 Signaling
Synaptogenesis Signaling
Axonal Guidance Signaling
GABA Receptor Signaling
Role of NFAT in Cardiac Hypertrophy
Heparan Sulfate Biosynthesis
Gαi Signaling
Heparan Sulfate Biosynthesis (Late)
Opioid Signaling
Gap Junction Signaling
-log10(P-value)
d
Gα 12/13
PI3K/AKT
RhoA
JNK
NF-κB
c-JUN
Cell proliferation & Differentiation
Y-27632 (ROCKi)
ROCK
Cell proliferation & Differentiation
Autophagy
Cell shape & Motility
Cell survival & Apoptosis
Vesicle dynamics
Cytoskeleton regulation
Cell growth & Regeneration
e
aNSC/NPC
Tension sensor
Average adhesion force (pN)
P = 0.032
P = 0.016
P = 0.016
Young no treatment
Young + ROCKi
Old no treatment
Old + ROCKi
f
aNSC/NPC
Tension sensor
Proportion of aNSC/NPC with force-producing adhesions
+ 38.5%
P = 0.006
- 86.5%
- 95.2%
n=306
n=158
n=298
n=162
Young no treatment
Young + ROCKi
Old no treatment
Old + ROCKi
g
aNSC/NPC
Tension sensor
Average adhesion area (µm2)
P = 0.016
P = 0.016
Young no treatment
Young + ROCKi
Old no treatment
Old + ROCKi
h
Old aNSC/NPC
PXN
No treatment
+ ROCKi
DAPI
PXN
20 µm
i
aNSC/NPC
PXN
Average number of focal adhesions per cell
P = 0.016
n.s.
P = 0.002
Young no treatment
Young + ROCKi
Old no treatment
Old + ROCKi
j
aNSC/NPC
PXN
Proportion of aNSC/NPC with focal adhesions
+ 45.7%
P < 0.001
- 38.8%
P < 0.001
- 58.2%
P < 0.001
n=214
n=241
n=241
n=242
Young no treatment
Young + ROCKi
Old no treatment
Old + ROCKi

Figure 4: Molecular tension sensors reveal an increase in the occurrence of force-producing adhesions in old aNSCs/NPCs which can be eliminated by ROCK inhibition

a, Diagram of RGD molecular tension sensor (adapted from previous work, see Methods). As cells adhere to the tension sensor-coated substrate, integrin heterodimers bind to the RGD cell-binding domain and exert force across a molecular spring, resulting in decreased FRET signal. RGD, peptide containing tripeptide Arg-Gly-Asp motif. FRET, Förster resonance energy transfer. **b,** Representative image of a young (3 months) (left) and old (21 months) (right) cultured aNSCs/NPCs seeded on RGD molecular tension sensors taken with bright field illumination (top) and FRET donor/acceptor fluorescence wavelengths to generate a high-resolution traction map of FRET efficiency (bottom). The colored bar reflects the FRET efficiency, a measure of adhesion strength, where low FRET efficiency indicates high force (red color) and high FRET efficiency indicates low force (blue color). Scale bar, 5 μm. **c,** Top 10 canonical pathways enriched for genes associated with differentially accessible peaks that open with age in freshly isolated aNSCs (FDR<0.05) generated by Ingenuity Pathway Analysis (IPA) and ranked by *P*-value. ATAC-seq peaks were annotated with their nearest gene using ChIPSeeker (v1.18.0) and *P*-values were calculated using Fisher's Exact Test by IPA. **d,** Diagram of the Gα 12/13 signaling pathway with selected targets including ROCK and downstream biological processes regulated by ROCK (adapted from the IPA canonical pathway diagram "Gα 12/13 Signaling" and previous work, see Methods). RhoA, Ras homolog family member A. ROCK, Rho-associated coiled-coiled kinase. PI3K, phosphoinositide 3-kinase. AKT, AKT serine/threonine kinase 1. NF-κB, Nuclear factor-kappa B. JNK, c-Jun N-terminal kinase. Y-27632, pharmacological inhibitor of ROCK. ROCKi, ROCK inhibitor. **e,** Quantification of average adhesion force (pN) exhibited by young (2.4-3 months) and old (20.5-21 months) cultured aNSCs/NPCs treated with H_2O vehicle (no treatment, solid dots) or 10 μM ROCKi (ROCKi treatment, open circles) determined using RGD molecular tension sensors. Each dot represents the average force produced by one cell (15– 89 cells per dot) in a primary culture derived from an individual mouse. $n = 5$ young male mice and $n = 5$ old male mice (no treatment), $n = 4$ young male mice and $n = 4$ old male mice (ROCKi treatment), combined over 5 independent experiments. Data are mean ± SEM. *P*-values were calculated using a two-tailed Mann-Whitney test. Data from independent experiments are in Source Data. **f,** Proportion of young (2.4-3 months) and old (20.5-21 months) cultured aNSCs/NPCs exhibiting force-producing adhesion patterns as determined from RGD tension sensor experiments, when treated with H_2O (no treatment, solid bars), or ROCKi (ROCKi treatment, open bars). Same experiment as in (e). Colored bars represent proportion of cells that have force-producing adhesions. *P*-values were calculated using a combined Fisher's exact test. Data from independent experiments are in Source Data. **g,** Quantification of average adhesion area under force-producing adhesions (μm^2) of young (2.4-3 months) and old (20.5-21 months) cultured aNSCs/NPCs treated with H_2O vehicle (no treatment, solid dots) or 10 μM ROCKi (ROCKi treatment, open circles) determined using RGD molecular tension sensors. Each dot represents the average adhesion area of force-producing adhesions from a single cell (15 – 89 cells per dot) in a primary culture derived from an individual mouse. Same experiment as in (e). Data are mean ± SEM. *P*-values were calculated using a two-tailed Mann-Whitney test. Data from independent experiments are in Source Data. **h,** Representative immunofluorescence staining of old (22 months) cultured aNSCs/NPCs on Matrigel treated with H_2O vehicle (top, no treatment) or 10 μM ROCKi (bottom, ROCKi treatment). Green, paxillin (PXN, focal adhesions); Blue, DAPI (nuclei). White arrows indicate PXN localization to focal adhesions. Scale bar, 20 μm. **i,** Quantification of average number of focal adhesions, determined using PXN staining, exhibited by young (2.5 months) and old (22.1 months) cultured aNSCs/NPCs treated with H_2O vehicle (no treatment, solid dots) or 10 μM ROCKi (ROCKi treatment, open circles). Each dot represents the average number of focal adhesions

per cell from a primary culture (30 cells per dot) derived from an individual mouse. $n = 7$ young male mice and $n = 8$ old male mice (no treatment) and $n = 8$ young male mice and $n = 8$ old male mice (ROCKi treatment), combined over 2 experiments. Data are mean ± SEM. *P*-values were calculated using a two-tailed Mann-Whitney test. Data from independent experiments are in Source Data. **j,** Proportion of young (2.5 months) and old (22.1 months) cultured aNSCs/NPCs exhibiting focal adhesions, determined using PXN staining, when treated with H_2O vehicle (no treatment, solid bars) or 10 μM ROCKi (ROCKi treatment, open bars) exhibiting focal adhesions. Same experiment as in (i). Colored bars represent proportion of cells that have focal adhesions. *P*-values were calculated using a combined Fisher's exact test. Data from independent experiments are in Source Data.

Figure 5

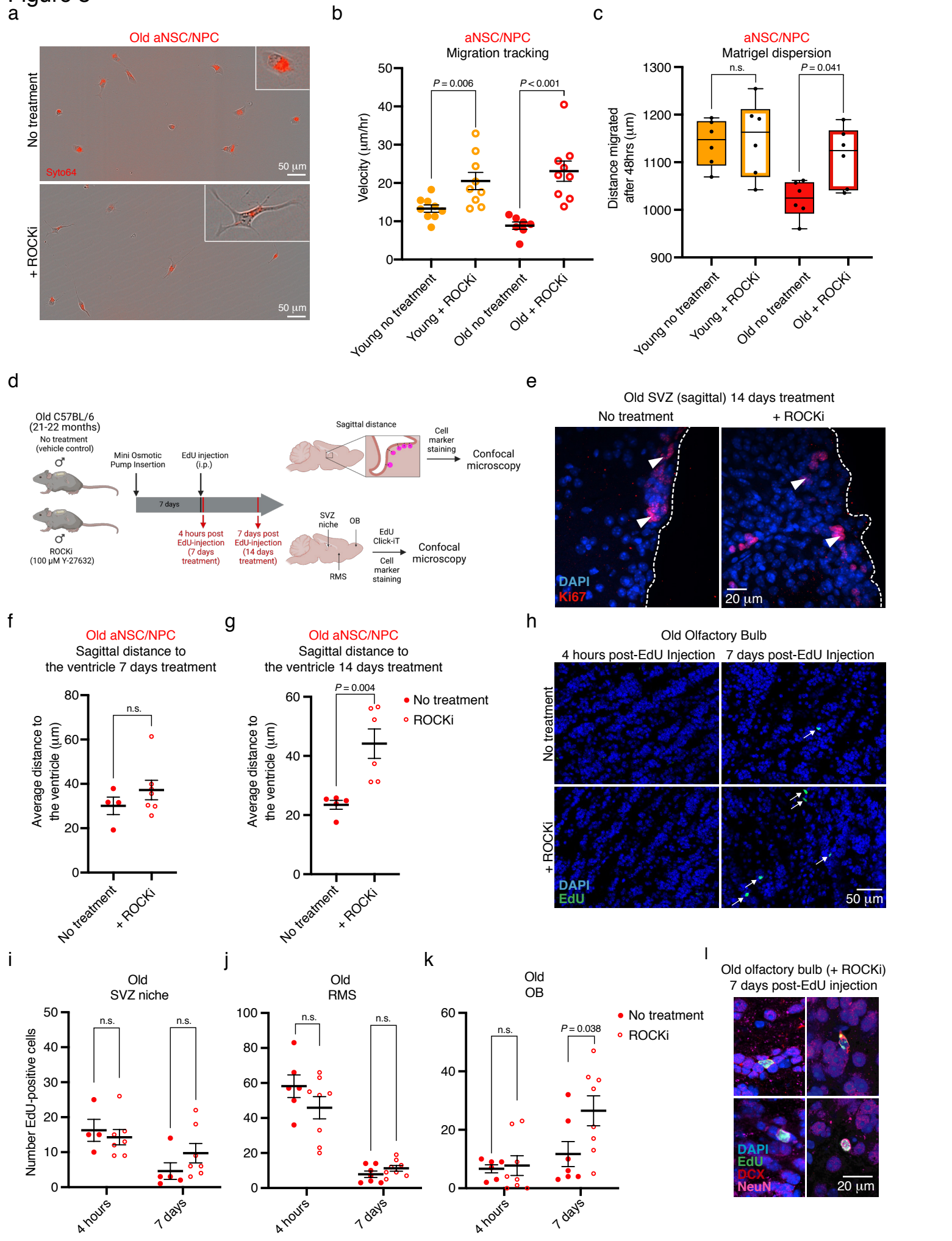
a
Old aNSC/NPC
No treatment
+ ROCKi
Syto64
50 µm
b
aNSC/NPC
Migration tracking
Velocity (µm/hr)
P = 0.006
P < 0.001
Young no treatment
Young + ROCKi
Old no treatment
Old + ROCKi
c
aNSC/NPC
Matrigel dispersion
Distance migrated after 48hrs (µm)
n.s.
P = 0.041
d
Old C57BL/6 (21-22 months)
No treatment (vehicle control)
ROCKi (100 µM Y-27632)
Mini Osmotic Pump Insertion
EdU injection (i.p.)
7 days
4 hours post EdU-injection (7 days treatment)
7 days post EdU-injection (14 days treatment)
Sagittal distance
Cell marker staining
Confocal microscopy
SVZ niche
OB
RMS
EdU Click-iT
e
Old SVZ (sagittal) 14 days treatment
No treatment
+ ROCKi
DAPI
Ki67
20 µm
f
Old aNSC/NPC
Sagittal distance to the ventricle 7 days treatment
Average distance to the ventricle (µm)
n.s.
No treatment
+ ROCKi
g
Old aNSC/NPC
Sagittal distance to the ventricle 14 days treatment
P = 0.004
No treatment
ROCKi
h
Old Olfactory Bulb
4 hours post-EdU Injection
7 days post-EdU Injection
No treatment
+ ROCKi
DAPI
EdU
50 µm
i
Old SVZ niche
Number EdU-positive cells
n.s.
4 hours
7 days
j
Old RMS
k
Old OB
P = 0.038
l
Old olfactory bulb (+ ROCKi) 7 days post-EdU injection
DAPI
EdU
DCX
NeuN
20 µm

Figure 5: Inhibition of ROCK boosts migration speed in aNSCs/NPCs cultured from aged brains and improves *in vivo* neurogenesis in old mice

a, Representative images of old (21-24 months) cultured aNSCs/NPCs 12 hours after plating onto Poly-D-Lysine-coated migration plates treated with H_2O vehicle (top, no treatment) or 10 μM ROCKi (bottom, ROCKi treatment). Images were taken with the Incucyte S3 system with phase contrast and red fluorescence imaging overlaid. Live cells were stained with Syto64, a cell-permeant red fluorescent nucleic acid stain, for migration tracking. Outlined inset (top-right) displays a representative magnified cell. Scale bar, 50 μm. **b,** Quantification of migration speed of young (3-4 months) and old (21-24 months) aNSCs/NPCs cultured on Poly-D-Lysine treated with H_2O vehicle (no treatment, solid dots) or with 10 μM ROCKi (ROCKi treatment, open circles). Each dot represents the average velocity over a 20-hour period of cultured cells (2-28) derived from one individual mouse. n = 9 young male mice and n = 7 old male mice (no treatment) and n = 9 young male mice and n = 9 old male mice (ROCKi treatment), combined over 3 experiments. Data are mean ± SEM. P-values were calculated using a two-tailed Mann-Whitney test. Data from independent experiments are in Source Data. **c,** Quantification of cell dispersion through Matrigel after 48 hours by young (3-4 months) and old (21-23 months) cultured aNSCs/NPCs treated with H_2O vehicle (no treatment, solid bars) or with 10 μM ROCKi (ROCKi treatment, open bars). Each dot represents the dispersion distance through Matrigel after 48 hours of cultured aNSCs/NPCs derived from an individual mouse. n = 6 young male mice and n = 6 old male mice for treated and untreated conditions, combined over 2 experiments. For each biological replicate, 1-4 technical replicates were evaluated, and dispersion distance was averaged. Boxplot displays median, and lower and upper quartile values. P-values were calculated using a two-tailed Mann-Whitney test. **d,** Design of *in vivo* ROCK inhibitor (ROCKi) immunofluorescence experiments to assess EdU-labelled NSC localization along migration path to the olfactory bulb. Mini-osmotic pumps with 100 μM of ROCKi or artificial cerebrospinal fluid vehicle control were stereotactically implanted into old (21-22 months) C57BL/6 male mice to continuously deliver ROCKi or vehicle control to the lateral ventricles for 7 or 14 days. After 7 days of treatment, animals were intraperitoneally injected with EdU, and then sacrificed and perfused with 4% PFA after a time interval of 4 hours (7 days treatment) or 7 days (14 days treatment). Perfused brains were sagittally cryosectioned at a thickness of 16 μm and stained for EdU and cell markers prior to quantification with confocal microscopy. EdU, 5-Ethynyl-2'-deoxyuridine. i.p., intraperitoneal. SVZ, subventricular zone niche. RMS, rostral migratory stream. OB, olfactory bulb. **e,** Representative images of immunofluorescence staining in sagittal sections of the SVZ of old (22 months) vehicle control (left, no treatment) and ROCKi-treated (right, ROCKi treatment) male mice after 14 days of treatment. Dotted line represents ventricle border. Arrowheads indicate aNSCs/NPCs (Ki67+/DCX-). Scale bar, 20 μm. **f,** Quantification of sagittal distance to the ventricle for aNSCs/NPCs (Ki67+/DCX-) in sagittal sections of old (21-22 months) SVZs treated with vehicle control (no treatment, solid dots) or ROCKi (ROCKi treatment, open circles) for 7 days (4 hours post-EdU injection). Each dot represents the mean distance from the ventricle of 18-47 cells in one sagittal section per mouse. n = 4 old male mice (no treatment) and n = 7 old male mice (ROCKi treatment), combined over 2 experiments. Data are mean ± SEM. P-values were calculated using a two-tailed Mann-Whitney. Data from independent experiments are in Source Data. **g,** Quantification of sagittal distance to the ventricle for aNSCs/NPCs (Ki67+/DCX-) in sagittal sections of old (21-22 months) SVZs treated with vehicle control (no treatment, solid dots) or ROCKi (ROCKi treatment, open circles) for 14 days (7 days post-EdU injection). Each dot represents the mean distance from the ventricle of 6-47 cells per individual mouse. n = 5 old male mice (no treatment) and n = 6 old male mice (ROCKi), combined over 2 experiments). Data are mean ± SEM. P-values were calculated using

a two-tailed Mann-Whitney. Data from independent experiments are in Source Data. **h,** Representative images of immunofluorescence staining in sagittal sections of the olfactory bulb from old (21 months) male C57BL/6 mouse with treated with vehicle control (top) or ROCKi (bottom) 4 hours (left) or 7 days (right) after intraperitoneal EdU injection. White arrows indicate EdU-positive cell. Green, EdU (proliferation marker); Blue, DAPI (nuclei). Scale bar, 50 μm. EdU, 5-Ethynyl-2'-deoxyuridine. **i-k,** Quantification of EdU+ cells counted in the SVZ **(i)**, RMS **(j)**, and OB **(k)** from sagittal sections 4 hours and 7 days post-injection of EdU in old (21-22 months) mice treated with vehicle control (no treatment, solid dots) or ROCKi (ROCKi treatment, open circles). Each dot represents the number of EdU+ cells counted in one sagittal section from a single mouse. n = 4-7 old male mice (no treatment), and n = 7-8 old male mice (ROCKi treatment) for each time point (4 hours, 7 days), combined over 2 experiments. Data are mean ± SEM. P-values were calculated using a two-tailed Mann-Whitney test. Data from independent experiments are in Source Data. **l,** Representative immunofluorescence images of old male mouse olfactory bulb (22.4 months) 7 days after EdU injection. EdU-positive cells in the olfactory bulb are DCX+ (top) or NeuN+ (bottom). Green, EdU; Red, DCX; Pink, NeuN. Blue, DAPI (nuclei). Scale bar, 20 μm.

Extended Data Figure 1

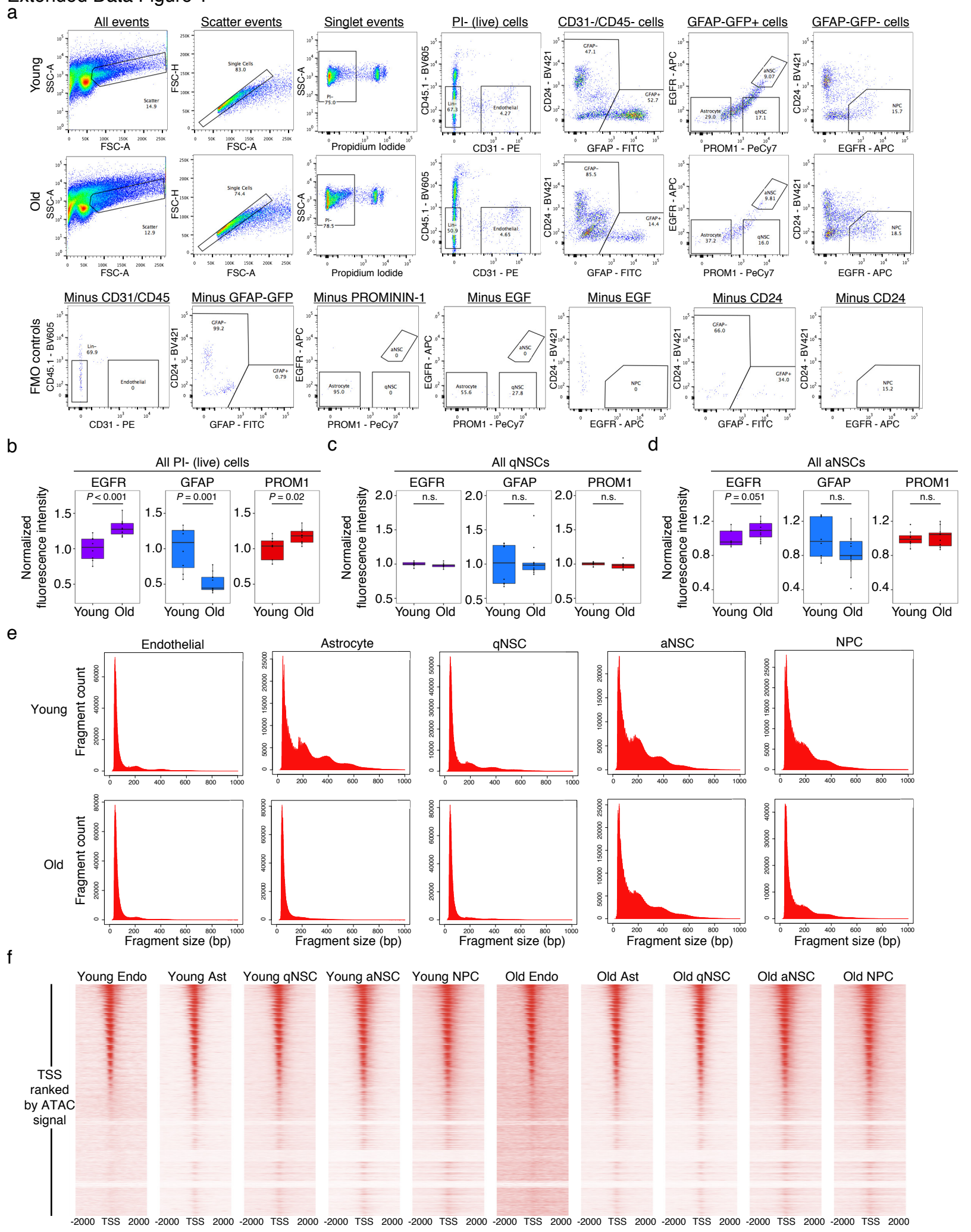

Extended Data Figure 1: Quality control metrics for FACS and *in vivo* ATAC-seq libraries
a, FACS gating scheme used to isolate 5 cell populations from the SVZ of young and old GFAP-GFP mice. Negative controls (fluorescence minus one (FMO) controls) for each stain are indicated. Negative controls (FMO controls) were stained with all antibodies other than the one(s) for which it was the negative control. **b,** Changes in FACS markers with age for all live cells. Normalized scaled fluorescence intensity of indicated FACS markers (EGFR, GFAP, and PROM1) of young (4-5 months) and old (20-24 months) PI-negative sorted cells used for generating ATAC-seq libraries from freshly isolated cells from the SVZ neurogenic niche. $n = 8$ young male and female GFAP-GFP mice and $n = 11$ old male and female GFAP-GFP mice combined over 2 experiments. Data normalized to young mean of each individual experiment. Boxplots display median, and lower and upper quartiles. Dots represent mean fluorescence intensity for an individual animal. *P*-values were calculated using a two-tailed Mann-Whitney test. Data from independent experiments are in Source Data. The change in marker expression in all live cells likely reflect changes in cell type composition that occur with age with age. **c,** Changes in FACS markers with age in quiescent NSCs. Normalized scaled fluorescence intensity of indicated FACS markers (EGFR, GFAP, and PROM1) of young (4-5 months) and old (20-24 months) FACS-purified quiescent NSCs used for generating ATAC-seq libraries from freshly isolated cells from the SVZ neurogenic niche. $n = 8$ young male and female GFAP-GFP mice and $n = 11$ old male and female GFAP-GFP mice combined over 2 experiments. Data normalized to young mean of each individual experiment. Note that EGFR raw values were very low, as expected, for quiescent NSCs (GFAP+PROM1+EGFR-). Boxplots display median, and lower and upper quartiles. Dots represent mean fluorescence intensity for an individual animal. *P*-values were calculated using a two-tailed Mann-Whitney test. Data from independent experiments are in Source Data. **d,** Changes in FACS markers with age in activated NSCs. Normalized scaled fluorescence intensity of indicated FACS markers (EGFR, GFAP, and PROM1) of young (4-5 months) and old (20-24 months) FACS-purified activated NSCs used for generating ATAC-seq libraries from freshly isolated cells from the SVZ neurogenic niche. $n = 8$ young male and female GFAP-GFP mice and $n = 11$ old male and female GFAP-GFP mice combined over 2 experiments. Data normalized to young mean of each individual experiment. Boxplots display median, and lower and upper quartiles. Dots represent mean fluorescence intensity for an individual animal. *P*-values were calculated using a two-tailed Mann-Whitney test. Data from independent experiments are in Source Data. **e,** Insert size distribution histograms of all paired-end reads from a single representative ATAC-seq library for each of the 5 cell types freshly isolated from the SVZ of both young and old animals. **f,** Heatmap of ATAC-seq enrichment at genome-wide transcription start sites (TSSs) ± 2000 base pairs for all 5 cell types in both young and old conditions.

Extended Data Figure 2

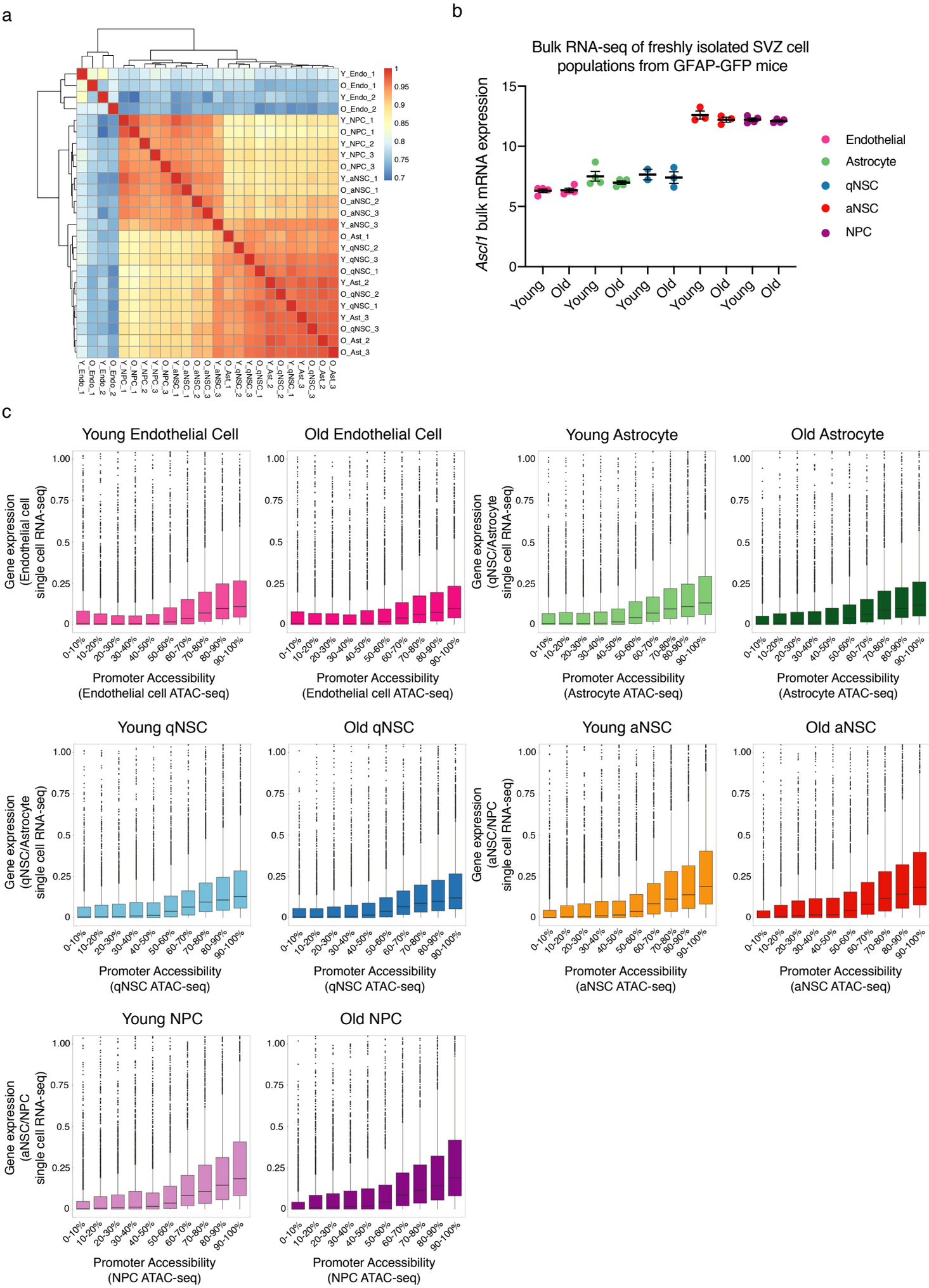

Extended Data Figure 2: Chromatin accessibility clustering and correlation with gene expression
a, Hierarchical clustering using Pearson's correlation of raw chromatin accessibility libraries (un-normalized) of all 5 cell types freshly isolated from the SVZ of young and old animals. Biological replicates are noted as numbers following age and cell type. **b,** mRNA expression of *Ascl1* in all 5 SVZ cell types in young and old conditions from bulk RNA-seq dataset (see Methods). Each dot represents the VST-normalized mRNA expression value from a single RNA-seq library (2-4 libraries per condition). Data are mean ± SEM. **c,** Decile plot of correlation between promoter accessibility levels (from ATAC-seq data) and mean gene expression values (from single cell RNA-seq data, see Methods). Promoters were binned into deciles based on accessibility level and boxplots were generated to correlate promoter bins with average gene expression for young and old endothelial cells, astrocytes, qNSCs, aNSCs, and NPCs. Each dot represents the gene expression level of an individual promoter binned based on chromatin accessibility signal. Y-axis constrained between 0 and 1 to facilitate boxplot visualization. Boxplot indicates median, and lower and upper quartiles.

Extended Data Figure 3

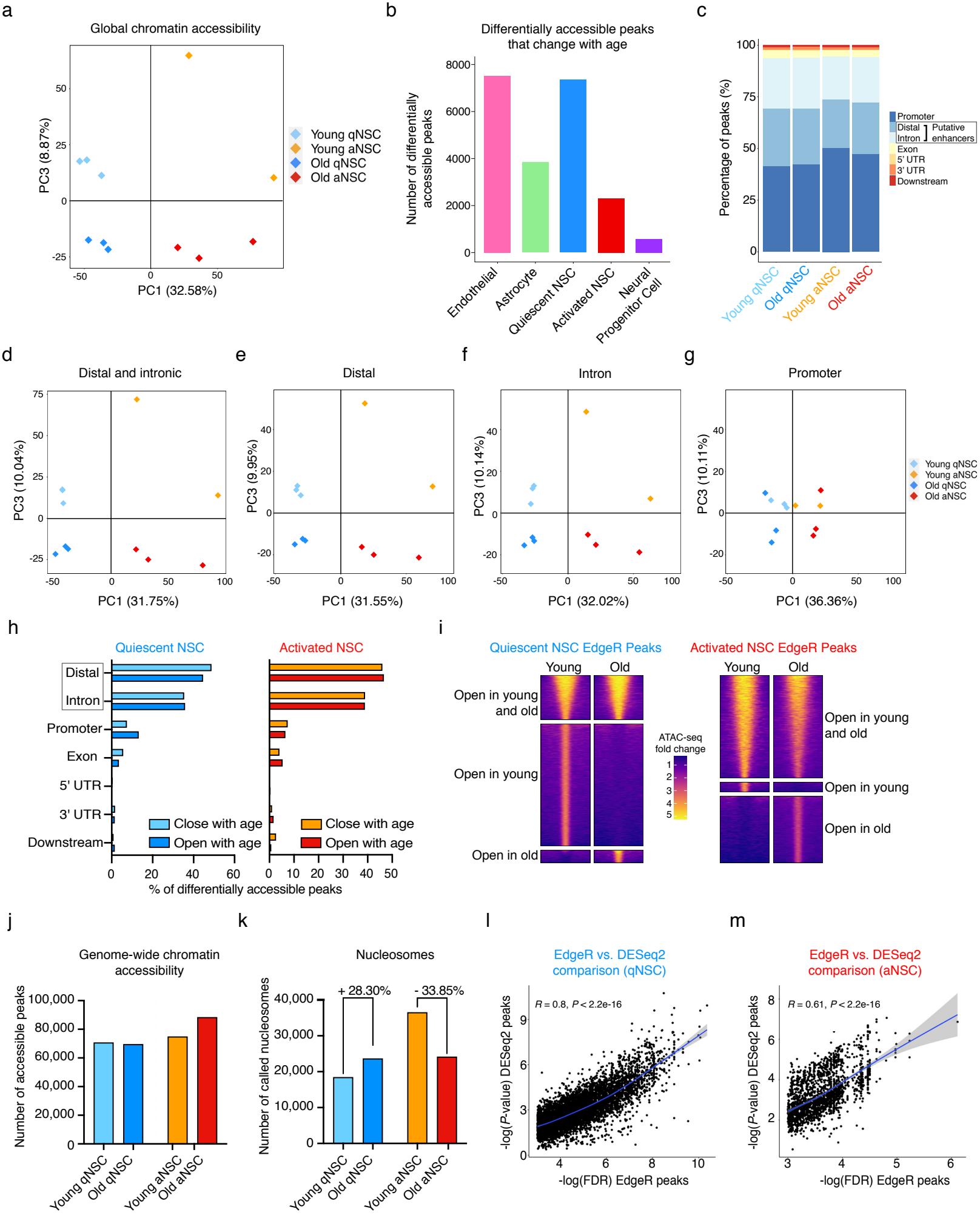

Extended Data Figure 3: Chromatin accessibility in quiescent and activated NSCs during aging
a, PCA on genome-wide chromatin peaks defining qNSCs and aNSCs freshly isolated from the young and old SVZ where each dot represents a single ATAC-seq library (PC1 vs. PC3). PCA was generated using the variance stabilizing transformation (VST)-normalized NSC consensus count matrix. PC, principal component. **b,** Barplot denoting the number of differentially accessible peaks that change with age (open and close) in freshly isolated endothelial cells, astrocytes, quiescent NSCs, activated NSCs, and neural progenitor cells. **c,** Stacked barchart representing the genomic distribution of open chromatin peaks for qNSCs and aNSCs in young and old conditions based on their pooled peaksets. ATAC-seq peaks were annotated with ChIPSeeker (v1.18.0). Grey box indicates distal and intronic peaks that likely contain putative enhancers. **d-g,** PCA on distal and intronic chromatin peaks **(d)**, exclusively distal **(e)**, exclusively intronic **(f)**, and exclusively promoter **(g)** chromatin peaks for qNSCs and aNSCs freshly isolated from the SVZ of young and old mice where each dot represents a single ATAC-seq library (PC1 vs. PC3). PCA was generated using the variance stabilizing transformation (VST)-normalized NSC consensus count matrix. PC, principal component. **h,** Frequency of differentially accessible ATAC-seq peaks that change with age in qNSCs (left) and aNSCs (right) associated with distal regions, introns, promoters, exons, 5' UTRs, 3' UTRs, and downstream regions. ATAC-seq peaks were annotated with ChIPSeeker (v1.18.0). Grey box denotes differentially accessible distal and intronic peaks that likely contain putative enhancers. **i,** Raw signal pileup plots illustrating chromatin accessibility signal of quiescent (left) and activated (right) NSC chromatin peaks separated based on whether they are common to qNSCs and aNSCs (top), open in young (middle), or open in old (bottom) as determined by the differential peak caller EdgeR. **j,** Barplot denoting the number of genome-wide chromatin peaks (non-differential) in freshly isolated young and old qNSCs and aNSCs. **k,** Number of nucleosome peaks called by NucleoATAC (v0.2.1) for freshly isolated young and old qNSC and aNSC chromatin landscapes. Nucleosome peaks were called using pooled, sub-sampled (to 30 million unique reads) ATAC-seq reads for each condition. **l,** Scatterplot illustrating correlation between significance levels of alternative differential peak calling methods: EdgeR FDR values vs DESeq2 P-values for peaks that are differentially open in young quiescent NSCs (called by EdgeR). Regression and *P*-values were respectively calculated using geom_smooth() and state_cor() in R. **m,** Scatterplot illustrating correlation between significance levels of alternative differential peak calling methods: EdgeR FDR values vs DESeq2 P-values for peaks that are differentially open in old activated NSCs (called by EdgeR). Regression and *P*-values were respectively calculated using geom_smooth() and state_cor() in R.

Extended Data Figure 4

a

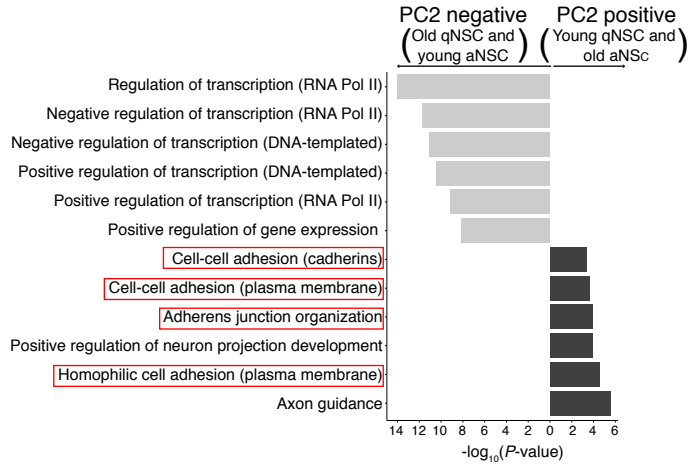

b

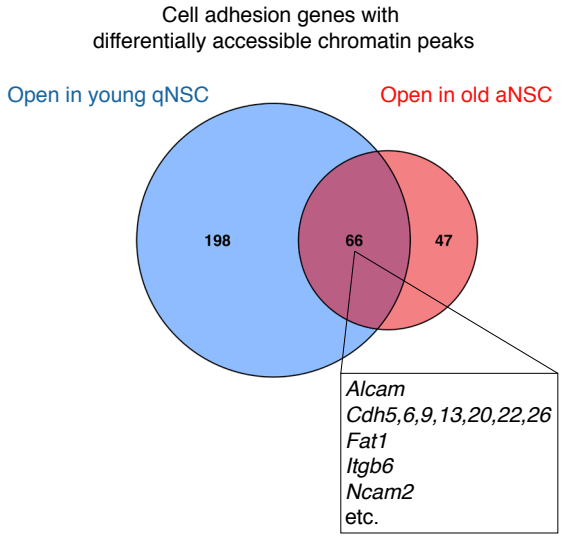

c

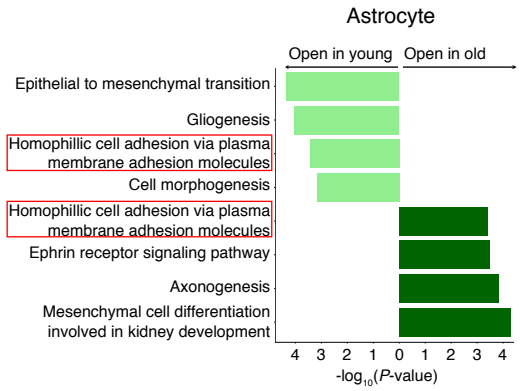

d

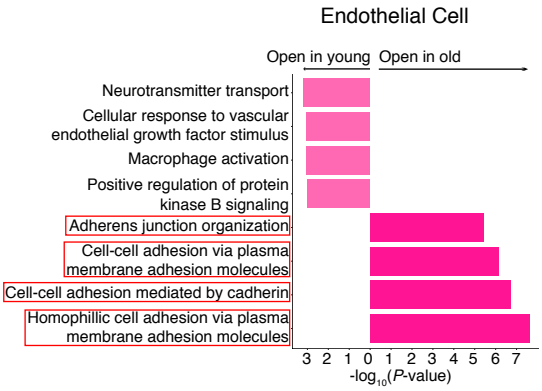

e

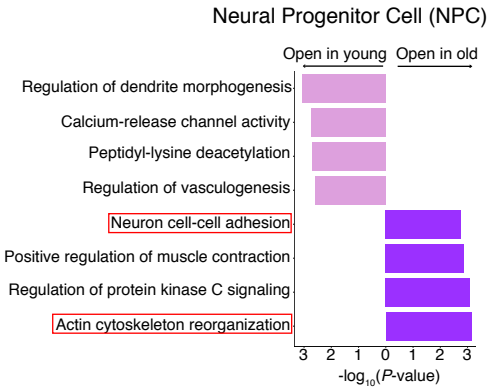

f

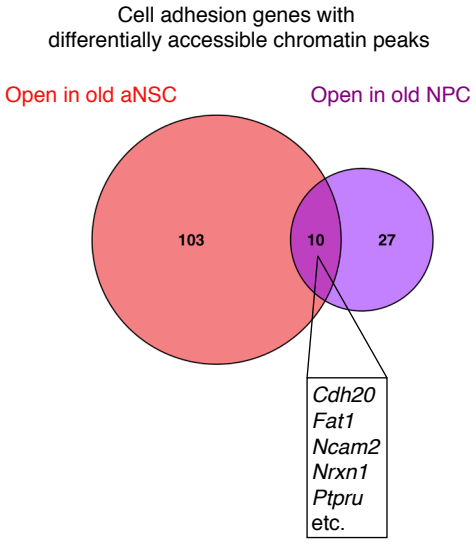

Extended Data Figure 4: Chromatin accessibility analysis in 5 different cell types
a, Top 6 GO terms associated with the top 1000 ATAC-seq peak-associated genes driving PC2 in the positive (young qNSCs and old aNSCs) and negative (old qNSCs and young aNSCs) direction. Red boxes indicate GO terms associated with cell adhesion. PC, principal component. **b,** Venn diagram illustrating overlap between genes in "Cell Adhesion" GO category (GO:0007155) with nearby chromatin peaks that are differentially open in young qNSCs (compared to old) and old aNSCs (compared to young). Box in overlap indicates select shared cell adhesion genes. **c-e,** Selected GO terms associated with differentially accessible ATAC-seq peaks (FDR<0.05) that change with age in freshly isolated astrocytes **(c)**, endothelial cells **(d)**, and neural progenitor cells (NPCs) **(e)** generated by EnrichR and ranked by *P*-value. ATAC-seq peaks were annotated with their nearest gene using ChIPSeeker (v1.18.0). Red boxes indicate GO terms associated with adhesion and migration. **f,** Venn diagram illustrating overlap between genes in "Cell Adhesion" GO category (GO:0007155) genes with nearby chromatin peaks that are differentially open in old aNSCs and old NPCs. Box in overlap indicates select shared cell adhesion genes.

Extended Data Figure 5

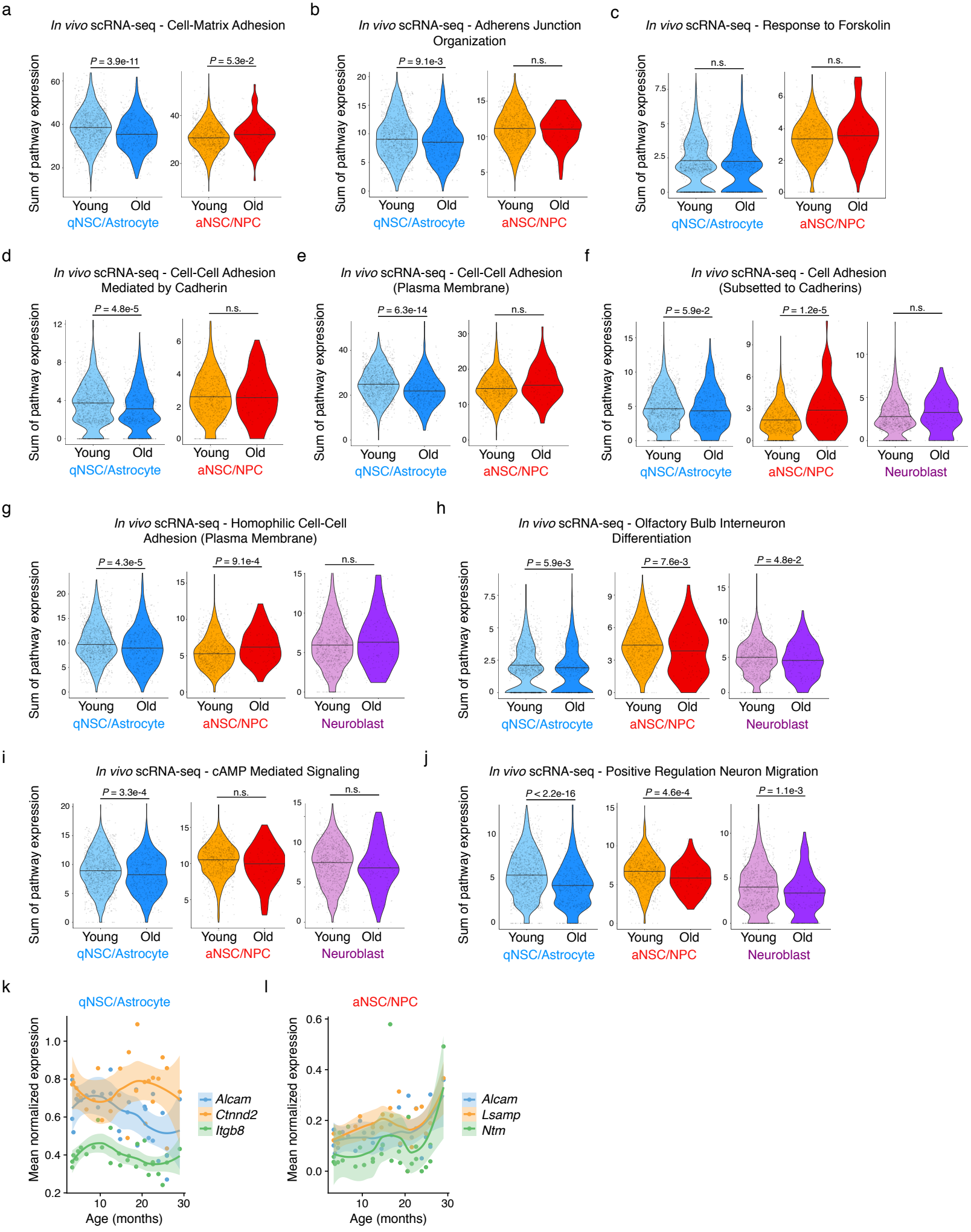

Extended Data Figure 5: Gene expression of cell adhesion and migration pathways in NSC lineage during aging by single cell RNA-seq

a-e, Violin plots of the distribution of single cell cumulative expression profiles of genes within the "Cell-matrix adhesion" GO category (GO:0007160) **(a)**, "Adherens junction organization" GO category (GO:0034332) **(b)**, "Response to forskolin" GO Category (GO:1904322) **(c)**, "Cell-cell adhesion mediated by cadherin" GO Category (GO:0044331) **(d)**, and "Cell-cell adhesion (plasma membrane)" GO Category (GO:0098742) **(e)** for young and old qNSCs/Astrocytes (left) and aNSCs/NPCs (right) from single cell RNA-seq data (see Methods). Each overlaid dot represents the cumulative expression of genes within the GO category in a single cell. *P*-values were calculated using a two-tailed Mann-Whitney test. **f-j,** Violin plots of the distribution of single cell cumulative expression profiles of genes within the "Cell adhesion" GO Category (GO:0007155) restricted to cadherins **(f)**, "Homophilic cell-cell adhesion (plasma membrane)" GO Category (GO:0007156) **(g)**, "Olfactory bulb interneuron differentiation" GO Category (GO:0021889) **(h)**, "cAMP mediated signaling" GO Category (GO:0019933) **(i)**, and "Positive regulation neuron migration" GO Category (GO:2001224) **(j)** for young and old qNSC/Astrocyte (left), aNSC/NPC (middle), and neuroblasts (right) from single cell RNA-seq data (see Methods). Each overlaid dot represents the cumulative expression of genes within the GO category in a single cell. *P*-values were calculated using a two-tailed Mann-Whitney test. **k,** Gene expression trajectories as a function of age of select cell adhesion genes (*Alcam, Ctnnd2, Itgb8*) in qNSCs/Astrocytes from single cell RNA-seq dataset (see Methods). **l,** Gene expression trajectories as a function of age of select cell adhesion genes (*Alcam, Lsamp, Ntm*) in aNSCs/NPCs from single cell RNA-seq dataset (see Methods).

Extended Data Figure 6

a

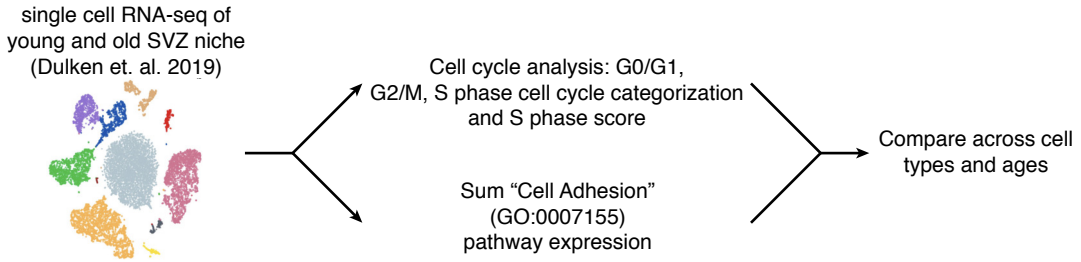

b

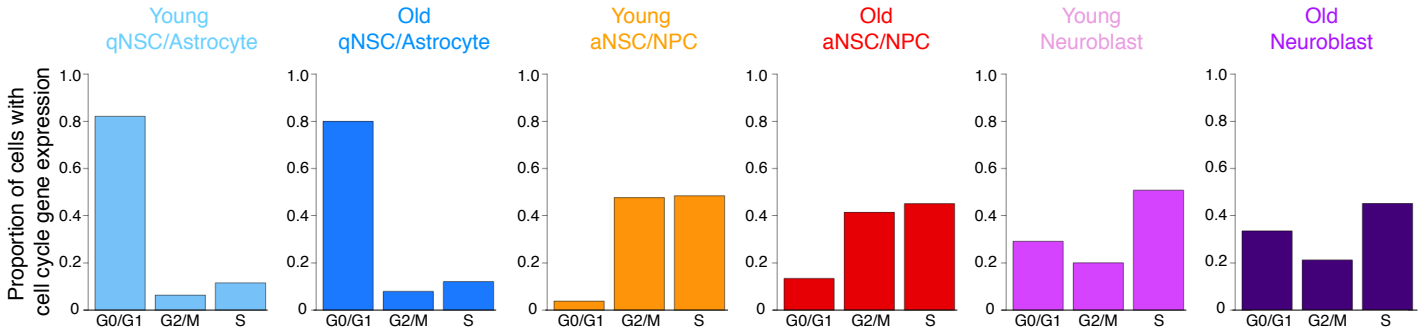

c

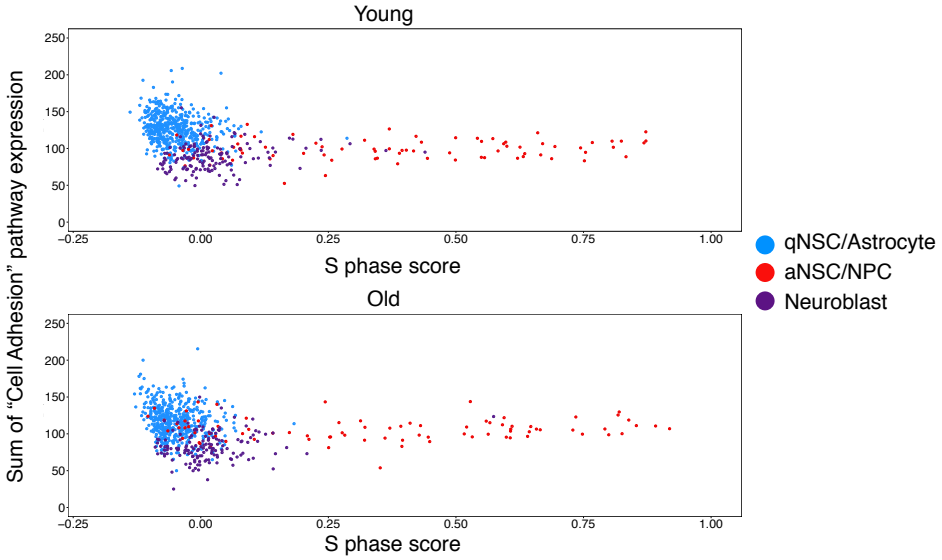

Extended Data Figure 6: Analysis of cell cycle and cell migration signatures in NSCs during aging by single cell RNA-seq

a, Single cell RNA-seq data was used to assess cell cycle gene expression and Cell Adhesion (GO:0007155) pathway expression for young and old qNSCs/astrocytes, aNSCs/NPCs, and neuroblasts (see Methods). **b,** Barplots illustrating the proportion of young and old qNSCs/astrocytes, aNSCs/NPCs, and neuroblasts in the GO/G1, G2/M, or S phase of the cell cycle based on gene expression signatures from single cell RNA-seq data (see Methods). **c,** Scatterplot of qNSCs/astrocytes, aNSCs/NPCs, and neuroblasts from young (top) and old (bottom) single cell RNA-seq data (see Methods) illustrating the relationship between Seurat's "S phase score" and the cumulative single cell expression levels of the genes in the "Cell Adhesion" GO category (GO:0007155). Young cells were downsampled to visualize the same number of young and old cells per cell type (480 qNSCs/astrocytes, 82 aNSCs/NPCs, and 146 neuroblasts).

Extended Data Figure 7

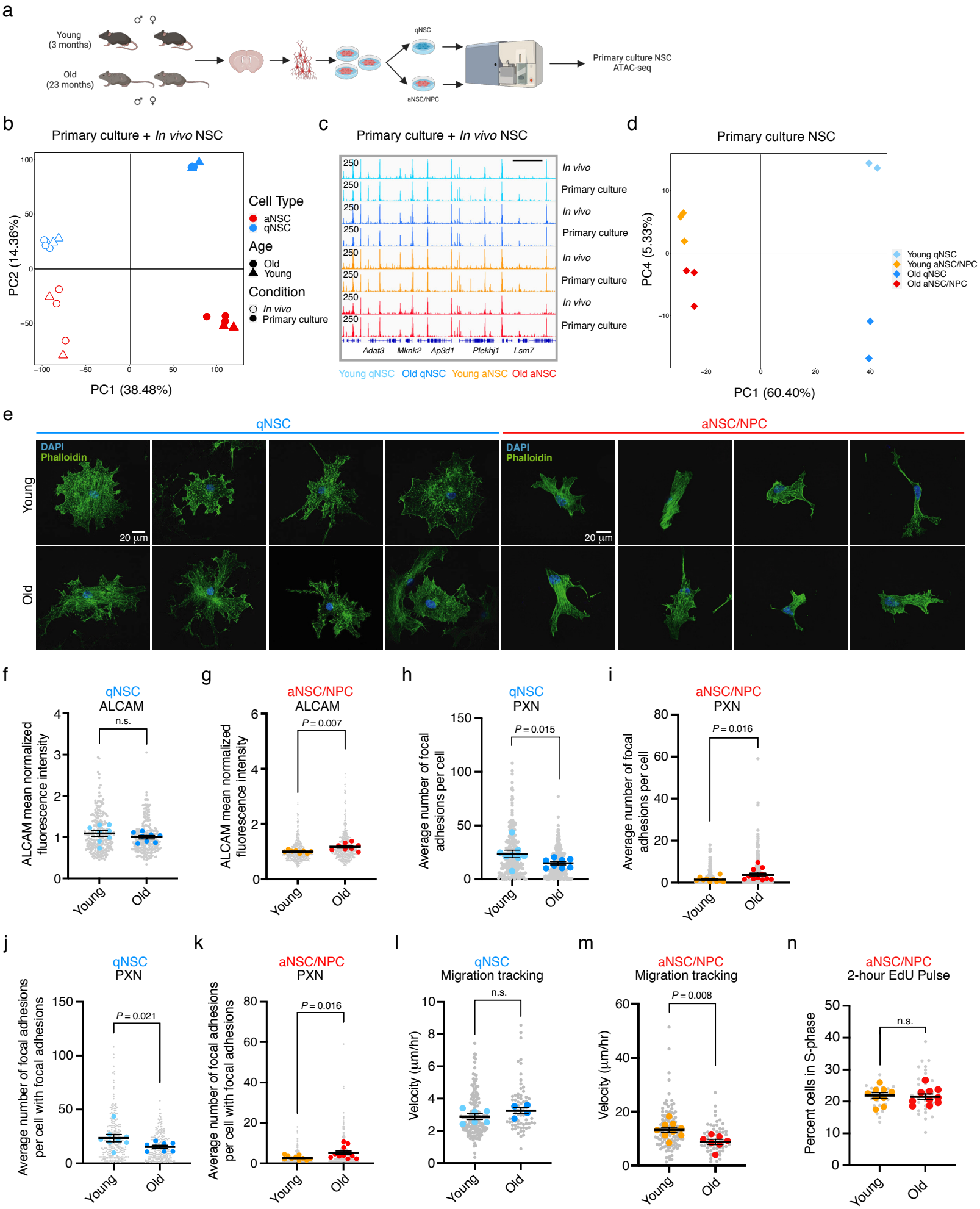

Extended Data Figure 7: Primary cultures of qNSCs and aNSCs/NPCs for ATAC-seq, immunostaining, and adhesion and migration assays

a, Experimental design for the generation of ATAC-seq libraries from quiescent and activated NSCs cultured from young (3 months) and old (23 months) mixed-sex C57BL/6 mice. For each library, fluorescence-activated cell sorted (FACS) was used to sort 10,000-15,000 live cells from cultures generated from mixed male and female C57BL/6 SVZs (see Methods). **b,** PCA on chromatin peaks defining cultured and *in vivo* qNSC and aNSC landscapes where each dot represents a single ATAC-seq library (PC1 vs. PC2). PCA was generated using the variance stabilizing transformation (VST)-normalized global consensus count matrix of all cultured and *in vivo* NSC peaks. PC, principal component. **c,** Genome browser (IGV) view of chromatin accessibility signal tracks on chromosome 10 of freshly isolated and cultured qNSC and aNSC from the young and old SVZ. *Adat3*, Adenosine Deaminase TRNA Specific 3. *Mknk2*, MAPK Interacting Serine/Threonine Kinase 2. *Ap3d1*, Adaptor Related Protein Complex 3 Subunit Delta 1. *Plekhj1*, Pleckstrin Homology Domain Containing J1. *Lsm7*, LSM7 Homology U6 Small Nuclear RNA and mRNA Degradation Associated. Scale bar, 50kb. **d,** PCA on chromatin peaks defining qNSC and aNSC/NPC cultured from young and old SVZs where each dot represents a single ATAC-seq library (PC1 vs. PC4). PCA was generated using the variance stabilizing transformation (VST)-normalized global consensus count matrix. PC, principal component. **e,** Representative immunofluorescent images of young (2.5-3 months) (top) and old (21-22.1 months) (bottom) of aNSC/NPC (left) and qNSC (right) highlighting heterogeneity in cell size and shape. Green, phalloidin (F-actin); Blue, DAPI (nuclei). Scale bar, 20 μm. **f, g,** ALCAM fluorescence intensity of young (2.5-3 months) and old (21-22.1 months) qNSC **(f)** and aNSC/NPC **(g)** on Matrigel. Each grey dot represents mean normalized fluorescent intensity per cell. Each colored dot represents mean normalized fluorescence intensity of 30 fields (each containing 1-3 cells) in a primary culture derived from an individual mouse, normalized by experiment and cell size. n = 8 young male mice, and n = 8 old male mice, combined over 2 (qNSC) or 3 (aNSC/NPC) independent experiments. Data are mean ± SEM. P-values were calculated using a two-tailed Mann-Whitney test comparing sample means. Data from independent experiments are in Source Data. **h,i,** Quantification of paxillin (PXN) immunostaining of young (2.5-3 months) and old (22.1-22.1 months) qNSCs **(h)** and aNSCs/NPCs **(i)** cultured on Matrigel. Each grey dot represents number of focal adhesions per cell. Each colored dot represents average number of focal adhesions per cell (28-32 cells per dot) in a primary culture derived from an individual mouse. n = 8 young male mice, and n = 8 old male mice (qNSCs), n = 10 young male mice, and n = 11 old male mice (aNSCs/NPCs), combined over 2 (qNSCs) or 3 (aNSCs/NPCs) independent experiments. Data are mean ± SEM. P-values were calculated using a two-tailed Mann-Whitney test comparing sample means. Data from independent experiments are in Source Data. **j,k,** Quantification of subpopulation of cells with at least one active focal adhesion as assessed with paxillin (PXN) immunostaining of young (2.5-3 months) and old (22.1-22.1 months) qNSCs **(j)** and aNSCs/NPCs **(k)** cultured on Matrigel. Each grey dot represents number of focal adhesions per cell. Each colored dot represents average number of focal adhesions per cell of cells that have at least once focal adhesion (4-23 cells per dot) from an individual mouse. n = 8 young male mice, and n = 8 old male mice (qNSCs), n = 10 young male mice and n = 11 old male mice (aNSCs/NPCs), combined over 2 (qNSCs) or 3 (aNSCs/NPCs) independent experiments. Same experiment as in (h) and (i). Data are mean ± SEM. P-values were calculated using a two-tailed Mann-Whitney test comparing sample means. Data from independent experiments are in Source Data. **l,** Migration speed of young (3-4 months) and old (23-24 months) qNSCs on Poly-D-Lysine. Each grey dot represents the average velocity of a single cell over a 20-hour period. Each dot represents the average velocity over a 20-hour period of 5-42 cells in a primary culture derived from an individual mouse. n = 6 young male mice and

n = 4 old male mice, combined over 2 independent experiments. Data are mean ± SEM. P-values were calculated using a two-tailed Mann-Whitney test comparing sample means. Data from independent experiments are in Source Data. **m,** Migration speed of young (3-4 months) and old (21-24 months) aNSCs/NPCs migrating on Poly-D-Lysine. Each grey dot represents the average velocity of a single cell over a 20-hour period. Each colored dot represents the average velocity per mouse over a 20-hour period of 6-28 cells. n = 9 young male mice and n = 7 old male mice, combined over 3 independent experiments. Data are mean ± SEM. P-values were calculated using a two-tailed Mann-Whitney test comparing sample means. Data from independent experiments are in Source Data. **n,** Percent cells that are EdU-positive (S-phase) after a 2-hour pulse for young (2.5-4 months) and old (21-23 months) aNSCs/NPCs on Poly-D-Lysine. Each grey dot represents percent of cells in given field that are EdU-positive. Each colored dot represents average percent cells EdU-positive for an individual mouse (average of 5-7 fields containing at least 100 cells each). n = 9 young male mice, and n = 10 old male mice, combined over 3 experiments. Data are mean ± SEM. P-values were calculated using a two-tailed Mann-Whitney test comparing sample means. Data from independent experiments are in Source Data.

Extended Data Figure 8

a

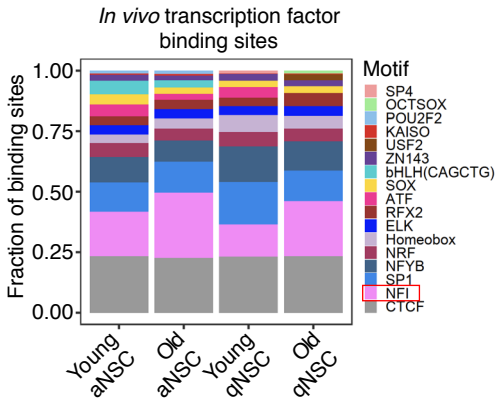

b

Transcription factor	HOMER pattern
NFIA	
NFIB	
NFIC	
NFIX	

c

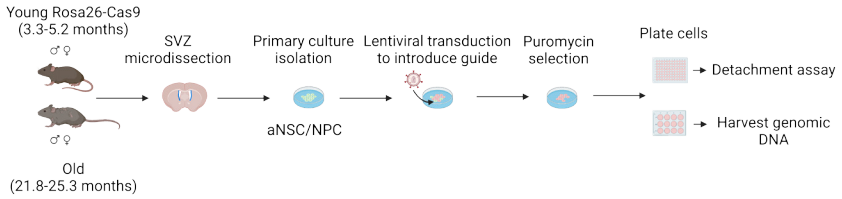

d

Guide name	Guide sequence	Synthego ICE knockout score range
Safe targeting control guide	GATAACCTGAACATGGACCA	58-84
NFIC targeting guide	GGCAGCAGCGCCTCGATGAA	56-79

e

Safe targeting control guide (example indel distribution)

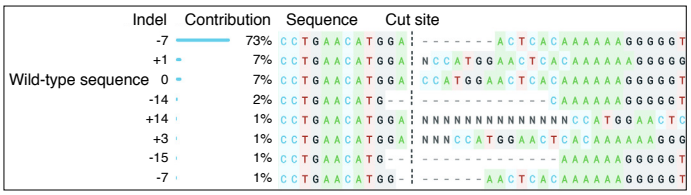

NFIC targeting guide (example indel distribution)

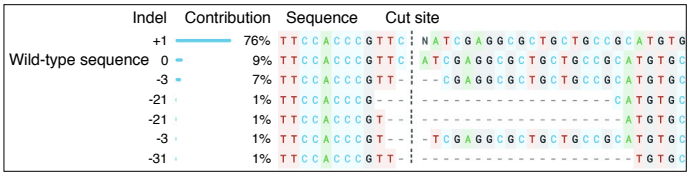

f

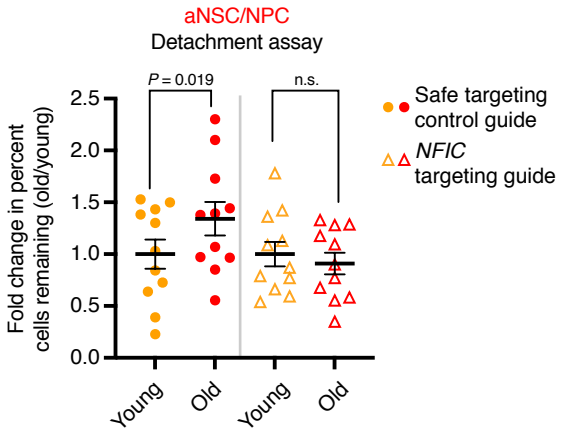

g

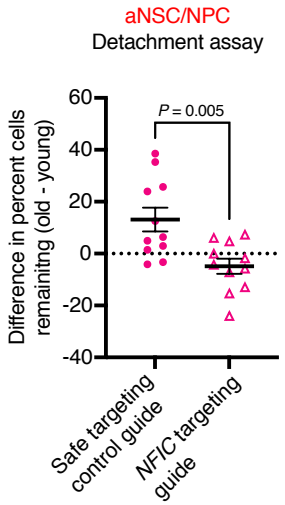

Extended Data Figure 8: NFI family of transcription factors during aging in activated NSCs
a, Distribution of transcription factor binding sites in accessible chromatin regions from freshly isolated young and old aNSCs and qNSCs identified using a deep learning model (see Methods). **b,** NFI family transcription factor binding site motifs for each NFI isoform from HOMER. **c,** Experimental pipeline for knocking out *NFIC* in primary cultures of young and old aNSCs/NPCs. Primary cultures derived from young and old Rosa26-Cas9 mixed male and female mice were infected with lentivirus to deliver guides of interest, puromycin selected, and then used for detachment assay and for harvesting genomic DNA to assess knockout efficiency (see Methods). **d,** Guide sequences used for safe targeting control guide which targets a safe harbor locus (gene that can be modified or disrupted with CRISPR-Cas9 without any adverse effect on the cell) and *NFIC* targeting guide from Bassik Lab mouse CRISPR Knockout library (see Methods) as well as Synthego ICE knockout score range achieved with each guide. With this tool, a score of 50 indicates 50% of the population sequenced was unedited (contains wild-type sequence). **e,** Sample traces for safe targeting control guide and *NFIC* targeting guide from Synthego ICE analysis tool indicating indel distribution and cut site. **f,** Detachment assay upon *NFIC* knockout in young and old aNSC/NPC using *NFIC* targeting guide. Quantification of percent of aNSCs/NPCs remaining after 3 minute Accutase incubation and wash with 1x PBS, normalized to young average from paired experiment. Each data point is average of 2-3 technical replicates per primary culture derived from an individual mouse. Safe targeting control guide samples (solid dot) were normalized to average of all young safe targeting control samples. *NFIC* targeting guide samples (open triangle) were normalized to average of all young *NFIC* targeting guide samples. Cells imaged and analyzed using Incucyte S3 system. Young (3.33-5.2 months) and old (21.8-25.3 months) aNSCs/NPCs were infected with lentivirus containing safe targeting control guide control or *NFIC* targeting guide. $n = 11$ young male and female mice, and $n = 11$ old male and female mice, combined over 7 experiments. Data are mean ± SEM. *P*-values were calculated using a Wilcoxon Matched-Pairs Signed Ranks Test, since experiments were performed in a paired manner (paired young and old). **g,** Detachment assay upon *NFIC* knockout in young and old aNSCs/NPCs using *NFIC* targeting guide. Same experiment as in (f). Quantification of difference of percent of aNSCs/NPCs remaining (old – young) after 3 minute Accutase incubation and wash with 1x PBS for safe targeting control guide samples (solid dot) and *NFIC* targeting guide samples (open triangle). Cells imaged and analyzed using Incucyte S3 system. Young (3.33-5.2 months) and old (21.8-25.3 months) aNSCs/NPCs were infected with lentivirus containing safe targeting control guide control or *NFIC* targeting guide. $n = 11$ young male and female mice, and $n = 11$ old male and female mice, combined over 7 experiments. Data are mean ± SEM. *P*-value was calculated using a two-tailed Mann-Whitney test.

Extended Data Figure 9

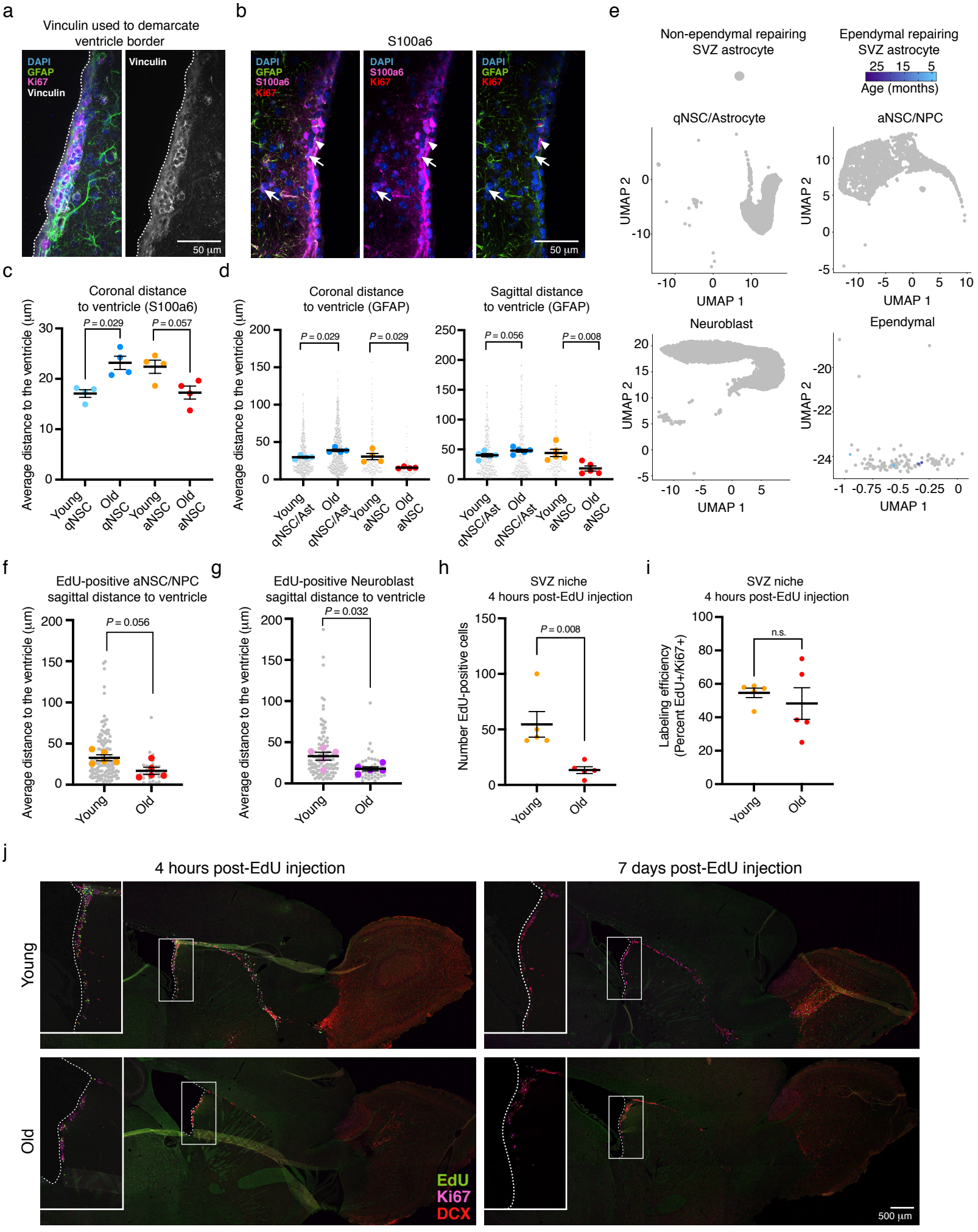

Extended Data Figure 9: *In vivo* location of EdU-labelled cells in the SVZ neurogenic niche
a, Representative image of vinculin immunofluorescence staining of old coronal section from GFAP-GFP mouse (Fig. 3c) indicating how vinculin (white) was used to demarcate ventricle border. The ventricular lining is indicated by a dotted white line. Green, GFAP (astrocyte/NSC marker); Pink, Ki67 (proliferation marker); Blue, DAPI (nuclei). Scale bar, 50 µm. **b,** Representative image of S100a6 immunofluorescent staining of old coronal section from GFAP-GFP mouse. White arrows: qNSC (S100a6+/Ki67- and GFAP+/Ki67-); white arrowheads aNSC (S100a6+/Ki67+ and GFAP+/Ki67+). Green, GFAP (astrocyte/NSC marker); Pink, S100a6 (NSC marker in the SVZ neurogenic niche); Red, Ki67 (proliferation marker); Blue, DAPI (nuclei). Scale bar, 50 µm. **c,** NSC distance to the ventricle was calculated for qNSCs (S100a6+/Ki67-) and aNSCs (S100a6+/Ki67+) in coronal sections of young (4 months) and old (18-26 months) SVZs. Each dot represents the mean distance from the ventricle of 140 – 574 cells in 6-11 fields per section (3 sections per dot) for an individual mouse. n = 4 mixed-sex young mice, and n = 4 mixed-sex old mice, combined over 4 independent experiments. Data are mean ± SEM. P-values were calculated using a two-tailed Mann-Whitney test comparing sample means. Data from independent experiments are in Source Data. **d,** NSC distance to the ventricle was calculated for qNSCs/astrocytes (GFAP+/Ki67-) and aNSCs (GFAP+/Ki67+) in coronal sections (left) of young (4 months) and old (18-26 months) SVZs from mixed sex GFAP-GFP mice and sagittal sections (right) of young (2-3 months) and old (21 months) SVZs from male C57BL/6 mice. Each grey dot represents the distance of a single cell from the ventricular lining. Each colored dot represents the mean distance from the ventricle of 19 - 231 cells in 3-7 fields per section (3 sections for coronal sections or 1 section for sagittal section) per individual mouse. Coronal sections: n = 4 young, and n = 4 old mixed-sex GFAP-GFP mice, combined over 4 independent experiments. Sagittal sections: n = 5 young male mice, and n = 5 old male C57BL/6 mice combined over 2 independent experiments. Data are mean ± SEM. P-values were calculated using a two-tailed Mann-Whitney test comparing sample means. Data from independent experiments are in Source Data. **e,** Single cell RNA-seq analysis of 28 C57BL/6 mice ranging in age from 3.3 months to 29 months (see Methods). Out of 21,458 cells, there are 4 cells expressing all markers of ependymal-repairing SVZ astrocytes (*S100b, Gfap, CD24a, Ctnnb1*) (see Methods). These cells are colored by age (4.7 months, 5.4 months, 16.83 months, and 18.87 months). Ependymal-repairing SVZ astrocytes are absent from qNSC/astrocyte, aNSC/NPC, and neuroblast clusters but are present in ependymal cell cluster. **f,** Distance to the ventricle was calculated for EdU+ aNSC/NPC (Ki67+/DCX-) in sagittal sections of young (2-3 months) and old (21 months) SVZs 4 hours after EdU injection. Each grey dot represents the distance of a single aNSC/NPC from the ventricle. Each colored dot represents the mean aNSC/NPC distance from the ventricle of 2-35 cells from 1 section per individual mouse. n = 5 young male mice, and n = 5 old male mice, combined over 2 experiments. Data are mean ± SEM. P-values were calculated using a two-tailed Mann-Whitney test comparing sample means. Data from independent experiments are in Source Data. **g,** Distance to the ventricle was calculated for EdU+ neuroblasts (DCX+) in sagittal sections of young (2-3 months) and old (21 months) SVZs 4 hours after EdU injection. Each grey dot represents the distance of a single neuroblast from the ventricle. Each colored dot represents the mean neuroblast distance from the ventricle of 3-25 cells from 1 section per individual mouse. n = 5 young male mice, and n = 5 old male mice, combined over 2 experiments. Data are mean ± SEM. P-values were calculated using a two-tailed Mann-Whitney test comparing sample means. Data from independent experiments are in Source Data. **h,** Quantification of number of EdU+ cells counted in the SVZ (along the entire length of the ventricle) from young (2-3 months) and old (21 months) sagittal sections 4 hours post-injection of EdU. n = 5 young male mice, and n = 5 old male mice, combined over 2 experiments. Data are mean ± SEM. P-values were calculated using a two-tailed Mann-Whitney test. Data from independent

experiments are in Source Data. **i,** Quantification of percent of Ki67+ cells that are EdU+ 4 hours post-injection of EdU in the SVZ (counting cells along the entire length of the ventricle). $n = 5$ young male mice, and $n = 5$ old male mice, combined over 2 experiments. Data are mean ± SEM. *P*-values were calculated using a two-tailed Mann-Whitney test. Data from independent experiments are in Source Data. **j,** Representative images of immunofluorescence staining of sagittal sections encompassing the SVZ, RMS, and OB regions from a young (2-3 months) (top) or old (21 months) (bottom) male C57BL/6 mouse 4hrs (left) or 7 days (right) after intraperitoneal EdU injection. White inset denotes SVZ. Dotted white line indicates ventricle lining. Green, EdU (proliferation marker); pink, Ki67 (aNSC/NPC/neuroblast marker); red, DCX (neuroblast marker). Scale bar, 500 μm.

Extended Data Figure 10

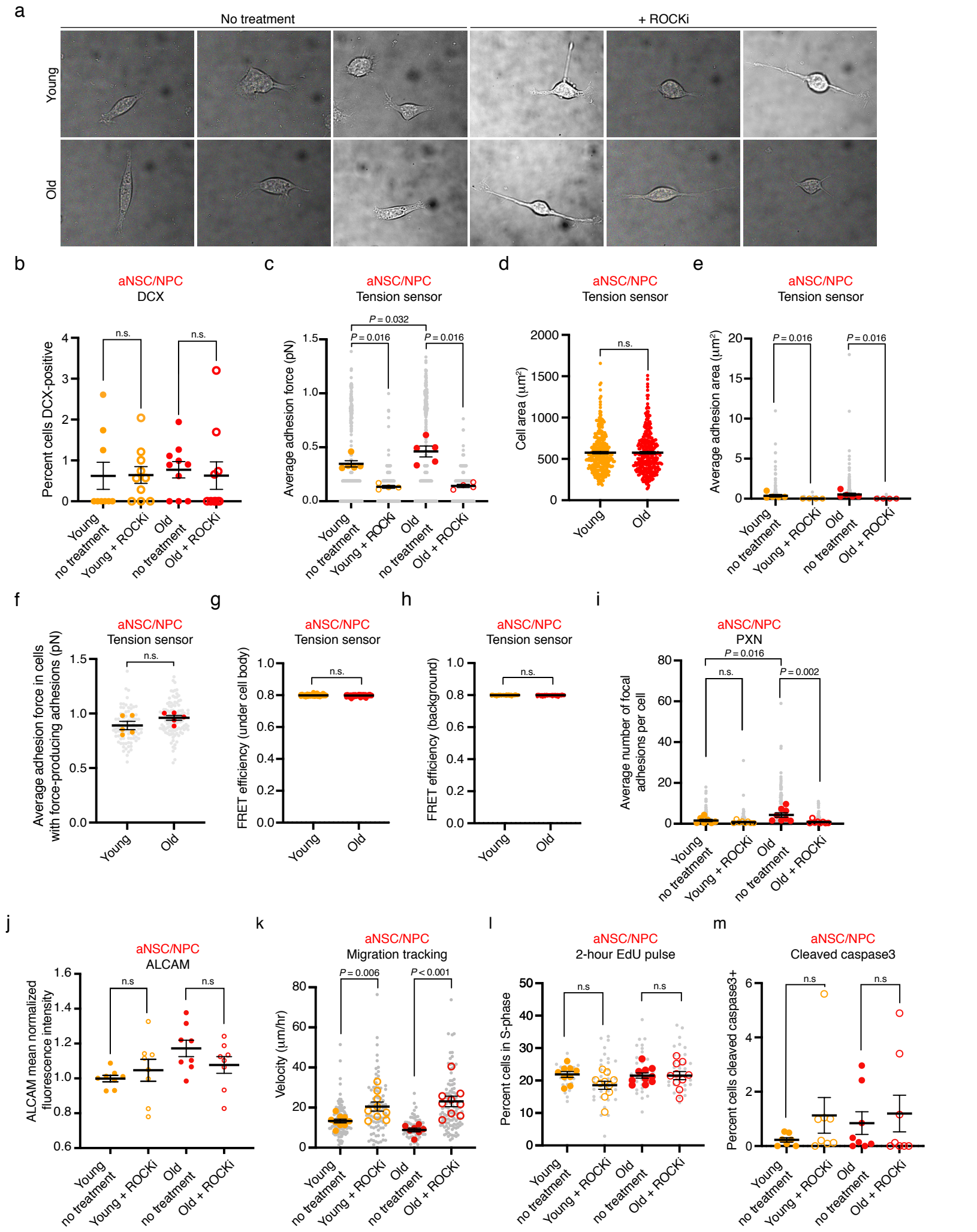

Extended Data Figure 10: Effect of ROCK inhibitor *in vitro* and *in vivo*

a, Representative brightfield images of young (2.4-3 months) (top) and old (20.5-21 months) (bottom) aNSCs/NPCs on RGD molecular tension sensors with H_2O vehicle (left) or 10 μM ROCKi (right). **b,** Percent cells that are positive for DCX staining in young (4 months) and old (22 months) aNSCs/NPCs treated with H_2O vehicle (no treatment, solid dots) or 10 μM ROCKi (ROCKi treatment, open circles) on Poly-D-Lysine. Each dot represents percent cells DCX-positive in a given field (containing 38-349 cells) for an individual animal (4-5 fields per animal). n = 2 young male mice and n = 2 old male mice (no treatment), and n = 2 young male mice and n = 2 old male mice (+ROCKi), combined over 1 experiment. Data are mean ± SEM. P-values were calculated using a two-tailed Mann-Whitney. Data from independent experiments are in Source Data. **c,** Quantification of average adhesion force (pN) exhibited by young (2.4-3 months) and old (20.5-21 months) cultured aNSCs/NPCs treated with H_2O vehicle (no treatment, solid dots) or 10 μM ROCKi (ROCKi treatment, open circles) determined using RGD molecular tension sensors. Each grey dot represents adhesion force produced by one cell. Each colored dot represents the average force produced by one cell (15– 89 cells per dot) in a primary culture derived from an individual mouse. n = 5 young male mice and n = 5 old male mice (no treatment), n = 4 young male mice and n = 4 old male mice (ROCKi treatment), combined over 5 independent experiments. Data are mean ± SEM. P-values were calculated using a two-tailed Mann-Whitney test comparing sample means. Data from independent experiments are in Source Data. **d,** Cell areas of young (2.4-3 months) and old (20.5-21 months) cultured aNSCs/NPCs determined using bright field images taken on RGD molecular tension sensors. n = 306 young aNSCs/NPCs, and n = 298 old aNSCs/NPCs, combined over 5 experiments. Data are mean ± SEM. P-values were calculated using a two-tailed Mann-Whitney test. Data from independent experiments are in Source Data. **e,** Quantification of average adhesion area under force-producing adhesions (μm^2) of young (2.4-3 months) and old (20.5-21 months) cultured aNSCs/NPCs treated with H_2O vehicle (no treatment, solid dots) or 10 μM ROCKi (ROCKi treatment, open circles) determined using RGD molecular tension sensors. Each grey dot represents adhesion area of force-producing adhesion from a single cell. Each colored dot represents the average adhesion area of force-producing adhesions from a single cell (15 – 89 cells per dot) in a primary culture derived from an individual mouse. Same experiment as in (c). Data are mean ± SEM. P-values were calculated using a two-tailed Mann-Whitney test comparing sample means. Data from independent experiments are in Source Data. **f,** Quantification of average adhesion force (pN) exhibited by young (2.4-3 months) and old (20.5-21 months) cultured aNSCs/NPCs that have at least one force-producing adhesion determined using RGD molecular tension sensors. Same experiment as in (c). Each grey dot represents adhesion force produced by one cell. Each colored dot represents the average force produced by one cell in cells that have at least one force-producing adhesion (8-29 cells per dot) in a primary culture derived from an individual mouse. n = 5 young male mice and n = 5 old male mice, combined over 5 independent experiments. Data are mean ± SEM. P-values were calculated using a two-tailed Mann-Whitney test comparing sample means. Data from independent experiments are in Source Data. **g,** FRET efficiency values underneath cell bodies of young (2.4-3 months) and old (20.5-21 months) cultured aNSC/NPC on RGD molecular tension sensors. n = 306 young aNSCs/NPCs, and n = 298 old aNSCs/NPCs, combined over 5 experiments. Same experiment as in (c). Data are mean ± SEM. P-values were calculated using a two-tailed Mann-Whitney test. Data from independent experiments are in Source Data. **h,** Background FRET efficiency values of young (2.4-3 months) and old (20.5-21 months) cultured aNSCs/NPCs on RGD molecular tension sensors. n = 306 young aNSCs/NPCs, and n = 298 old aNSCs/NPCs, combined over 5 experiments. Same experiment as in (c). Data are mean ± SEM. P-values were calculated using a two-tailed Mann-Whitney test. Data from independent experiments are in Source

Data. **i,** Quantification of average number of focal adhesions, determined using paxillin (PXN) staining, exhibited by young (2.5 months) and old (22.1 months) cultured aNSCs/NPCs treated with H_2O vehicle (no treatment, solid dots) or 10 μM ROCKi (ROCKi treatment, open circles). Each grey dot represents number of focal adhesions per cell. Each colored dot represents the average number of focal adhesions per cell from a primary culture (30 cells per dot) derived from an individual mouse. n = 7 young male mice and n = 8 old male mice (no treatment) and n = 8 young male mice and n = 8 old male mice (ROCKi treatment), combined over 2 experiments. Data are mean ± SEM. P-values were calculated using a two-tailed Mann-Whitney test comparing sample means. Data from independent experiments are in Source Data. **j,** Quantification of ALCAM fluorescence intensity of young (2.5-3 months) and old (21-22.1 months) aNSCs/NPCs on Matrigel treated with H_2O vehicle (no treatment, solid dots) or 10 μM ROCKi (ROCKi treatment, open circles). Each dot represents mean-normalized fluorescence intensity of 30 fields (each containing 1-3 cells) in a primary culture derived from an individual mouse, normalized by experiment and cell size. n = 8 young male mice and n = 8 old mice (no treatment) and n =8 young male mice and n = 8 old male mice (ROCKi treatment), combined over 2 experiments. Data are mean ± SEM. P-values were calculated using a two-tailed Mann-Whitney test comparing sample means. Data from independent experiments are in Source Data. **k,** Quantification of migration speed of young (3-4 months) and old (21-24 months) aNSC/NPC cultured on Poly-D-Lysine ± treatment with 10 μM ROCKi. Each grey dots represents average velocity of a single cell over a 20-hour period. Each colored dot represents the average velocity over a 20-hour period of cells (2-28) from one culture derived from one individual mouse. n = 9 young male mice and n = 7 old male mice (no treatment, solid dots) and n = 9 young male mice and n = 9 old male mice (ROCKi treatment, open circles), combined over 3 experiments. Data are mean ± SEM. P-values were calculated using a two-tailed Mann-Whitney test comparing sample means. Data from independent experiments are in Source Data. **l,** Percent cells that are EdU-positive (S-phase) after a 2 hour pulse for young (2.5-4 months) and old (21-23 months) aNSCs/NPCs treated with H_2O vehicle (no treatment, solid dots) or 10 μM ROCKi (ROCKi treatment, open circles) on Poly-D-Lysine. Each grey dot represents percent of cells in given field that are EdU-positive. Each colored dot represents average percent cells EdU-positive for an individual mouse (average of 5-7 fields containing at least 100 cells each). n = 9 young male mice and n = 10 old male mice (no treatment), and n = 10 young male mice and n = 10 old male mice (ROCKi treatment) combined over 3 experiments. Data are mean ± SEM. P-values were calculated using a two-tailed Mann-Whitney test comparing sample means. Data from independent experiments are in Source Data. **m,** Percent cells that are positive for cleaved-caspase 3 staining in young (3-4 months) and old (21-23 months) aNSCs/NPCs treated with H_2O vehicle (no treatment, solid dots) or 10 μM ROCKi (ROCKi treatment, open circles) on Poly-D-Lysine. Each dot represents average percent cells cleaved caspase3-positive for an individual mouse (average of 5 fields containing at least 100 cells). n = 7 young male mice and n = 8 old male mice (no treatment), and n = 8 young male mice and n = 8 old male mice (+ROCKi), combined over 2 experiments. Data are mean ± SEM. P-values were calculated using a two-tailed Mann-Whitney test comparing sample means. Data from independent experiments are in Source Data.